

FIST PROGRAM

Project No.: SR/FST/PSI-176/2012

(Level – I)

PROJECT COMPLETION REPORT

**Submitted to
Department of Science & Technology
New Delhi**

By



**School of Physics & Materials Science
Thapar Institute of Engineering & Technology
(Thapar University)
Patiala – 147004
PUNJAB**

June 2018

DST – Fund for Improvement in S&T Infrastructure (Level – I)

Name of Department: School of Physics & Materials Science (SPMS), Thapar Institute of Engineering and Technology, Patiala - 147004

Project No.: SR/FST/PSI-176/2012 dated 15th November, 2012

Brief Outline of the Department:

School of Physics & Materials Science (SPMS) was established in 1956 along with the inception of the Thapar Institute of Engineering and Technology, Patiala. Within the University, SPMS is recognized as premier academic and R&D department of the University. With its current faculty strength of 19, SPMS offers two PG programs in addition to undergraduate engineering programs. It also offers highly rated Ph.D. program in advance and diverse fields of materials engineering and technology, theoretical high energy physics, non-linear optics and computation physics.

Teaching & Research Activities:

SPMS offers two post graduate Programs (M.Sc. in Physics and M. Tech in Materials and Metallurgical Engineering). Both master's program have 30 seats each. SPMS is also offering Ph.D. in diverse field of science and technology in subjects related to core physics like nuclear & particle physics, computation physics, non-linear optics, condensed matter physics, etc. to multidisciplinary sciences like nanomedicine, green energy technologies, thin film technology, etc. SPMS has 29 on-going projects worth 3.60 crores.

Facilities Created:

1. Vibrating Sample Magnetometer



Model and Make: 7404; Lakeshore, USA

Total Cost: Rs. 1.12 crore (DST contribution: 35 lakhs; TU contribution: 77 lakhs)

Salient Features:

Dynamic range 0.5×10^{-6} emu to 10^3 emu

Noise 0.5×10^{-6} emu at 1.0" gap

Field accuracy in gauss 1% of reading or $\pm 0.05\%$ of full scale

Field stability in gauss $\pm 0.05\%$ of full scale

Maximum field strength ± 14.5 kG with air gap of 0.9"; 10 kG @ 1.6" gap

Temperature range: 77 K – 950 K (with single stage cryostat-oven)

2. Inductively coupled plasma atomic emission spectrophotometer (ICP-AES)

Model and Make: *Prodigy*; Teledyne Leeman Lab, USA

Total Cost: Rs. 38.68 lakhs (DST contribution: 19 lakhs; TU contribution: 19.68 lakhs)

Salient Features:

Simultaneous ICP spectrophotometer

Modes: Radial, Axial and Dual

RF power output: 600 – 2000 W at 40 MHz

Wavelength Range: 165-900 nm

Polychromator: Echelle optics

Detection limit: < 1 ppm for most of the elements (sample dependent)

: < 1 ppb for hydride generating elements

Funding:

Total Cost of the FIST (level – I): **1.63 Crore**

DST contribution: **81.5 lakhs (54 lakhs released; 27.5 lakhs to be released)**

TU contribution: **81.5 lakhs (96.68 lakhs released)**

Funding for other sources during the reporting period: **734.04 lacs**

For further details contact:

Professor Manoj K. Sharma

Head, School of Physics & Materials Science and FIST Program Coordinator

Thapar Institute of Engineering and Technology, Patiala – 147004, Punjab

Email: msharma@thapar.edu

Tel. No. (O) +91-175-2393893 (M) +91-9592780056

Report for utilization of FIST support

1. Name of the Department: School of Physics & Materials Science (SPMS)

2. Address for communication:

Professor Manoj K. Sharma
 Head, School of Physics & Materials Science and FIST Program Coordinator
 Thapar Institute of Engineering and Technology, Patiala – 147004, Punjab
 Email: msharma@thapar.edu
 Tel. No. (O) +91-175-2393893 (M) +91-9592780056

3. Date and ref. No. of DST Sanction letter: May 30, 2013; SR/FST/PSI-176/2012

4. Details of the Grants

<i>Budget Heads</i>	<i>Amount Sanctioned with Date</i>	<i>Amount Received with Date</i>
<i>a. Equipment</i>	150 lakh (75DST; 75 TU) Dt. 28/06/2013	54 lakhs
<i>b. Infrastructure</i>	0	0
<i>c. Networking</i>	0	0
<i>d. Maintenance</i>	13 lakhs (6.5 DST; 6.5 TU) Dt. 28/06/2013	0
<i>e. Total</i>	163 lakhs (81.5 DST; 81.5 TU) Dt. 28/06/2013	54 lakhs 17/07/2013

5. Equipment ordered/purchased/installed:

<i>Name (with Model & Make)</i>	<i>Order date</i>	<i>Installation date</i>	<i>Cost in INR</i>
Vibrating Sample Magnetometer (VSM)			
Model: 7404	25.03.2015	30.04.2015	112 lakhs
Make: Lakeshore, USA			
Inductively Coupled Plasma Atomic Emission Spectrophotometer (ICP-AES)			
Model: Prodigy	21.01.2014	10.03.2015	38.68 lakhs
Make: Teledyne Leeman Lab, USA			

6. Details of Infrastructure developed: N.A.

7. Details of Networking: (Specify if the Internet facility is available to UG/PG/research students)

Entire campus (academic blocks / hostels and residential area) has wi-fi enabled internet connectivity for 24×7.

8. Utilization of the facilities created under FIST support:

- a. **For teaching:** SPMS offers an advance course on characterization and measurements techniques to PG (M.Sc. and M.Tech) students and a similar course is also being offered to Ph.D. students during their course work. Infrastructure facility (VSM and ICP) created under FIST program is being extensively used by the concern faculty to teach fundamentals of these two techniques, their design, measurement aspects and result analysis.
- b. **For research:** PG students are using the facilities created under FIST program (VSM and ICP) extensively while working on their Masters Dissertation. Doctoral students are also using them on regular basis. Following is the list of user groups of these facilities:

Condensed Matter / Materials Science Group (SPMS)
 School of Chemistry and Biochemistry
 School of Energy and Environment
 Department of Biotechnology
 Department of Chemical Engineering
 Department of Mechanical Engineering

In addition, PG and Ph.D. students of various undergraduate colleges in and around Patiala and research groups of various Universities of Punjab are also using these facilities.

9. Details of full length research publications (in peer-reviewed journals) during the period under report.

Annexure – P1

10. Sponsored research projects in operation during the period under report (please provide name/s of PI/Co-PIs, title of the project, funding agency and total quantum of external support)

No. of projects = 35

Total Amount = 734.04 lacs

S. No.	Name of the Investigator	Title of the project and duration	Amount sanctioned (Rs. in lacs)	Funding Agency
1	Puneet Sharma	Synthesis and Characterization of Multiferroics AFe_2O_4 - $BiFeO_3$ (A= Co, Ni, Zn) Nanocomposite Films.	10.00	UGC
2	Puneet Sharma	Development of barium hexaferrite ($BaFe_{12}O_{19}$) thick films for micro/millimeter wave device application.	16.00	CSIR

3	Puneet Sharma	Development of M type hexaferrite films for microwave device application.	47.46	DST
4	Puneet Sharma	Development of exchange coupled hard/soft ferrite nanocomposites for tunable microwave application.	21.56	CSIR
5	B.N.Chudasama	Nanoengineering of magnetic carriers for drug delivery of anticancer therapeutics.	13.75	DST
6	B.N.Chudasama	Studies on antimicrobial properties of metal and metal oxide nanostructures.	27.10	UGC
7	B.N.Chudasama	Development of Magnetic Therapeutic Agents for Thermo-Chemotherapy of Cancer.	48.78	DST
8	B.N.Chudasama	Magnetic core supported heterogeneous catalysts for the glycerol carbon synthesis.	19.60	CSIR
9	Manoj Sharma	Study of nuclear reaction dynamics involved with heavy ion collisions.	12.50	DST
10	Manoj Sharma	Study of different versions of nuclear proximity potentials in the formation and decay path of nuclear systems	12.70	UGC
11	Manoj Sharma	Exploring the incomplete processes and features which effect the same.	20.00	CSIR
12	Manoj Sharma	Decay analysis of light particle induced reactions and related structural effects.	17.80	DST
13	Alka Upadhyay	Study of heavy-Light D and B mesons using HQET.	10.00	UGC
14	Alka Upadhyay	Low energy properties of baryon $J_p=1/2^+$ octets and $J_p=3/2^+$ Decuplets using phenomenological model.	17.39	DST
15	Poonam Uniyal	Study of Size-dependent multiferroics properties of doped BiFeO_3 nanostructures.	24.14	BRNS
16	Poonam Uniyal	Synthesis of $\text{BiFeO}_3 - (\text{K}_{0.5}\text{Na}_{0.5})\text{NbO}_3$ thin films for device applications	13.92	UGC
17	Poonam Uniyal	Lead free relax or ferroelectric ceramics for Electrocaloric applications.	39.40	CSIR
18	B. C. Mohanty	Investigation of growth dynamics and kinetic surface roughening of some solution processed technologically important binary sulfides.	6.00	UGC
19	B. C. Mohanty	Photovoltaic and Grain Boundary Characteristics of Single Target Sputtered $\text{Cu}_2\text{ZnSn}(\text{SSe})_4$ Thin Film Solar Cell.	55.26	SERB-DST
20	Soumendu Jana	Moving And Colliding Cavity Solitons and Cavity Soliton Molecules	6.00	UGC-BSR
21	Debabrata Deb	Substrate mediated phase transition in two-dimensional liquid crystal systems.	26.45	SERB-DST
22	D. P. Singh	Development of transition metal oxide decorated graphene - polypyrrole nanocomposites as Radar absorbing materials.	9.91	DRDO

23	S. D. Tiwari	Determination of Neel Temperature for ferritin.	18.75	UGC
24	S. D. Tiwari	Effect of magnetic anisotropy and particle size distribution on the magnetization of antiferromagnetic NiO nanoparticles.	9.91	CSIR
25	Kulvir Singh	Study of Alkaline earth metals substitution in Bi based mixed ion conductor for solid oxide fuel cell application.	14.42	DRDO
26	Kulvir Singh	Study of La doped mixed conductor for solid electrolyte.	34.50	DST
27	O.P. Pandey	Synthesis and characterization of novel 2D metal carbides (MXenes) for energy conversion and storage applications	40.66	DST
28	O.P. Pandey	Synthesis and Characterization of Na ₂ S-P ₂ S ₅ glass/glass-ceramic based solid electrolytes for Na-ion batteries	28.00	DST
29	O.P. Pandey	Study of alkali metal oxide containing calcium silicate glasses as substrate for solar cell application	23.70	DST
30	O.P. Pandey	Synthesis and characterization of molybdenum carbide nanoparticles for electrochemical applications.	2.13	UGC-DAE
31	O.P. Pandey	Development of Transition Metal Oxides decorated Graphene-Polypyrrole nanocomposites as RADAR Absorbing Materials	9.91	DRDO
32	O.P. Pandey	Corrosion Resistant behaviour of Glass - steel interface.	9.03	UGC
33	O.P. Pandey	Synthesis of nano tungsten carbide powder from wolframite ore.	33.00	DST
34	O.P. Pandey	Synthesis of WC nano powder through thermo-chemical reduction and its application for the development of WC-Composite	27.00	DST
35	O.P. Pandey	Synthesis and Characterization of Vanadium Carbide Nanoparticles	7.34	UGC, DAE, CSR

11. Utilization of Equipment from outside the Department:

User groups from following departments are using Facilities created under FIST program:

School of Chemistry and Biochemistry
School of Energy and Environment
Department of Biotechnology
Department of Chemical Engineering
Department of Mechanical Engineering

User groups of UG colleges:

Khalsa College, Patiala
Government Mohindra College, Patiala
Multani Mal Modi College, Patiala
Bhai Gurdas Institute of Engineering and Technology, Sangrur
Baba Banda Singh Bahadur College of Engineering, Fatehgarh Sahib

User Groups of other Universities/Institutes:

Punjabi University, Patiala
Punjab University, Chandigarh
CSIO, Chandigarh
IIT, Ropar
Gurugranth Sahib World Sikh University, Fatehgarh Sahib
Arni University, Kangra
Chandigarh University, Chandigarh

12. SELF-ASSESSMENT OF THE IMPACT OF FIST SUPPORT: Please specify if any of the following activity emerged/ improved as a consequence of the FIST support:

a. New class-room experiments at B.Sc/ M.Sc. or other levels

SPMS has introduced an advance course on Material Characterization and Measurement Techniques. This course is being offered to PG students of M.Sc., M.Tech and Ph.D. (Experimental Condensed Matter Physics). Few Ph.D. students of School of Chemistry and Biochemistry, Department of Chemical Engineering, Department of Mechanical Engineering and Department of Biotechnology also peruse this course during the course work. Instrument facilities (ICP and VSM) created under the FIST program is being extensively utilized in laboratory teaching of this course.

b. Success of students at national level tests (various PG/Ph.D. entrance tests and tests for JRF, etc):

Most of our PG students after completing their PG degrees opt for Ph.D. programs at Institute of National / International repute. Many of them join various IITs by cracking their respective interest tests. Few students are also pursuing their Ph.D. in abroad. However, success rate in NET/JRF tests remained poor. From our school, only two students have cleared JRF test. School is focusing on this lacuna and we are expecting to improve this number in near future.

c. Any new research project that emerged on the basis of the FIST support:

School has its core competency in designing materials for various technological uses. Some important breakthroughs in recent years is fabrication of low frequency high dielectric materials from agriculture waste, nanoantibiotics which has better efficiency and no multidrug resistance, low cost high efficiency semiconductor for solar cell applications.

School has received funding from various national agencies for 35 major research projects worth 734 lakhs during the tenure of DST-FIST level – I. It has also published over 400 publications in renowned SCI journals during the period of this report.

c. Any new research project that emerged on the basis of the FIST support:

S. No.	Name of the Investigator	Title of the project and duration	Amount sanctioned (Rs. in lacs)	Funding Agency
1	Puneet Sharma	Development of barium hexaferrite (BaFe ₁₂ O ₁₉) thick films for micro/millimeter wave device application.	16.00	CSIR
2	Puneet Sharma	Development of M type hexaferrite films for microwave device application.	47.46	DST
3	Puneet Sharma	Development of exchange coupled hard/soft ferrite nanocomposites for tunable microwave application.	21.56	CSIR
4	B.N.Chudasama	Studies on antimicrobial properties of metal and metal oxide nanostructures.	27.10	UGC
5	B.N.Chudasama	Development of Magnetic Therapeutic Agents for Thermo-Chemotherapy of Cancer.	48.78	DST
6	B.N.Chudasama	Magnetic core supported heterogeneous catalysts for the glycerol carbon synthesis.	19.60	CSIR
7	Poonam Uniyal	Synthesis of BiFeO ₃ - (K _{0.5} Na _{0.5})NbO ₃ thin films for device applications	13.92	UGC
8	Poonam Uniyal	Lead free relax or ferroelectric ceramics for Electrocaloric applications.	39.40	CSIR
9	B. C. Mohanty	Investigation of growth dynamics and kinetic surface roughening of some solution processed technologically important binary sulfides.	6.00	UGC
10	B. C. Mohanty	Photovoltaic and Grain Boundary Characteristics of Single Target Sputtered Cu ₂ ZnSn(SSe) ₄ Thin Film Solar Cell.	55.26	SERB-DST
11	D. P. Singh	Development of transition metal oxide decorated graphene - polypyrrole nanocomposites as Radar absorbing materials.	9.91	DRDO
12	S. D. Tiwari	Effect of magnetic anisotropy and particle size distribution on the magnetization of antiferromagnetic NiO nanoparticles.	9.91	CSIR
13	O.P. Pandey	Synthesis and characterization of novel 2D metal carbides (MXenes) for energy conversion and storage applications	40.66	DST
14	O.P. Pandey	Synthesis and Characterization of Na ₂ S-P ₂ S ₅ glass/glass-ceramic based solid electrolytes for Na-ion batteries	28.00	DST
15	O.P. Pandey	Study of alkali metal oxide containing calcium silicate glasses as substrate for	23.70	DST

		solar cell application		
16	O.P. Pandey	Synthesis and characterization of molybdenum carbide nanoparticles for electrochemical applications.	2.13	UGC-DAE
17	O.P. Pandey	Development of Transition Metal Oxides decorated Graphene-Polypyrrole nanocomposites as RADAR Absorbing Materials	9.91	DRDO

d. Did the newly created facility lead to betterment of quality of research publications?

Yes.

No. of publications before FIST program (5 years): **201**

No. of publications after FIST program (5 years): **420**

Average impact factor of publication before FIST program (5 years): **1.52**

Average impact factor of publication after FIST program (5 years): **2.298**

No. of Ph.D. award before FIST (5 years): **25**

No. of Ph.D. award after FIST (5 years): **49**

e. Any training program/ workshop organized by the department during the period of report, especially those involving the newly created facility):


1. 58th DAE Solid State Physics Symposium (DAE-SSPS – 2013) (December 2013)
2. Seminar cum Exhibition on “Nuclear Technology for Future needs” (March 2014)
3. National Workshop on Carrier in Physics (March 2015)
4. 2nd Conference on Microscopy in Materials Science and 2nd Annual meeting of Academy of Microscope Science and Technology (AMST), February 25-27, 2016
5. Summer School on Magnetism, July 11- 15, 2016
6. DAE-BRNS symposium on Nuclear Physics, December 20-24, 2017

Apart from these major events, SPMS invites leading experts from across the globe for invited lectures under its Materials and Physics Society Expert Lecture Series throughout the year.

13. Is any problem faced in utilization of the grant/facilities?

Release of second instalment of the grant for the third approved instrument (Electron Paramagnetic Resonance) is pending with DST. This release may be considered during the next phase of the program. An application for DST-FIST (level – II) has already been submitted for the kind consideration of the Department.

Details of Equipment acquired under FIST Program

Name of the Equipment	Inductively coupled Plasma Atomic Emission Spectrophotometer (ICP-AES)
Model Number	Prodigy
Complete Specifications	Simultaneous ICP spectrophotometer Modes: Radial, Axial and Dual RF power output: 600 – 2000 W at 40 MHz Wavelength Range: 165-900 nm Polychromator: Echelle optics Detection limit: < 1 ppm for most of the elements : < 1 ppb for hydride generating elements
Details of Manufacturer	
Name	Teledyne Leeman Labs
Address	6 Wentworth Drive
City	Hudson
PIN	NH 03051
State	USA
Phone	+1 513.229.7082
Fax	--
Email	Wayne.Mozer@teledyne.com
Details of Local Agent / Supplier	
Name	Labindia Analytical Instruments Pvt Ltd
Address	G-4 Palmohan Sadan, 26/32 East Patel Nagar,
City	New Delhi
PIN	110008
State	Delhi
Phone	011-43306001-10
Fax	011-25851066
Email	kumara@labindia.com
Actual Cost (in Foreign Exchange)	64000 USD
Actual Cost (in Indian Rupees)	Rs. 38.68 lakhs
Used for	Elemental analysis of trace metals
Scanned Photograph of the Equipment (Front View)	
	
ICP-AES at Thapar Institute of Engineering and Technology (Thapar University), Patiala	

Name of the Equipment	Vibrating Sample Magnetometer (VSM)
Model Number	7404 with 74035 single stage cryostat oven
Complete Specifications	Dynamic range 0.5×10^{-6} emu to 10^3 emu Noise 0.5×10^{-6} emu at 1.0" gap Field accuracy in gauss 1% of reading or $\pm 0.05\%$ of full scale Field stability in gauss $\pm 0.05\%$ of full scale Maximum field strength ± 14.5 kG with air gap of 0.9"; 10 kG @ 1.6" gap Temperature range: 77 K – 950 K (with single stage cryostat-oven)
Details of Manufacturer	
Name	Lakeshore Cryotronics Inc
Address	575 McCorkle, Boulevard
City	Westerville
PIN	OH 43082
State	Ohio
Phone	001- (614) 891-2244
Fax	001-(614) 818-1600
Email	sales@lakeshore.com
Details of Local Agent / Supplier	
Name	Specialise Instruments Marketing Company
Address	305,Kailas Industrial Complex, A-Wing, 3rd Floor, Building No.2, Parksite, Vikroli (West)
City	Mumbai
PIN	400079
State	Maharashtra
Phone	+91-22-25171922/23
Fax	+91-22-25171924
Email	specmcol@vsnl.com
Actual Cost (in Foreign Exchange)	154315 USD
Actual Cost (in Indian Rupees)	Rs. 112 lakhs
Used for	Magnetic Characterization of bulk, thin films and nanomaterials.

Scanned Photograph of the Equipment (Front View)



VSM at Thapar Institute of Engineering and Technology (Thapar University), Patiala

Details of Assets Acquired under FIST Program

Sr. No.	Name of the Equipment/ Item	Cost in FE	Cost in INR
1	Inductively Coupled Plasma Atomic Emission Spectrophotometer (ICP-AES)	64000 USD	38.68094 lakhs
2	Vibrating Sample Magnetometer (VSM)	154315 USD	Rs. 111.43545 lakhs

Head wise Expenditure Details:

1. Equipment Head (E):

Sr. No.	Name of the Equipment/ Item	Total Cost (total cost of equipment after paying all charges)	Date of Installation
1	Inductively Coupled Plasma Atomic Emission Spectrophotometer (ICP-AES)	38.68094 lakhs	21.01.2014
2	Vibrating Sample Magnetometer (VSM)	Rs. 111.43545 lakhs	25.03.2015
Total		150.11639 lakhs	

2. Networking Head (NW): NA

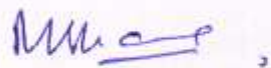
Sr. No.	Name of Item procured for computer lab	Total Cost (total cost of equipment after paying all charges)	Date of Installation
1			
Total			

3. Infrastructure Head (IF): NA

Sr. No.	Name of the Item procured/activities carried out including Books acquired	Total Cost (total payment towards renovation, up gradation of labs, Books acquired, etc)	Date of Completion of Work/Date of acquiring of items, Books etc.
1			

4. Maintenance Head (M): Nil

Sr. No.	Name of Items	Total Cost	Date on which expenditure was made
1			


Professor Manoj K. Sharma
Coordinator, DST-FIST (Level – I)
Head, School of Physics & Materials Science
Thapar Institute of Engineering and Technology, Patiala – 147004, Punjab
Email: msharma@thapar.edu
Tel. No. (O) +91-175-2393893 (M) +91-9592780056

HEAD
School of Physics & Materials Science
Thapar Institute of Engineering & Technology
Patiala - 147004.

List of Research Publications only in SCI Journals

Sr. No.	Authors	Title of paper	Name of journal	Year	Vol No. / Page No.	Impact Factor
1	Pallavi Gupta, Alka Upadhyay	Analysis of strong decays of charmed mesons $D_2(2460)$, $D_0(2560)$, $D_2(2740)$, $D_1(3000)$, $D_2(3000)$ and their spin partners $D_1(2680)$, $D_3(2760)$ and $D_0(3000)$	Phys. Rev. D	2018	97, 014015	4.568
2	P. Jha, S.S. Danewalia, G. Sharma, K Singh	Antimicrobial and bioactive phosphate-free glass-ceramics for bone tissue engineering applications	Mater. Sci. Engg.:C	2018	86 (2018) 9-17	4.164
3	N. Bansal, G. Kaur, K. Singh	Braunite phase embedded $Y_2O_3/MnO_2-Al_2O_3-CaO-SiO_2$ glass ceramics and their properties	Materials Research Bulletin	2018	98, 34-40	2.446
4	L Khanna, NK Verma, SK Tripathi	Burgeoning tool of biomedical applications-Superparamagnetic nanoparticles	Journal of Alloys and Compounds	2018	752, 332-353	3.133
5	Baldeep Kaur and Soumendu Jana	Cavity Soliton Molecules and All-Optical Push-broom Effect	Journal of lightwave technology	2018	36 (12), 2463 - 2470	2.862
6	Motoharu Imai, Mukesh Kumar, Yoshitaka Matsushita, Naoto Umezawa	Crystal structure and electronic properties of Sr-substituted disilicide $Ba_{1-x}Sr_xSi_2$ for solar cells: computational and experimental studies	Acta Materialia	2018	148, 462-498	5.301
7	Kanishka Sharma, Gudveen Sawhney, Manoj K.Sharma, Raj K.Gupta	Decay of Plutonium isotopes via spontaneous and heavy-ion induced fission paths	Nucl. Phys. A	2018	972, 1-17	1.916
8	Pallavi Gupta, Alka Upadhyay	Decay width and coupling constants of charm and bottom mesons.	PoS Hadron	2018	2017, 025	1.09
9	Neha Grover, Kirandeep Sandhu, and Manoj K. Sharma	Dynamics of $^{17}F + ^{58}Ni$ reaction via complete and incomplete fusion processes at above barrier energies	Nucl. Phys. A	2018	974, 56-71	1.916
10	Gurjit Kaur, Kirandeep Sandhu, Amandeep Kaur, and Manoj K. Sharma	Dynamics of Db isotopes formed in reactions induced by ^{238}U , ^{248}Cm , and ^{249}Bk across the Coulomb barrier	Phys. Rev. C	2018	97, 054602	3.82
11	P Kaur, BN Chudasama	Effect of Colloidal Medium on the Shelf-Life and Stability of Gold Nanorods Prepared by Seed-Mediated Synthesis	Journal of Nanoscience and Nanotechnology	2018	18 (3), 1665-1674	1.483
12	S. Sharma, T. Nanda, O.P. Pandey	Effect of dual particle size (DPS) on dry sliding wear behaviour of LM30/sillimanite composites	Tribology International	2018	123, 142-154	2.903

13	Sandeep Sharma, Tarun Nanda and O.P. Pandey	Effect of particle size on dry sliding wear behaviour of sillimanite reinforced aluminium matrix composites	Ceramics International	2018	44 (1), 104-114	2.986
14	Shivani Jindal, Kamaldeep Kaur, N.K. Verma, & Puneet Sharma	Effect of Tb ³⁺ ions substitution on structural, optical and magnetic properties of CdS nanoparticles	J Mater Sci: Mater Electron	2018	29, 86-90	2.019
15	N Kaur, BN Chudasama	Effect of thermal aging on stability of transformer oil based temperature sensitive magnetic fluids	Journal of Magnetism and Magnetic Materials	2018	451, 647-653	2.63
16	B. C. Mohanty , K. Bector, R. Laha,	Elucidating doping driven microstructure evolution and optical properties of lead sulfide thin films grown from a chemical bath	Appl. Surf. Sci.	2018	435, 444-451	3.387
17	Aayush Gupta, Varun Singhal and O.P. Pandey	Facile in-situ synthesis of NbB ₂ nanoparticles at low temperature	Journal of Alloys and Compounds	2018	736, 306-313	3.133
18	R Bains, P Sharma, RA Mir, S Jeet, G Kaur, O.P. Pandey	Influence of CuO/MgO ratio on the gene expression, cytocompatibility, and antibacterial/anticancerous/analgesic drug loading kinetics for (15-x)CuO-xMgO-10P2O5-60SiO2-10CaO-5ZnO (2.5 ≤ x ≤ 12.5) mesoporous bioactive glasses	J Biomed Mater Res A	2018	10.1002/jbm.a.36415	3.076
19	Rameez Mir Ahmad and O.P. Pandey	Influence of graphitic/amorphous coated carbon on HER activity of low temperature synthesized β-Mo ₂ C@C nanocomposites	Chemical Engineering Journal	2018	10.1016/j.cej.2018.05.041	6.216
20	K. J. Cook, I. P. Carter, E. C. Simpson, M. Dasgupta, D. J. Hinde, L. T. Bezzina, Sunil Kalkal , C. Sengupta, C. Simenel, B. M. A. Swinton-Bland, K. Vo-Phuoc, and E. Williams.	Interplay of charge clustering and weak binding in reactions of ⁸ Li	Phys. Rev. C	2018	97, 021601 (R)	3.82
21	S.S. Danewalia, K. Singh	Intriguing role of TiO ₂ in glass-ceramics: Bioactive and magneto-structural properties	J. Am. Ceram. Soc.	2018	101, 2819-2830	2.841
22	Deepshikha and Suneel Kumar	Investigation of nuclear stopping observable in heavy ion collisions	Nuclear Physics A	2018	975, 29-47	1.916
23	N. Kaur, G. Kaur, D. Kumar, K. Singh	Mechanical and thermal properties of SrO/BaO modified Y ₂ O ₃ -Al ₂ O ₃ -B ₂ O ₃ -SiO ₂ glasses and their compatibility with solid oxide fuel cell components	J Phys Chem Solids	2018	118, 248-254	2.048

24	G Dhir, P Uniyal, NK Verma	Multiferroic properties of Sr-doped BiFeO ₃ nanoparticles	Physica B: Condensed Matter	2018	531, 51-57	1.386
25	C Khurana, BN Chudasama	Nanoantibiotics: strategic assets in the fight against drug-resistant superbugs	International journal of nanomedicine	2018	13, 3	4.383
26	Kamaldeep Kaur and Suneel Kumar	On the study of rotational effects in mass asymmetric colliding nuclei at intermediate energies	Nuclear Physics A	2018	973, 149–163	1.916
27	G. Sharma, S.K. Arya, K. Singh,	Optical and thermal properties of glasses and glass-ceramics derived from agricultural wastes	Ceramic International	2018	44, 947-952	2.758
28	Deepshikha and Suneel Kumar	Participation of nucleons among different harmonics of anisotropic flow.	Canadian Journal of Physics, (ja).	2018		0.724
29	M. Mittal, A. Gupta and O.P. Pandey	Role of oxygen vacancies in Ag/Au doped CeO ₂ nanoparticles for fast photocatalysis	Solar Energy	2018	165, 206-216	4.018
30	Amandeep Kaur, Gudveen Sawhney, Manoj K. Sharma and Raj K. Gupta	Spontaneous fission of the end product in alpha-decay chain of recoiled super heavy nucleus: a theoretical study	Int. J. of Mod. Phys E (IJMPE)	2018	27 (5), 1850043	1.916
31	Baldeep Kaur, Anu Mittal, S.S. Mallick, Peter Wypych and Soumendu Jana	Stability and phase space analysis of fluidized-dense phase pneumatic transport system	Powder Technology	2018	330, 190-200	2.942
32	Pallavi Gupta, Alka Upadhyay	Strong Decays and Coupling Constants of 1P and 1D Bottom Meson	Springer Proc.Phys.	2018	203, 885-888	-
33	H.K. Sidana, Rameez Ahmad Mir and O.P. Pandey	Synthesis of molybdenum nitride (Mo ₂ N) nanoflakes via in-situ reduction-nitridation	Journal of Alloys and Compounds	2018	736, 255-265	3.133
34	S Jeet, O.P. Pandey	Template free synthesis route to monophasic BaMgAl ₁₀ O ₁₇ : Eu ²⁺ with high luminescence efficiency	Journal of Alloys and Compounds	2018	750, 85-91	3.133
35	Aayush Gupta and O.P. Pandey	Visible irradiation induced photodegradation by NbC/C nanocomposite derived from smoked cigarette litter (filters)	Solar Energy	2018	163, 167-176	4.018
36	Neha Grover, Ishita Sharma, Gurvinder Kaur, Manoj K. Sharma	Analysis of dynamical behavior of reactions associated with ^{118,120,122} Xe* isotopes	Nuclear Physics A	2017	959, 10–26	1.916
37	Mandeep Kaur, Bir Bikram Singh, Manoj K.Sharma, Raj K. Gupta	Analysis of intermediate and light mass fragments from composite systems ^{26–29} Al* formed in ^{16,18} O + ^{10,11} B reactions	Nucl. Phys. A	2017	969, 14	1.916
38	Gudveen Sawhney, Amandeep Kaur, Manoj K. Sharma	Analysis of spontaneous fission in super heavy mass region using the dynamical cluster-decay model	Acta Physica Polonica B	2017	48, 3	0.904

39	S. Kumar, S.K. Sharma and O.P. Pandey	Analysis of volume dependence of thermal expansivity for NaCl	Indian Journal of Pure & Applied Physics	2017	55 (4), 293-296	0.521
40	S. Garg, S. Thakur, Aayush Gupta, G. Kaur and O.P. Pandey	Antibacterial and anticancerous drug loading kinetics for (10-x) CuO-xZnO-20CaO-60SiO ₂ -10P ₂ O ₅ (2 ≤ x ≤ 8) mesoporous bioactive glasses	J. Mater. Sci.: Mater. Med.	2017	28, 11	2.325
41	Ankita Goyal, S Bansal, B Chudasama , KB Tikoo, V Kumar, Sonal Singhal	Augmenting the catalytic performance of spinel nanoferrites (CoFe ₂ O ₄ and NiFe ₂ O ₄) via incorporation of Al into the lattice	New Journal of Chemistry	2017	41, 8320-8332	3.277
42	Mukesh Kumar , Naoto Umezawa, Wei Zhou and Motoharu Imai	Barium disilicide as a promising thin-film photovoltaic absorber: structural, electronic, and defect properties	Journal of Materials Chemistry A	2017	5, 25293 – 25302	8.867
43	G. Singla, K. Singh , O.P. Pandey	Catalytic activity of tungsten carbide-carbon (WC@C) core-shell structured for ethanol electro-oxidation	Materials Chemistry and Physics	2017	186, 19-28	2.084
44	Amandeep Kaur and Manoj K Sharma	Competing analysis of α and 2p _{2n} - emission from compound nuclei formed in neutron induced reactions	Nuclear Phys. A	2017	957, 274–288	1.916
45	Manjeet Singh Gautam, Neha Grover and Manoj K. Sharma	Complete and incomplete fusion dynamics of 6,7Li + 159Tb reactions near the Coulomb barrier	Eur. Phys. J. A	2017	53:12:00	2.833
46	N Kaur, G. Kaur, S Khan, K Singh	Conductivity, dielectric and structural studies of (30-x) SrO-xBaO-10Al ₂ O ₃ -45-SiO ₂ -5B ₂ O ₃ -10Y ₂ O ₃ (5<x<25) glasses	Ionics	2017	1-11.	2.112
47	Khushboo, Nikhar Bhargava, Khyati Anand, Praveen Malik, Puneet Sharma , Divya Jayoti & K. K. Raina	Dielectric and polarization switching studies in nickel nanoparticles dispersed ferroelectric liquid crystal mixtures	Integrated Ferroelectrics	2017	184, 192-198	0.457
48	Kadam Bhambri , Gurkirpal Singh , Neena Gupta, Debabrata Deb , Soumendu Jana	Dispersion Managed Dissipative Solitons with Higher Order Nonlinearity and Frequency-Selective Feedback	Optical and Quantum Electronics	2017	49, 376	1.055
49	GS Parmar, Soumendu Jana , BA Malomed	Dissipative soliton fiber lasers with higher-order nonlinearity, multiphoton absorption and emission, and random dispersion	JOSA B	2017	34 (4), 850-860	1.843
50	Neha Grover, Kanishka Sharma, and Manoj K. Sharma	Dynamics of 47V* formed in 20Ne + 27Al reaction in view of fusion-fission and DIC mechanism	Eur. Phys. J. A	2017	53 (12), 239	2.833

51	Kaur, G., Sriranganathan, N., Waldrop, S.G., Sharma, P., Chudasama, B.N.	Effect of copper on the up-regulation/down-regulation of genes, cytotoxicity and ion dissolution for mesoporous bioactive glasses	Biomedical Materials	2017	12(4), 045020	3.361
52	S.S. Danewalia, N. Gupta, S. Aggarwal, K. Singh	Effect of mixed oxide/fluoride bonding on the dielectric properties of oxyfluoride glasses	Journal of Materials Science: Materials in Electronics	2017	28,18986-18993	2.019
53	N Bansal, GC Mohanta, K. Singh,	Effect of Mn ²⁺ and Cu ²⁺ co-doping on structural and luminescent properties of ZnS nanoparticles	Ceramics International	2017	43 (9) 7193-7201.	2.758
54	Tarun Nanda, B. Ravi Kumar, Sailaja Sharma, Vishal Singh and O.P. Pandey	Effect of thermal cycling process parameters on recrystallization kinetics for processing of fine-grained pure copper	Materials and Manufacturing Processes	2017	32 (1), 34-43	2.274
55	S. Khan, G. Kaur, K. Singh,	Effect of ZrO ₂ on dielectric, optical and structural properties of yttrium calcium borosilicate glasses,	Ceramic International	2017	43 (1)722-727	2.758
56	P Jena, SK Gupta, NK Verma, AK Singh, RM Kadam	Energy transfer dynamics and time resolved photoluminescence in BaWO ₄ : Eu ³⁺ nanophosphors synthesized by mechanical activation	New Journal of Chemistry	2017	41 (17), 8947-8958	3.277
57	Pallavi Gupta, Ashok Kumar, Monika Tomar, Vinay Gupta, Dwijendra P. Singh	Enhanced dielectric properties and suppressed leakage current density of PVDF composites flexible film through small loading of submicron Ba _{0.7} Sr _{0.3} TiO ₃ crystallites.	Journal of Materials Science: Materials in Electronics	2017	28 (16), 11806-11812	2.019
58	P. Singla, O.P. Pandey, K. Singh,	Enhanced photocatalytic degradation of diethyl phthalate using Zn doped rutile TiO ₂ ,	Indian Journal of Pure & Applied Physics	2017	55, 710-715	0.521
59	M. Morjean, D. J. Hinde, C. Simenel, D. Y. Jeung, M. Airiau, K. J. Cook, M. Dasgupta, A. rouart, D. Jacquet, S. Kalkal, C. S. Palshetkar, E. Prasad, D. Rafferty, E. C. Simpson, L. Tassan-Got, K. Vo-Phuoc, and E. Williams	Evidence for the role of proton shell closure in quasifission reactions from X-ray fluorescence of mass -identified fragments.	Phys. Rev Lett.	2017	119, 222502	8.462
60	Deepak Kumar, M. Sharma, D. Haranath, O.P. Pandey	Facile route to produce spherical and highly luminescent Tb ³⁺ doped Y ₂ O ₃ nanophosphors	Journal of Alloys and Compounds	2017	695, 726-736	3.133

61	Amandeep Kaur, Manoj K. Sharma	Fragmentation analysis of α -induced reactions using clusterization approach	Nucl. Phys. A	2017	969, 30	1.916
62	Ishita Sharma, Manjeet Singh Gautam and Manoj K. Sharma	Fusion dynamics of $^{30}\text{Si} + ^{238}\text{U}$ reaction using variety of interaction potentials	Int. J. of Mod. Phys E	2017	26 (11), 1750077	1.597
63	B Kaur, Soumendu Jana	Generation and dynamics of one- and two-dimensional cavity solitons in a vertical-cavity surface-emitting laser with a saturable absorber and frequency-selective feedback	JOSA B	2017	34 (7), 1374-1385	1.843
64	D.H. Yeon, B.C. Mohanty , C. Y. Lee, S. M. Lee, and Y.S. Cho	High-Efficiency Double Absorber PbS/CdS Heterojunction Solar Cells by Enhanced Charge Collection Using a ZnO Nanorod Array	ACS Omega	2017	2, 4894-4899	N/A
65	D.H. Yeon, B.C. Mohanty , C. Y. Lee, S. M. Lee, and Y.S. Cho	High-Efficiency Double Absorber PbS/CdS Heterojunction Solar Cells by Enhanced Charge Collection Using a ZnO Nanorod Array	ACS Omega	2018	2, 4894-4900	N/A
66	Pankaj Kumar, Vandna Sharma, Chinky, Divya Jayoti, Kuldeep Kumar Raina & Praveen Malik	Impact of dye on the switching responses of polymer dispersed ferroelectric liquid crystal	Molecular Crystals and Liquid Crystals	2017	647, 385-394	0.571
67	Rajni, Deepika Jain, Ishita Sharma, Manoj K. Sharma	Impact of spin orbit density dependent potential in heavy ion reaction forming Se nuclei,	Eur. Phys. J. A	2017	53 (10), 208	2.833
68	M. Kaur, G. Kaur, O.P. Pandey, K. Singh and V. Kumar	Influence of CaO/MgO ratio on the crystallization kinetics and interfacial compatibility with Crofer 22APU and YSZ of strontium based aluminoborosilicate glasses for SOFC applications	International Journal of Hydrogen Energy	2017	42 (25), 16244-16257	3.582
69	Bhupinder Kaur, K. Singh, O.P. Pandey and Samita Thakur	Influence of modifier on dielectric and ferroelectric properties of aluminosilicate glasses	Journal of Non-Crystalline Solids	2017	465, 26-30	2.124
70	Rajni Mittal, Deepika Jain, Manoj K. Sharma	Influence of sticking vs non-sticking limits of moment of inertia and higher order deformations in the decay of $^{214,216}\text{Rn}^*$ compound systems	Nucl. Phys. A	2017	968, 436-452	1.916
71	P. Jha, S.S. Danewalia, K. Singh ,	Influence of thermal stability on dielectric properties of $\text{SiO}_2\text{-K}_2\text{O-CaO-MgO}$ glasses	Journal of Thermal Analysis and Calorimetry	2017	128 (2) 745-754.	1.953

72	Rupal Malik, Jaspreet Kaur, Anupama Kaushik, Ankush Sheoran, Bhupendra Chudasama , Vinod Kumar, KB Tikoo, Sonal Singhal	Interesting structural transformation of CdS from zinc blende into wurtzite during minuscule loading of magnetic nanoparticles: emergence of heterojunctions with enhanced photocatalytic performance	New Journal of Chemistry	2017	41, 14088-14102	3.277
73	P Sharma, P Uniyal	Investigating thermal and kinetic parameters of lithium titanate formation by solid-state method	Journal of Thermal Analysis and Calorimetry	2017	128 (2), 875-882	1.953
74	Amanpreet Kaur, Pallavi Gupta, Alka Upadhyay	Low energy properties of $J^P = 1/2^+$ octet baryons using statistical model	Prog. Theor. Exp. Phys.	2017	063B02	2.294
75	Anu Gupta, S.D. Tiwari	Magnetic Properties of Undoped and Al doped Layered α -Co(OH) ₂	Physica B: Condensed Matter	2017	525, 21-25	1.386
76	Anu Mittal, Baldeep Kaur; Soumya S Mallick, Renhu Pan, Soumendu Jana	Numerical Simulation of Fluidized Dense-Phase Pneumatic Conveying of Powders towards Developing Improved Model for Solids Friction Factor	Particuology	2017	35, 42-50	2.621
77	B Kaur, A Mittal, P Wypych, SS Mallick, Soumendu Jana	On developing improved modelling and scale-up procedures for pneumatic conveying of fine powders	Powder Technology	2017	305, 270-278	2.942
78	Amandeep Kaur and Suneel Kumar	On the global and local nuclear stopping in mass asymmetric nuclear collisions using density-dependent symmetry energy	Indian Journal of Physics	2017	91(9), 1095-1102	0.988
79	Kamaldeep Kaur and Suneel Kumar	On the rapidity distribution of nucleons participating in elliptical flow at intermediate energies.	Modern Physics Letters A	2017	32(01), 1750001	1.338
80	Paramjyot Kumar Jha, O.P. Pandey, K. Singh	Optimization of high conducting Na ₃ Zr ₂ Si ₂ PO ₁₂ phase by new phosphate salt for solid electrolyte	Silicon	2017	9 (3), 411-419	0.829
81	Pankaj Kumar, Vandna Sharma, Chinky Jaggi, Praveen Malik & Kuldeep Kumar Raina	Orientalional control of liquid crystal molecules via carbon nanotubes and dichroic dye in polymer dispersed liquid crystal	Liquid Crystals	2017	44, 843-853	2.661
82	C Rani, SD Tiwari	Phase transitions in two-line ferrihydrite nanoparticles	Applied Physics A	2017	123 (8), 532	1.455
83	I. Sharma, Raj Kumar , and M. K. Sharma	Probing the role of Skyrme interactions on the fission dynamics of ⁶ Li+ ²³⁸ U reaction	Eur. Phys. J. A	2017	53, 140	2.833
84	P Kaur, BN Chudasama	Seedless co-surfactant-based dimensional and optical tunability of gold nanorods with simultaneous pH regulation	Journal of Materials Science	2017	52 (19), 11675-11687	2.599

85	Khushboo, P. Sharma , P. Malik & K. K. Raina	Size-dependent studies in ferromagnetic nanoparticles dispersed ferroelectric liquid crystal mixtures	Liquid Crystals	2017	45(6), 896-906	2.661
86	Kanishka Sharma, Gudveen Sawhney , and Manoj K. Sharma	Spontaneous fission and competing ground state decay modes of actinide and transactinide nuclei	Phys. Rev. C	2017	96, 054307	3.82
87	Samita Thakur, K. Singh and O.P. Pandey	Sr doped BiMO ₃ (M= Mn, Fe, Y) perovskites: Structure correlated thermal and electrical properties	Materials Chemistry and Physics	2017	187, 96-103	2.084
88	RK Singh, NK Verma , S Chandriya	Structural analysis of a cracked cantilever beam with an arbitrary cross-section of a finiteelement model	Advances in Mechanical, Industrial, Automation and Management Systems	2017	12, 110	
89	Chhavi Pahwa, Santhoshkumar Mahadevan, Sukhleen Bindra, Puneet Sharma	Structural magnetic and microwave properties of exchange coupled and non-exchange coupled BaFe ₁₂ O ₁₉ /NiFe ₂ O ₄ nanocomposites	J. Alloys Compounds	2017	725, 1175-1181	3.133
90	Santhoshkumar Mahadevan, Chhavi Pahwa, Sukhleen Bindra Narang, Puneet Sharma	Structural, dielectric and magnetic properties of BaFe _{12-x} Al _x O ₁₉ hexaferrite thick films, Journal of Magnetism and Magnetic Materials	Journal of Magnetism and Magnetic Materials	2017	441, 465-474	2.63
91	N Kaur, BN Chudasama	Structure induced tunable magnetic properties of Zn substituted Mn _{1-x} Zn _x Fe ₂ O ₄ (x= 0-1) NPs	Micro & Nano Letters	2017	12 (3), 151-156	0.91
92	Gurjit Kaur, Kirandeep Sandhu, Manoj K. Sharma ,	Study of cold fusion reactions using collective clusterization approach	Commun. Theor. Phys.	2017	68, 4	1.042
93	M Kaur, P Uniyal	Study on Structural, Multiferroic, Optical and Photocatalytic Properties of Ferroelectromagnetic Nanoparticles: Bi _{0.9} Ba _{0.1} Fe _{0.8} Ti _{0.2} O ₃	Journal of Superconductivity and Novel Magnetism	2017	30 (2), 431-439	1.18
94	C Rani, SD Tiwari	Superparamagnetic behavior of antiferromagnetic six lines ferrihydrite nanoparticles	Physica B: Condensed Matter	2017	513, 58-61	1.386
95	D Kumar, CB Singh, NK Verma , AK Singh	Synthesis and structural investigations on multiferroic Ba _{1-x} Sr _x MnO ₃ perovskite manganites	Ferroelectrics	2017	518 (1), 191-195	0.551
96	Khushboo, Praveen Malik, Divya Jayoti, Puneet Sharma , and K. K. Raina	Textural and optical studies of magneto-mesogen material for display applications, Molecular crystals and liquid crystals	Molecular crystals and liquid crystals	2017	647, 201-206	0.571

97	Khushboo, P. Sharma , P. Malik and K. K Raina	Textural, thermal, optical and electrical properties of Iron nanoparticles dispersed 4'-(Hexyloxy)-4-biphenylcarbonitrile liquid crystal mixture	Liquid Crystals	2017	44,1717-1726	2.661
98	Rameez Ahmad Mir, Piyush Sharma and O.P. Pandey	Thermal and structural studies of carbon coated Mo ₂ C synthesized via in-situ single step reduction carburization	Scientific Reports	2017	7, 3518	4.259
99	R. Kaur, P. Singla, K. Singh ,	Transition metals (Mn,Ni, Co) doping in TiO ₂ nanoparticles and their effect on degradation of diethyl phthalate	Int. Journal of Environmental Science and Technology	2017	1-10,	2.19
100	Baldeep Kaur, Soumendu Jana	A generic travelling wave solution in dissipative laser cavity	Pramana	2016	87 (4), 53	0.52
101	S.S. Danewalia, Gaurav Sharma, Samita Thakur, K. Singh	Agricultural wastes as a resource of raw materials for developing low-dielectric glass-ceramics	Scientific Reports	2016	6,1-12.	4.259
102	Amandeep Kaur, Deepshikha, Karan Singh Vinayak and Suneel Kumar	Analyzing fragment production in mass-asymmetric reactions as a function of density dependent part of symmetry energy	Physics of Atomic Nuclei	2016	79(4), 474-480	0.411
103	Sunil Kalkal , E. C. Simpson, D. H. Luong, K. J. Cook, M. Dasgupta, D. J. Hinde et al.	Asymptotic and near-target direct breakup of ⁶ Li and ⁷ Li.	Phys. Rev. C.	2016	93, 044605	3.82
104	Baldeep Kaur, Soumendu Jana , Qin Zhou, Anjan Biswas, Milivoj Belic	Bright and exotic solitons in laser cavity with frequency selective feedback	J. of Optoelectronics and Advanced Materials	2016	18 (5-6), 428-434	0.29
105	Gurbinder Kaur, O.P. Pandey , K. Singh , B. Chudasama and V. Kumar	Combined and individual doxorubicin/vancomycin drug loading, release kinetics and apatite formation for the CaO–CuO–P ₂ O ₅ –SiO ₂ –B ₂ O ₃ mesoporous glasses	RSC Advances	2016	6, 51046-51056	3.108
106	N Grover, G Kaur, Manoj K Sharma	Decay analysis of pre actinide and trans actinide nuclei formed using various projectiles on ¹⁹⁷ Au	Phys. Rev. C	2016	93, 014603	3.82
107	Khushboo, Puneet Sharma , Praveen Malik & K.K. Raina	Dielectric and electro-optical studies of a nickelferrite-nanoparticle- doped ferroelectric liquid crystal mixture	Phase Transitions	2016	89, 144-154	1.06
108	E. C. Simpson, K. J. Cook, D. H. Luong, Sunil Kalkal , I. P. Carter, M. Dasgupta, D. J. Hinde, and E.	Disintegration locations in ⁷ Li→ ⁸ Be transfer- triggered Breakup at near-barrier energies.	Phys. Rev. C	2016	93, 024605	3.82

	Williams					
109	Rajni, Gurvinder Kaur, and Manoj K. Sharma	Dynamics of 16,18O induced reactions using Ni, Ge and Mo targets	Int. J. of Mod. Phys E	2016	25 (11), 1650091	1.597
110	I. Gupta and B. C. Mohanty	Dynamics of surface evolution in semiconductor thin films grown from a chemical bath	Scientific Reports	2016	6, 33136	4.259
111	Shiwani Sharma, Alok Mishra, P. Saravanan, O. P. Pandey and Puneet Sharma	Effect of Gd - substitution on the ferroelectric and magnetic properties of BiFeO ₃ processed by high-energy ball milling	J. Magn. Magn. Mater.	2016	418, 188–193	
112	Praveen Jha, K. Singh ,	Effect of MgO on bioactivity, hardness, structural and optical properties of SiO ₂ -K ₂ O-CaO-MgO glasses	Ceramic international,	2016	42 (1) 436-444.	2.758
113	G Dhir, P Uniyal, NK Verma	Effect of particle size on the multiferroic properties of Tb-doped BiFeO ₃ nanoparticles	Journal of Superconductivity and Novel Magnetism	2016	29 (10), 2621-2628	1.18
114	Aayush Gupta, Gourav Singla, O.P. Pandey	Effect of synthesis parameters on structural and thermal properties of NbC/C nano composite synthesized via in-situ carburization reduction route at low temperature	Ceramics International	2016	42 (11), 13024-13034	2.986
115	S.K. Arya, G. Kaur, K. Singh	Effect of Vanadium on the optical and physical properties of lithium borate glasses,	Journal of Non-Crystalline Solids	2016	433,14-19	2.124
116	S.K. Arya, S.S.Danewalia, M. Arora, K. Singh	Effect of Variable Oxidation States of Vanadium on Structural, Optical and dielectric properties of B ₂ O ₃ -Li ₂ O-ZnO-V ₂ O ₅ Glasses	The Journal of Physical Chemistry B	2016	120 (47) 12168-12176.	3.187
117	Khushboo, Puneet Sharma , Praveen Malik & K. K. Raina	Electro-optic, dielectric and optical studies of NiFe ₂ O ₄ -ferroelectric liquid crystal: a soft magnetoelectric material	Liquid Crystals	2016	43, 1671-1681	2.661
118	Soumendu Jana , Shivani, Gurkirpal Singh Parmar, Baldeep Kaur, Qin Zhou, Anjan Biswas, Milivoj Belic	Evolution of bell-shaped dissipative optical solitons from super-gaussian pulse in parabolic law medium with bandwidth limited amplification	Optoelectronics and Advanced Materials – Rapid Communications	2016	10(3-4), 143-150	0.449
119	Mittal, Manish; Sharma, Manoj; O.P. Pandey	Fast and quick degradation properties of doped and capped ZnO nanoparticles under UV-Visible light radiations	SOLAR ENERGY	2016	125, 51-64	4.018

120	SK Arya, S. S. Danewalia, K. Singh	Frequency independent low-k lithium borate nanocrystalline glass ceramic and glasses for microelectronic applications	Journal of Materials Chemistry C	2016	4, 3328-3336.	5.066
121	Shiwani Sharma, P. Saravanan, O.P. Pandey , and Puneet Sharma	Grain size distribution dependent magnetic and ferroelectric properties in sol-gel driven BiFeO ₃ thin films	J Mater Sci: Mater Electronics	2016	27 (6), 5909-5915	2.019
122	Meenakshi Batra, Alka Upadhyay , Pallavi Gupta	Heavy–light charm mesons spectroscopy and decay widths	Prog. Theor. Exp. Phys	2016	053B02	2.294
123	Devender Kumar, K. Singh ,	High hardness- High Toughness WC-20Co Nanocomposites: Effect of VC Variation and Sintering Temperature	Materials Science & Engineering A	2016	663, 21-28.	2.647
124	M Dhiman, S Bhukal, BN Chudasama , S Singhal	Impact of metal ions (Cr ³⁺ , Co ²⁺ , Ni ²⁺ , Cu ²⁺ and Zn ²⁺) substitution on the structural, magnetic and catalytic properties of substituted Co–Mn ferrites synthesized by sol–gel route	Journal of Sol-Gel Science and Technology	2016	3 (81), 831-843	1.575
125	K. J. Cook, E. C. Simpson, D. H. Luong, Sunil Kalkal , M. Dasgupta, and D. J. Hinde	Importance of lifetime effects in breakup and suppression of complete fusion in reactions Of weakly bound nuclei.	Phys. Rev. C.	2016	93, 064604	3.82
126	Manju Middha, Rishi Kumar & K. K. Raina	Improved Electro Optical Response of Induced Chiral Nematic Liquid Crystal Doped with Multi Walled Carbon Nanotubes	Ferroelectrics	2016	495, 75-86	0.551
127	I. J. Choi, J. W. Jang, B. C. Mohanty , S. M. Lee, and Y. S. Cho	Improved Photovoltaic Characteristics and Grain Boundary Potentials of CuIn _{0.7} Ga _{0.3} Se ₂ Thin Films Spin-Coated by Na-Dissolved Nontoxic Precursor Solution	ACS Appl. Mater. Interfaces	2016	8, 17011–17015	7.504
128	C Khurana , AK Vala, N Andhariya, OP Pandey , BN Chudasama	Influence of antibiotic adsorption on biocidal activities of silver nanoparticles	IET nanobiotechnology	2016	10 (2), 69-74	1.463
129	M Kaur, P Uniyal	Investigation on the effect of Ti doping on dielectric, impedance and magnetic properties of Ba ²⁺ -substituted BiFeO ₃ ceramics	Journal of Materials Science: Materials in Electronics	2016	27 (12), 12539-12549	2.019
130	Amanpreet Kaur, Alka Upadhyay	J/P=1/2+, J/P=3/2+ masses in statistical model	Eur. Phys. J. A	2016	52, 332	2.736
131	S.S. Danewalia, K. Singh	Magnetic and bioactive properties of MnO ₂ /Fe ₂ O ₃ modified Na ₂ O-CaO-P ₂ O ₅ -SiO ₂ glasses and nanocrystalline glass-ceramics,	Ceramics International	2016	42(10) 11858-11865.	2.986

132	Shiwani Sharma, P. Saravanan, O.P. Pandey , V.T.P. Vinod, Miroslav Černík and Puneet Sharma	Magnetic behaviour of sol–gel driven BiFeO ₃ thin films with different grain size distribution	J. Magn. Magn. Mater.	2016	401,180–187	
133	Amanpreet Kaur, Alka Upadhyay	Magnetic moments of JP = 3/2+ decuplet baryons using statistical model	Eur. Phys. J. A	2016	52, 105	2.736
134	M Kaur, KL Yadav, P Uniyal	Multiferroic and optical studies on the effects of Ba ²⁺ ions in BiFeO ₃ nanoparticles	Journal of Materials Science: Materials in Electronics	2016	27 (5), 4475-4482	2.019
135	A Gupta, SD Tiwari , D Kumar	Nature of magnetic interactions in β-Co (OH) ₂ nanoparticles	physica status solidi (b)	2016	253 (9), 1795-1798	1.674
136	Paramjyot Kumar Jha, O.P. Pandey , K. Singh	Non-isothermal crystallization kinetics of K ₂ O modified sodium-phosphate glasses	Journal of Non-Crystalline Solids	2016	440, 76-84	2.124
137	Rishi Kumar & K.K. Raina	Optical and electrical control of circularly polarised fluorescence in CdSe quantum dots dispersed polymer stabilised cholesteric liquid crystal	Liquid Crystals	2016	43, 994–1001	2.661
138	K. Sood, K. Singh, S. Basu and O.P. Pandey	Optical, thermal, electrical and morphological study of La _{1-x} Ca _x GaO _{3-δ} (x= 0, 0.05, 0.10, 0.15 and 0.20) electrolyte	Journal of the European Ceramic Society	2016	36 (13), 3165-3171	3.411
139	Manju Middha, Rishi Kumar & K.K. Raina	Photoluminescence tuning and electro optical memory in chiral nematic liquid crystals doped with silver nanoparticles	Liquid Crystals	2016	43, 1002-1008	2.661
140	G kaur, K Sandhu, Manoj K Sharma	Properties of fission fragments for Z=112-116 superheavy nuclei.	Phys. Rev. C	2016	94, 014615	3.82
141	Loveleen K Brar, Gourav Singla and O.P. Pandey	Role of carbon in structural evolution during single step synthesis of nano Tantalum Carbide	RSC Advances	2016	6, 109174-109184	3.108
142	M K Sharma, R N Panda, Manoj K Sharma , S K Patra	Search for halo structure in ³⁷ Mg using a Glauber model and microscopic relativistic mean-field densities,	Phys. Rev. C	2016	93, 014322	3.82
143	Ramneek Kaur & K. K. Raina	Self assembling effects of nano particles in mesomorphic LB films	Ferroelectrics	2016	495, 87–96	0.551
144	S. Verma, O.P. Pandey , A. Paesano, P. Sharma	Structural and magnetic properties of Co Ti substituted barium hexaferrite thick films	Journal of Alloys and Compounds	2016	678, 284-289	3.133
145	N Aggarwal, K Kaur, A Vasishth, NK Verma	Structural, optical and magnetic properties of Gadolinium-doped ZnO nanoparticles	Journal of Materials Science: Materials in Electronics	2016	27 (12), 13006-13011	2.019

146	Pallavi Gupta, Alka Upadhyay	Study of 1D stranded-charm meson family using HQET	Advances In High Energy Phys.,	2016	4957236	1.74
147	Singla, P.; O.P. Pandey; Singh, K.	Study of photocatalytic degradation of environmentally harmful phthalate esters using Ni-doped TiO ₂ nanoparticles	Int. J. of Env. Sci. & Tech.	2016	13 (3), 849-856	1.915
148	Singla, Gourav; Singh, K.; O.P. Pandey	Study on single step solid state synthesis of WC@C nanocomposite and electrochemical stability of synthesized WC@C & Pt/WC@C for alcohol oxidation (methanol/ethanol)	J. Alloys Compounds	2016	665, 186-196	3.133
149	Vishalli, K.K. Raina , D.K. Avasthi, Alok Srivastava, Keya Dharamvir	Swift heavy ion induced modifications of single walled carbon nanotube thin films	Nuclear Instruments and Methods in Physics Research B	2016	373, 28–34	1.109
150	Chandni Khurana , Purnima Sharma, O.P. Pandey, B. Chudasama	Synergistic effect of metal nanoparticles on the antimicrobial activities of antibiotics against biorecycling microbes	Journal of Materials Science & Technology	2016	32, 524-532	2.764
151	Sanjay Kumar, S.K.Sharma, O.P.Pandey	Volume dependence of Grüneisen parameter for solids under extreme compression	Pramana-Journal of Physics	2016	87 (2), 21	0.52
152	Niyti, G. Sawhney , Manoj K. Sharma, R. K. Gupta	Alpha-decay chains of recoiled superheavy nuclei: A theoretical study.	Phys. Rev. C	2015	91, 054606	3.82
153	Kumar, Sanjay; Sharma, S. K.; O.P. Pandey	Analysis of thermodynamic properties in the limit of infinite pressure	High Temp. High Pressure	2015	44 (5)	0.408
154	GS Parmar, Soumendu Jana	Bistable dissipative soliton in cubic-quintic nonlinear medium with multiphoton absorption and gain dispersion	JEMWA	2015	29, 1410-1429	0.86
155	Manoj K Sharma and G. Kaur	Cluster decay analysis and related structure effects of fissionable heavy and superheavy nuclei,	Pramana J. Phys.	2015	85 (3), 431-437	0.692
156	Sood, Kapil; Singh, K.; O.P. Pandey	Co-existence of cubic and orthorhombic phases in Ba-doped LaInO ₃ and their effect on conductivity	Physica B	2015	456, 250-257	1.386
157	PK Jha, OP Pandey, K. Singh ,	Crystallization and Glass Transition Kinetics of Na ₂ S-P ₂ S ₅ -Based Super-Ionic Glasses	Particulate Science and Technology	2015	33, 166-171	0.784

158	M. Kaur, B B Singh, Manoj K. Sharma and Raj K. Gupta.	Decay analysis of compound nuclei with masses A approx 30--200 formed in reactions involving loosely bound projectiles" by	Phys. Rev. C.	2015	92, 024623	3.82
159	G Sawhney , A. Kaur, Manoj K Sharma and R K Gupta	Decay of $^{297}118$ formed in reaction $^{249}\text{Cf}+^{48}\text{Ca}$ using dynamical cluster decay model.	Phys. Rev. C	2015	92, 064303	3.82
160	G Kaur, Rajni and Manoj K Sharma,	Decay of Zr isotopes and related nuclear structure effects using collective clusterization approach.	Phys. Scr. T	2015	166 014013.	1.194
161	Sakshi Gupta, K. Singh,	Dielectric, optical and structural properties of $\text{Bi}_4\text{V}_2-x\text{Sr}_x\text{O}_{11-\delta}$ ($0.05 \leq x \leq 0.20$)	Journal of Physics and Chemistry of Solids	2015	85 , 18- 25.	2.048
162	D.H. Yeon, B.C. Mohanty , S. M. Lee, and Y.S. Cho,	Effect of band-aligned double absorber layers on photovoltaic characteristics of chemical bath deposited PbS/CdS thin film solar cells,	Scientific Reports	2015	5, 14353	4.259
163	Sakshi Gupta, K. Singh,	Effect of dopants ionic radii on dielectric properties of $\text{Bi}_4\text{V}_2-x\text{MExO}_{11-\delta}$ (where $x=0.0$ and 0.15 ; ME=Mg, Ca, Sr and Ba)	Applied Physics A 121 (2015) 1251-1259. (1.694)	2015	121, 1251- 1259	1.455
164	Mahajan, Tarlochan Singh; O.P. Pandey	Effect of Electric and Magnetic Treatments on Germination of Bitter Gourd (Momordica charantia) Seed	Int. J. of Agriculture Biology	2015	17 (2)	0.746
165	Singh, Harjinder; O.P. Pandey	Effect of Extended Milling of Scheelite Ore with Activated Charcoal on Direct Synthesis of Nanotungsten Carbide	Particulate Science and Technology	2015	33(6), 587-592	0.784
166	S Kumar, HC Jeon, TW Kang, J Sekhon, NK Verma , HS Bhatti	Effect of ferromagnetic dopants on laser induced optical parameters of bismuth doped CaS phosphors	Russian Journal of Physical Chemistry A	2015	89 (13), 2482- 2486	0.581
167	P. Jha, K. Singh	Effect of Field Strength and Electronegativity of CaO and MgO on Structural and Optical Properties of $\text{SiO}_2\text{-K}_2\text{O-CaO-MgO}$ Glasses	Silicon	2015	8(3), 437- 442	0.829
168	Satwinder Singh, G. Kalia, K. Singh,	Effect of intermediate oxide (Y_2O_3) on thermal, structural and optical properties of lithium borosilicate glasses	Journal of Molecular Structure	2015	1086 , 239-245.	1.753
169	Sharma, Anju; Kumar, Suresh; Singh, Gurmel; O.P. Pandey	Effect of Particle Size on Wear Behavior of Al-Garnet Composites	Particulate Science and Technology	2015	33(3), 234-239	0.784
170	Kaur, Jagdeep; Sharma, Manoj; O.P. Pandey	Effect of pH on Size of ZnS Nanoparticles and Its Application for Dye Degradation	Particulate Science and Technology	2015	33(2), 184-188	0.784

171	Devender Kumar and K. Singh	Effect of Processing Methods and Die Design Parameters on Green Properties of WC–Co Nano powder Pellets	Materials and Manufacturing Processes	2015	30, 1329-1341.	2.274
172	Singla, Gourav; Singh, K. ; O.P. Pandey	Effect of Processing Variables on WC Nanoparticles Synthesized by Solvothermal Route	Particulate Science and Technology	2015	33(1), 47-52	0.784
173	S. Gupta, K. Singh,	Effect of two different dopants (Mg ²⁺ and Ca ²⁺) and processing parameters on γ -phase stabilization and conductivity of Bi ₄ V ₂ O ₁₁ - δ ,	Ceramics International,	2015	41(8), 9496-9504	2.986
174	Ramneek Kaur & K.K. Raina	Effects of nanoparticle doping on the phase transitional behaviour of ferroelectric liquid crystal Langmuir–Blodgett composite films	Phase Transitions	2015	88, 1213-1224	1.06
175	T. C. Yang, Y. S. Cheng, Y. C. Ju, Y. T. Lin, C. F. Huang, H. C. Lu, S. F. Wang, Puneet Sharma , A. Cheng	Effects of Thickness Ratio of Co to Pt Layer on Magnetic Properties and Microstructure of [Co/Pt] Multilayer Films	IEEE Trans. Magn.	2015	51, 2301904	1.243
176	SUMIT BHARDWAJ, JOGINDER PAUL, SUBHASH CHAND, K.K. RAINA , RAVI KUMAR	Electroactive Phase Induced Bi ₄ Ti ₃ O ₁₂ –Poly(Vinylidene Difluoride) Composites with Improved Dielectric Properties	Journal of ELECTRONIC MATERIALS	2015	44(10), 3710-3723	1.579
177	Y.S. Chen, A. C. Sun, H.Y. Lee, H. C. Lu, S. F. Wang and Puneet Sharma	Enhanced coercivity of HCP Co–Pt alloy thin films on a glass substrate at room temperature for patterned media	J. Magn. Magn. Mater.	2015	391, 12–16	2.63
178	T. H. You, Y. S. Chen, Y. C. Ju, Y. T. Lin, H. C. Lu, S. F. Wang, Puneet Sharma , and An-Cheng Sun	Enhanced Perpendicular Magnetic Anisotropy of Co-Rich Type Co–Pt Film by Inserting Pt Underlayer	IEEE Trans. Magn.	2015	51, 3201804	1.243
179	C Rani, SD Tiwari , D Kumar	Estimation of Particle Concentration in a Nanocomposite Using Magnetization Data	IEEE Transactions on Magnetism	2015	51 (12), 1-5	1.243
180	C Rani, SD Tiwari	Estimation of particle magnetic moment distribution for antiferromagnetic ferrihydrite nanoparticles	Journal of Magnetism and Magnetic Materials	2015	385, 272-276	2.63
181	Brar, Loveleen K. ; Singla, Gourav; O.P. Pandey	Evolution of structural and thermal properties of carbon-coated TaC nanopowder synthesized by single step reduction of Ta-ethoxide	RSC ADVANCES	2015	5(2), 1406-1416	3.108

182	K Kaur, NK Verma	Ferromagnetic behavior of Cd 1–x Ni x S nanorods: a novel study	Journal of Materials Science: Materials in Electronics	2015	26 (11), 8285-8291	2.019
183	A. Kaur, G. Kaur, Manoj K. Sharma,	Fission decay analysis of n-induced reaction using collective clusterization approach.	Nucl. Phys. A	2015	941 152-166.	1.916
184	M S Gautam, A Kaur and Manoj K Sharma	Formation and decay analysis of 98,104Cd* isotopes in 40Ca induced reactions.	Phys. Rev. C	2015	92, 054605	3.82
185	P.K. Jha, O.P. Pandey, K. Singh	FTIR spectral analysis and mechanical properties of sodium phosphate glass-ceramics	Journal of Molecular Structure	2015	1083, 278-283	1.753
186	K Kaur, NK Verma	Hydrothermally synthesized CdS nanoparticles: effect of Fe doping on optical and magnetic properties	Journal of Superconductivity and Novel Magnetism	2015	28 (11), 3317-3322	1.18
187	Mintu Tyagi, Ratnamala Chattarjee and Puneet Sharma	Improved dielectric and magnetic properties of multiferroic BiFeO3–NiFe2O4 nanocomposite thin films	J. Sol-Gel Sci. Technol.	2015	74, 692-697	1.575
188	Y. H. Jo, J. W. Jang, B. C. Mohanty, H. B. Kang, and Y. S. Cho,	Improved photovoltaic and grain boundary characteristics of single elementary target-sputtered Cu2ZnSnSe4 thin films by post sulfurization/selenization process,	J. Phys D	2015	48, 245103.	2.588
189	ParveenKumar, SangeetaSingh, J.K.Juneja, ChandraPrakash, K.K.Raina	Improved properties of BPT ceramics using microwave sintering	Materials Letters	2015	142, 84–86	2.572
190	Arora, Rama; Kumar, Suresh; Singh, Gurmel; O.P. Pandey	Influence of particle size and temperature on the wear properties of rutile-reinforced aluminium metal matrix composite	JOURNAL OF COMPOSITE MATERIALS	2015	49(7), 843-852	1.494
191	Mahajan, Mani; Rajpoot, Shalini; O.P. Pandey	In-situ synthesis of chromium carbide (Cr3C2) nanopowders by chemical-reduction route	Int. J. of Refractory Metals and Hard Metals	2015	50, 113-119	2.155
192	S Kumar, NK Verma	Investigation of the Magnetic and Optical Properties of Wurtzite Fe-Doped ZnS Nanorods	Journal of Electronic Materials	2015	44 (8), 2829-2834	1.579
193	Mintu Tyagi, Mukesh Kumari, Ratnamala Chatterjee and Puneet Sharma	Large magnetoelectric response in modified BNT based ternary piezoelectric [72.5(Bi1/2Na1/2TiO3)-22.5(Bi1/2K1/2TiO3)-5(BiMg1/2Ti1/2O3)]-magnetostrictive (NiFe2O4) particulate (0-3) composites	Appl. Phys. Lett.	2015	106, 202904	3.411

194	I Kaur, NK Verma	Magnetic and electric properties of BFO–NFO nanocomposites	Materials Science in Semiconduct or Processing	2015	33, 32-35	2.359
195	Kaur, Gurbinder; Pickrell, G.; Kumar, V.; O.P. Pandey ; Singh, K. ; Arya, S. K.	Mechanical, dielectric and optical assessment of glass composites prepared using milling technique	Bull. Mater. Sci.	2015	38(4), 1003-1008	0.899
196	Manju Middha, Rishi Kumar & K.K. Raina	Memory effects in chiral nematic liquid crystals doped with functionalised single walled carbon nanotubes	Liquid Crystals	2015	42, 1028–1035	2.661
197	Rishi Kumar & K.K. Raina	Morphological control and switchable photoluminescence responses of silica nanoparticles modified polymer dispersed liquid crystal composite films	Liquid Crystals	2015	42, 119–126	2.661
198	Kumar, Deepak; Sharma, Manoj; O.P. Pandey	Morphology controlled Y ₂ O ₃ :Eu ³⁺ nanophosphors with enhanced photoluminescence properties	J. Luminescence	2015	158, 268-274	2.686
199	J Singh, A Vasishth, NK Verma	Multiferroic Properties of Zn _{1-x} Mg _x O Nanoparticles	Journal of Superconductivity and Novel Magnetism	2015	28 (10), 3069-3074	1.18
200	Singh, Harjinder; O.P. Pandey	Novel process for synthesis of nanocrystalline WC from wolframite ore	Ceramics Int.	2015	41(9), 10481-10487	2.986
201	Raj Kumar , J. A. Lay, and A. Vitturi	Nuclear fusion as a probe for octupole deformation in ²²⁴ Ra	Phys. Rev. C	2015	92, 054604	3.82
202	M. K. Sharma, R. N. Panda, Manoj K. Sharma , S. K. Patra.	Nuclear Structure study of some bubble nuclei in light mass region using mean field formalism.	Chinese Physics C	2015	39 (6), 064102.	5.082
203	S.K. Arya, B.Kaur, G.Kaur, K. Singh	Optical and thermal properties of (70-x) SiO ₂ -xNa ₂ O-15CaO-10Al ₂ O ₃ -5TiO ₂ (10 ≤ x ≤ 25) glasses	Journal of Thermal Analysis and Calorimetry	2015	120, 1163-1171.	1.953
204	G Dhir, P Uniyal , NK Verma	Particle size dependent multiferroic properties of Bi _{0.95} Tb _{0.05} FeO ₃ nanoparticles	Journal of Materials Science: Materials in Electronics	2015	26 (6), 3538-3544	2.019
205	Kaur, Jagdeep; Sharma, Manoj; O.P. Pandey	Photoluminescence and photocatalytic studies of metal ions (Mn and Ni) doped ZnS nanoparticles	Optical Mater.	2015	47, 7-17	2.238
206	Rishi Kumar & K.K. Raina	Polarisation switching and molecular relaxation behaviour of anthraquinone dye dispersed polymer stabilised ferroelectric liquid crystal composites	Liquid Crystals	2015	42,18–23	2.661

207	Sood, Kapil; Singh, K. ; Basu, Suddhasatwa; O.P. Pandey	Preferential occupancy of Ca ²⁺ dopant in La _{1-x} Ca _x InO _{3-δ} (x=0-0.20) perovskite: structural and electrical properties	IONICS	2015	21(10), 2839-2850	2.062
208	M.S. Gautam, Rajni, Manoj K. Sharma	Role of Barrier modification and inelastic surface excitations in sub barrier fusion of 32S+94Zr reaction	Braz. J. of Phys.	2015	46:133–142	1.042
209	Arora, Rama; Kumar, Suresh; Singh, Gurmel; O.P. Pandey	Role of Different Range of Particle Size on Wear Characteristics of Al-Rutile Composites	Particulate Science and Technology	2015	33(3), 229-233	0.784
210	Kumar, Suresh; O.P. Pandey	Role of fine size zircon sand ceramic particle on controlling the cell morphology of aluminum composite foams	J. Manufacturing Practice	2015	20, 172-180	2.322
211	S Kumar, NK Verma	Room temperature investigations on optical and magnetic studies of Co _x Zn _{1-x} nanorods	Journal of Magnetism and Magnetic Materials	2015	374, 548-552	2.63
212	NKV , Sunil Kumar	Room temperature magnetism induced in Co-doped ZnS nanoparticles	Journal of Superconductivity and Novel Magnetism	2015	28 (1), 137-142	1.18
213	Y. H. Jo, B. C. Mohanty , D. H. Yeon, S. M. Lee and Y. S. Cho,	Single Elementary Target-Sputtered Cu ₂ ZnSnSe ₄ Thin Film Solar Cells,	Solar Energy Mater. Solar Cells	2015	132, 136-141	4.784
214	G Dhir, P Uniyal, NK Verma	Sol-gel synthesized BiFeO ₃ nanoparticles: Enhanced magnetoelectric coupling with reduced particle size	Journal of Magnetism and Magnetic Materials	2015	394, 372-378	2.63
215	Meenakshi Batra, Alka Upadhyay	Strong Decay widths and coupling constant of recent charm mesons states	Eur. Phys. J. C	2015	75, 319	5.331
216	SK Arya, K. Singh ,	Structural and optical properties of 30Li ₂ O–55B ₂ O ₃ –5ZnO–xTiO ₂ –(10-x)V ₂ O ₅ , (0 ≤ x ≤ 10) glasses	Journal of Non-Crystalline Solids	2015	414, 51-58	2.124
217	Kaur, Jagdeep; Sharma, Manoj; O.P. Pandey	Structural and optical studies of undoped and copper doped zinc sulphide nanoparticles for photocatalytic application	Super lattice and Microstructure	2015	77, 35-53	2.123
218	Dipti, J. K. Juneja, Sangeeta Singh, K. K. Raina , R. K. Kotnala & Chandra Prakash	Structural Dielectric and Magnetolectric Properties of xCo _{0.8} Ni _{0.2} Fe ₂ O ₄ ·xPbZr _{0.55} Ti _{0.45} O ₃ Composites	Ferroelectrics Letters	2015	42, 97–106	0.267

219	M. Mahajan, K. Singh , OP Pandey	Structural Investigation of Catalytically Grown Carbon Nanotubes	Materials and Manufacturing Processes	2015	31(8) 989-994.	2.274
220	Sood, Kapil; Singh, K. ; O.P. Pandey	Structural, Conductivity, and Dielectric Relaxation Studies of La _{0.9} Ba _{0.1} GaO ₃ -delta System	Particulate Science and Technology	2015	33(2), 113-118	0.784
221	Samiksha Verma, S. K. Dhawan, Andrea Paesano Jr, O.P. Pandey and Puneet Sharma	Structural, magnetic and microwave properties of barium hexaferrite thick films with different Fe/Ba mole ratio	J. Magn. Magn. Mater.	2015	396, 308–312	2.63
222	Mintu Tyagi, Ratnamala Chatterjee and Puneet Sharma	Structural, optical and ferroelectric behavior of pure BiFeO ₃ thin films synthesized by the sol–gel method	J Mater Sci: Mater Electron	2015	26,1987-1992	2.019
223	S Kumar, NK Verma	Structural, optical and magnetic investigations on Fe-doped ZnS nanoparticles	Journal of Materials Science: Materials in Electronics	2015	26 (5), 2754-2759	2.019
224	Thakur, Samita; O.P. Pandey ; Singh, Kulvir	Structural, Thermal, and Electrical Study of Bi _{0.5} Sr _{0.5} MnO ₃	Particulate Science and Technology	2015	33(2), 178-183	0.784
225	Jha, Paramjyot Kumar; O.P. Pandey ; Singh, K.	Structure and crystallization kinetics of Li ₂ O modified sodium-phosphate glasses	JOURNAL OF MOLECULAR STRUCTURE	2015	1094, 174-182	1.753
226	M. K. Sharma, R. N. Panda, Manoj K. Sharma , S. K. Patra.	Study of reaction cross section of light mass nuclei using Glauber formalisms.	Braz J Phys.	2015	45, 138-146	1.042
227	L Khanna, NK Verma	Study on novel, superparamagnetic and biocompatible PEG/KFeO ₂ nanocomposite	Journal of Applied Biomedicine	2015	13 (1), 23-32	1.302
228	Mahajan, Mani; Lalla, N. P.; Singh, K. ; O.P. Pandey	Synthesis and photoluminescence, properties of in-situ synthesized core-shell (m-VC@C) nanocomposites	Mater Chem Phys	2015	160, 48-58	2.084
229	Singla, Gourav; Singh, K. ; O.P. Pandey	Synthesis of carbon coated tungsten carbide nano powder using hexane as carbon source and its structural, thermal and electrocatalytic properties	Int. J. Hydrogen Energy	2015	40(16), 5628-5637	3.582
230	Singh, Amandeep; Kaur, Ramanjot; O.P. Pandey ; Wei, Xueyong; Sharma, Manoj	Synthesis of fluorescent core-shell nanomaterials and strategies to generate white light	J. Appl. Phys.	2015	118(4), 044305	2.068

231	Mahajan, Mani; Singla, Gourav; Singh, K.; O.P. Pandey	Synthesis of grape-like carbon nanospheres and their application as photocatalyst and electrocatalyst	J. Solid State Chem.	2015	232, 108-117	2.299
232	C Khurana, OP Pandey, BN Chudasama	Synthesis of visible light-responsive cobalt-doped TiO ₂ nanoparticles with tunable optical band gap	Journal of Sol-Gel Science & Technology	2015	75,424-435	1.53
233	S.M. Lee, D.H. Yeon, B.C. Mohanty , and Y.S. Cho,	Tensile Stress-Dependent Fracture Behavior and Its Influences on Photovoltaic Characteristics in Flexible PbS/CdS Thin-Film Solar Cells,	ACS Appl. Mater. Interfaces	2015	7, 4573-4578	7.504
234	S.K. Arya, K. Singh ,	Thermal and kinetic parameters of 30Li ₂ O–55B ₂ O ₃ –5ZnO–xTiO ₂ –(10–x)V ₂ O ₅ (0 ≤ x ≤ 10) glasses	Journal of Thermal Analysis and calorimetry	2015	122, 189-195	1.953
235	Brar, Loveleen K.; Singla, Gourav; Kaur, Navjot; O.P. Pandey	Thermal stability and structural properties of Ta nanopowder synthesized via simultaneous reduction of Ta ₂ O ₅ by hydrogen and carbon	J. Thermal Analysis and Calorimetry	2015	119(1), 175-182	1.953
236	Sakshi Gupta and K. Singh	γ-Phase stabilized Bi ₄ BaxV ₂ – xO ₁₁ – δ (0.0 ≤ x ≤ 0.20): Structural, thermal and conducting properties	Solid state ionics	2015	278, 233-238.	2.112
237	Thakur, Samita; O.P. Pandey; Singh, K.	A comparative structural, thermal and electrical study of Ca ²⁺ , Sr ²⁺ substituted BiMnO ₃	Solid state ionics	2014	268, 23-30	2.354
238	G. Kaur, O.P. Pandey, K. Singh , D. Homa, B. Scott, G. Pickrell	A review of bioactive glasses: Their structure, properties, fabrication and apatite formation	J. Biomedical Materials Research Part A	2014	102 (1) 254-274	2.84
239	M. Kaur, M K Sharma, Manoj K. Sharma	Analysis of fragment distribution and associated effects in ¹² C, ¹³ C induced reactions	Int. J. Mod. Phys. E	2014	23 (5) 1450030	1.597
240	C Khurana, AK Vala, N Andhariya, OP Pandey, BN Chudasama	Antibacterial activities of silver nanoparticles and antibiotic-adsorbed silver nanoparticles against biorecycling microbes	Environmental Science: Processes Impacts	2014	16, 2191–2198	2.17
241	C Khurana, AK Vala, N Andhariya, OP Pandey, BN Chudasama	Antibacterial activity of silver: the role of hydrodynamic particle size at nanoscale	Journal of Biomedical Materials Research Part A	2014	102 (10), 3361-3368	3.361
242	L Khanna, NK Verma	Biocompatibility and superparamagnetism in novel silica/CaFe ₂ O ₄ nanocomposite	Materials Letters	2014	128, 376-379	2.572
243	M Kaur, NK Verma	CaCO ₃ /TiO ₂ nanoparticles based dye sensitized solar cell	Journal of Materials Science & Technology	2014	30 (4), 328-334	2.764

244	Samiksha Verma, Puneet Sharma, O.P. Pandey , Andrea Paesano Jr., An-Cheng Sun	Comparison of structural and magnetic properties of La ³⁺ substituted BaFe ₁₂ O ₁₉ prepared by different substitution methods	Physica B	2014	448, 57–59	1.386
245	J Singh, NK Verma	Correlation between structure and ferromagnetism in cobalt-doped CdSe nanorods	Journal of Superconductivity and Novel Magnetism	2014	27 (10), 2371–2377	1.18
246	G. Kaur, V. Kumar, K. Singh, O.P. Pandey , G. Pickrell	Correlation of glass stability (GS) and heating rates using inflection point temperature	Physics and chemistry of glasses: European Journal of glass Science and Technology part B	2014	55, 57–62	0.76
247	K. Sandhu, Manoj K. Sharma , A. Kaur, R. K. Gupta	Decay and related stability aspects of ²⁶⁶ Rf nucleus formed in ¹⁸ O+ ²⁴⁸ Cm reaction	Phys. Rev. C	2014	90, 034610	3.82
248	Kirandeep Sandhu and Manoj K. Sharma	Decay Mechanism of ^{290,292} 114 Superheavy Nuclei Formed in ⁴⁸ Ca-Induced Reactions.	Braz J Phys	2014	44: 64–72	1.042
249	Sumit Bhardwaj, Joginder Paul, K.K.Raina , N.S.Thakur, Ravi Kumar	Dielectric modulus and magneto capacitance behavior of Bi _{3.7} Sm _{0.3} Ti _{2.7} Fe _{0.3} O ₁₂ multiferroic	Physica B	2014	448, 194–198	1.386
250	Rekha Rani, Sangeeta Singh, J. K. Juneja, K. K. Raina , Chandra Prakash	Dielectric, ferroelectric and ferromagnetic properties of x Ni _{0.8} Zn _{0.2} Fe ₂ O ₄ -(1-x) Pb _{0.99} La _{0.02} Zr _{0.65} Ti _{0.35} O ₃ composites	Journal of Electroceramics	2014	32, 141–145	1.238
251	Manoj K. Sharma and G. Kaur.	Dynamics of light, heavy and super heavy nuclear systems formed in heavy ion collisions	Pramana J. Phys	2014	82 (5)	0.692
252	K. Sandhu, G. Kaur, Manoj K. Sharma	Dynamics of ^{40,48} Ca+ ²³⁸ U→ ^{278,286} 112* reactions across the Coulomb barrier using dynamical cluster decay model.	Nuclear Physics A	2014	921 114–130.	1.916
253	S. Thakur, O.P. Pandey, K. Singh	Effect of Ca substitution on structural, magnetic and dielectric properties of BiFeO ₃	Phase Transition,	2014	87(6), 527–540.	1.04
254	Kumar, Deepak; Sharma, Manoj; O.P. Pandey	Effect of co-doping metal ions (Li ⁺ , Na ⁺ and K ⁺) on the structural and photoluminescent properties of nano-sized Y ₂ O ₃ :Eu ³⁺ synthesized by co-precipitation method	OPTICAL MATERIALS	2014	36(7), 1131–1138	2.238

255	Supreet, R. Pratibha, S. Kumar & K.K. Raina	Effect of dispersion of gold nanoparticles on the optical and electrical properties of discotic liquid crystal	Liquid Crystals	2014	41, 933-939	2.661
256	Satwinder Singh, K. Singh,	Effect of in-situ reduction of Fe ³⁺ on physical, structural and optical properties of calcium sodium silicate glasses and glass ceramics	J. Non-crystalline solids	2014	386, 100-104	1.71
257	J Singh, S Kumar, NK Verma	Effect of Ni-doping concentration on structural, optical and magnetic properties of CdSe nanorods	Materials Science in Semiconductor or Processing	2014	26, 1-6	2.359
258	S Kumar, NK Verma	Effect of Ni-doping on optical and magnetic properties of solvothermally synthesized ZnS wurtzite nanorods	Journal of Materials Science: Materials in Electronics	2014	25 (2), 785-790	2.019
259	G Dhir, P Uniyal, NK Verma	Effect of particle size on magnetic and dielectric properties of nanoscale Dy-doped BiFeO ₃	Journal of Superconductivity and Novel Magnetism	2014	27 (6), 1569-1577	1.18
260	G Dhir, P Uniyal, NK Verma	Effect of particle size on multiferroism of barium-doped bismuth ferrite nanoparticles	Materials Science in Semiconductor or Processing	2014	27, 611-618	2.359
261	Ravi Kumar Shukla & Kuldeep Kumar Raina	Effect of solvent polarity on the self-assembly and dielectric dynamics of non-aqueous lyotropic liquid crystalline phases	Liquid Crystals	2014	41, 701-706	2.661
262	Kumar, Vishal; Kaur, Gurbinder; Lu, Kathy; O.P. Pandey.; Singh, Kulvir	Effect of Thermal Treatment on Chemical Interaction Between Yttrium Borosilicate Glass Sealants and YSZ for Planar Solid Oxide Fuel Cells	Int. J. Appl. Glass Sci.	2014	5(4), 410-420	1.79
263	Gourav Singla, K. Singh	Effect of TiO ₂ on the photocatalytic properties of bismuth oxide	Environmental Technology	2014	35, 1520-1524.	1.19
264	Rupanjit Kaur, S. Thakur, K. Singh	Effect of two different sites substitution on structural and optical properties of Bi ₄ V ₂ O _{11-δ}	Physica B: Condensed Matter	2014	440, 78-82.	1.386
265	Mintu Tyagi, Mukesh Kumari, Ratnamala Chatterjee, An-Cheng Sun and Puneet Sharma	Electrical and Magnetic Properties of Multiferroic (1-x) BiFeO ₃ -x CoFe ₂ O ₄ nanocomposite thin films derived by Sol-gel process	IEEE Trans. Magn.	2014	1, 2500704	1.243
266	Rishi Kumar & K.K. Raina	Electrically modulated fluorescence in optically active polymer stabilised cholesteric liquid crystal shutter	Liquid Crystals	2014	41, 228-233	2.661

267	Kaur, Gurbinder; O.P. Pandey ; Singh, K	Electronic microscopic, thermal and electrical properties of Bi ₂ V _{1-x} Ti _x O _{5.5-delta} (0.05 ≤ x ≤ 0.20) oxide ion conductors	Ind. J. Pure & Appl. Phys.	2014	52(4), 262-270	0.521
268	NK Verma , I Kaur, K Kaur, GS Lotey	Enhanced Efficiency of Au-Deposited BiFeO ₃ Nanoparticles Based Dye-Sensitized Solar Cells	Advanced Materials Research	2014	856, 184-187	
269	Rishi Kumar & K.K. Raina	Enhanced ordering in polymer stabilised ferroelectric liquid crystal guest host composites evidence by polarised fluorescence spectroscopy	Liquid Crystals	2014	41, 694-700	2.661
270	Raj Kumar , J. A. Lay, and A. Vitturi	Enhanced sub-barrier fusion for proton halo nuclei	Phys. Rev. C	2014	89, 027601	3.82
271	Dipti, J.K. Juneja, Sangeeta Singh, K.K. Raina , Chandra Prakash	Enhancement in magnetoelectric coupling in PZT based composites	Ceramics International	2014	41(4), 6108-6112	2.986
272	J Singh, S Kumar, NK Verma	Enhancement of room temperature ferromagnetism in Cd _{1-x} Ni _x Se nanoparticles	Journal of Materials Science: Materials in Electronics	2014	25 (5), 2267-2272	2.019
273	Raj Kumar and D. Jain	Entrance channel effect with stable and radioactive beams using dynamical cluster decay model	Nucl. Phys. A	2014	929, 169-183	1.916
274	Kumar, Sanjay; Sharma, S. K.; O.P. Pandey	Estimation of volume dependence of Grüneisen parameter for NaCl and epsilon-Fe	Ind. J. Pure & Appl. Phys.	2014	52(8), 541-544	0.521
275	Alka Upadhyay , J.P. Singh	Eta prime Gluonic contribution to the nucleon self-energy in an effective theory	Advance in High energy Physics	2014	841703	1.74
276	B. B Singh, S Kumar, Manoj K Sharma , S K Patra	Extensions of Natural Radioactivity to 4th-Type and of the Periodic Table to Super-heavy Nuclei:	J. of Nucl. Phys. MSRA	2014	1 (2), 133-143	0.86
277	Ravi Kumar Shukla, Kuldeep Kumar Raina & Wolfgang Haase	Fast switching response and dielectric behaviour of fullerene ferroelectric liquid crystal nanocolloids	Liquid Crystals	2014	41, 1726-1732	2.661
278	S Kumar, NK Verma	Ferromagnetic and weak superparamagnetic like behavior of Ni-doped ZnS nanocrystals synthesized by reflux method	Journal of Materials Science: Materials in Electronics	2014	25 (2), 1132-1137	2.019
279	K Kaur, GS Lotey, NK Verma	Ferromagnetism in Gd-doped CdS dilute magnetic semiconducting nanorods	Journal of Materials Science: Materials in Electronics	2014	25 (1), 311-316	2.019
280	Rajni, Raj Kumar , and M. K. Sharma	Formation and decay of ²⁰⁰ Pb* using different incoming channels	Phys. Rev. C	2014	90, 044604	3.82

281	Gurvinder Kaur and Manoj K. Sharma	Fragment mass identification and related aspects in the decay of $^{40}\text{Ca}^*$ and $^{39}\text{K}^*$ nuclei.	Int. J. of Mod. Phys. E	2014	23 (10) 1450063.	1.597
282	Meenakshi Batra, Alka Upadhyay	Importance of Non-Perturbative QCD Parameters for Bottom Mesons,	Advance in High energy Physics	2014	619783	1.74
283	Dipti, Parveen Kumar, J.K Juneja, Sangeeta Singh, K.K. Raina , Chandra Prakash	Improved dielectric and magnetic Properties in modified lithium-ferrites	Ceramics International	2014	41(2), 3293-3297	2.986
284	J. S. Kim, B. C. Mohanty , C. S. Han, S. J. Han, G. H. Ha, L. Lin, Y. S. Cho,	In situ magnetic field-assisted low temperature atmospheric growth of GaN nanowires via the vapor-liquid-solid mechanism,	ACS Appl. Mater. Interfaces	2014	6, 116-121	7.504
285	Thakur, Samita; O.P. Pandey ; Singh, K.	Influence of Ca^{2+} substitution on thermal, structural, and conductivity behavior of $\text{Bi}_{1-x}\text{Ca}_x\text{FeO}_{3-y}$ (0.40 a parts per thousand currency sign x a parts per thousand currency sign 0.55)	J. Thermal Analysis and Calorimetry	2014	118(1), 255-262	1.953
286	Ramneek Kaur & K.K. Raina	Influence of single wall carbon nanotubes on Langmuir Blodgett films of ferroelectric liquid crystals as studied by atomic force microscopy	Liquid Crystals	2014	41, 1065–1072	2.661
287	Kumar, V.; O.P. Pandey ; Singh, K. ; Lu, K.	Interaction Study of Yttria-Based Glasses with High-Temperature Electrolyte for SOFC	Fuel Cells	2014	14(4), 635-644	1.706
288	Mahajan, Tarlochan Singh; O.P. Pandey	Magnetic-time model at off-season germination	Int. Agrophys.	2014	28(1), 57-62	0.967
289	Neeraj, K.K.Raina	Multi wall carbon nanotubes doped ferro electric liquid crystal composites: A study of modified electrical behavior	Physica B	2014	434,1–6	1.386
290	P Uniyal , GS Lotey, A Gautam, NK Verma , KL Yadav	Multiferroic Properties of $(\text{Bi}_{0.9}\text{Gd}_{0.1}\text{FeO})_{1-x}(\text{BaTiO}_3)_x$ Ceramics	Journal of Superconductivity and Novel Magnetism	2014	27 (2), 569-574	1.18
291	Satwinder Singh and K. Singh ,	Nanocrystalline glass ceramics: structural, physical and optical properties	J. Molecular Structure	2014	1081,211-216	1.59
292	G. Sawhney , Manoj K. Sharma and R. K. Gupta J. Phys. G:	Neutron-halo structure of light nuclei studied with effects of deformations and orientations included.	Nucl. Part. Phys.	2014	41 (5), 055101	NA
293	Kumar, Akshay; Singh, K. ; O.P. Pandey	One Step Synthesis and Growth Mechanism of Carbon Nanotubes	J. Mater. Sci. & Tech.	2014	30(2), 112-116	2.764
294	K Kaur, GS Lotey, NK Verma	Optical and magnetic properties of Fe-doped CdS dilute magnetic semiconducting nanorods	Journal of Materials Science: Materials in Electronics	2014	25 (6), 2605-2610	2.019

295	Kaur, Gurbinder; Pickrell, Gary; Kumar, Vishal; O.P. Pandey; Singh, Kulvir ; Homa, Daniel	Optical, mechanical and TEM assessment of titania-doped Bi ₂ V _{1-x} Ti _x O _{5.5-delta} bismuth vanadate oxides	Bull. Mater. Sci.	2014	37(7), 1647-1656	0.899
296	Sumit Bhardwaj, Joginder Paul, Subhash Chand, K. K. Raina , Ravi Kumar	Oxygen vacancy induced dielectric relaxation studies in Bi ₄₂ xLaxTi ₃ O ₁₂ (x = 0.0, 0.3, 0.7, 1.0) ceramics	J Mater Sci: Mater Electron	2014	25, 4568–4576	2.019
297	Singla, Pooja; Sharma, Manoj; O.P. Pandey; Singh, K.	Photocatalytic degradation of azo dyes using Zn-doped and undoped TiO ₂ nanoparticles	Appl Phys. A	2014	116(1), 371-378	1.455
298	Mittal, Manish; Sharma, Manoj; O.P. Pandey	Photocatalytic Studies of Crystal Violet Dye Using Mn Doped and PVP Capped ZnO Nanoparticles	J. Nanosci Nanotech	2014	14(4), 2725-2733	1.483
299	Niyti, Manoj K. Sharma , K. Sandhu, R. K. Gupta.	Probing Nuclear Matter at the Extremes through application of Dynamical Cluster-decay Model to Superheavy Nuclei	Int. Rev. of Phys. IREPHY	2014	8 (3), 86.	0.9
300	Khushboo, Divya Jayoti, Praveen Malik, Ashok Chaudhary, Rohit Mehra & K.K. Raina	Properties of Ferroelectric Liquid Crystal Multiwall Carbon Nanotube Doped Composite	Integrated Ferroelectrics	2014	158, 123-130	0.457
301	M. Tyagi, Mukesh Kumari, R. Chatterjee and Puneet Sharma	Raman scattering spectra, magnetic and ferroelectric properties of BiFeO ₃ -CoFe ₂ O ₄ nano-composite thin films structure	Physica B.	2014	448, 128–131	1.386
302	B. C. Mohanty , D. H. Yeon, J. H. Yun, K. H. Yoon and Y. S. Cho,	RF power dependence of refractive index of room temperature sputtered ZnO:Al thin films,	Appl. Phys. A	2014	115, 347-351	1.455
303	G. Sawhney , K. Sandhu, Manoj K. Sharma , R. K. Gupta.	Role of nuclear deformations and proximity interactions in heavy particle radioactivity.	Euro. Phys. J. A	2014	50 (11), 175	2.833
304	G. Kaur, N. Grover, K. Sandhu, Manoj K. Sharma.	Role of rotational energy and deformations in the dynamics of ⁶ Li+ ⁹⁰ Zr reaction.	Nuclear Physics A	2014	927 232–248.	1.916
305	Thakur, Samita; O.P. Pandey; Singh, K.	Role of Sr ²⁺ substitution on structural, thermal and conducting behavior of Bi _{1-x} Sr _x FeO ₃ (0.40 ≤ x ≤ 0.55)	Ceramics Int.	2014	40(10), 16371-16379	2.986
306	Kaur, Gurbinder; O.P. Pandey .; Singh, Kulvir	Self-Healing Behavior of Barium-Lanthanum-Borosilicate Glass and Its Reactivity with Different Electrolytes for SOFC Applications	Int. J. Appl. Ceramics Tech.	2014	11(1), 136-145	1.048
307	Soumendu Jana , Ajitpal Singh, K. Porsezian, T. Mithun	Self-trapped elliptical super-Gaussian beam in cubic–quintic media	Optics Communications	2014	332, 311-320	1.45
308	P Kaur, BN Chudasama	Single step synthesis of pluronic stabilized IR responsive gold nanoplates	RSC Advances	2014	4,36006–360112014	3.84

309	Meenakshi Batra, Alka Upadhyay	Strange and non-strange sea quark-gluon effects in nucleons	Nuclear Physics A	2014	922, 126–139	1.916
310	Ravi Kumar Shukla & Kuldeep Kumar Raina	Structural and dielectric behaviour of non aqueous lyotropic mixtures influence of amphiphile chain lengths and counter ions	Liquid Crystals	2014	41, 1090–1096	2.661
311	Singh, Kapil Sood K.; O.P. Pandey	Structural and electrical behavior of Ba-doped LaGaO ₃ composite electrolyte	J. Renewable and Sustainable Energy	2014	6(6), 063112	1.135
312	Mahajan, Mani; Singh, K.; O.P. Pandey	Structural and growth kinetics of in-situ reduced V ₂ O ₅	Int. J. Refractory metals and Hard Metals	2014	46, 90-95	2.155
313	Thakur, Samita; O.P. Pandey; Singh, K.	Structural and optical properties of Bi(1-x)A(x)FeO(3) (A = Sr, Ca; 0.40 ≤ x ≤ 0.55)	J. Molecular Structure	2014	1074, 186-192	1.753
314	S. Thakur, M. Devi, K. Singh	Structural and optical properties of La and Gd substituted Bi _{4- x} M _x V ₂ O _{11-δ} (0.1 ≤ x ≤ 0.3)	Ionics	2014	20 (1)73 - 81.	1.83
315	Sakshi Gupta, K. Singh	Structural and optical properties of quenched and heat-treated Bi ₄ V _{2- x} Mg _x O _{11-δ} (0.0 ≤ x ≤ 0.20)	Ceramics International	2014	40(9) (2014) 14801-14808.	2.986
316	Singla, Gourav; Singh, K.; O.P. Pandey	Structural and thermal analysis of in situ synthesized C-WC nanocomposites	Ceramic Int.	2014	40(4), 5157-5164	2.986
317	Kaur, Ravneet; Singh, Surinder; O.P. Pandey	Structural variation in gamma ray irradiated PbO-Na ₂ O-B ₂ O ₃ -SiO ₂ glasses	Solid State Comm.	2014	188, 40-44	1.554
318	Parveen Kumar, Pratibha Singh, J.K. Juneja, K.K. Raina , R.P. Pant, Chandra Prakash, Sangeeta Singh	Structural, dielectric and ferroelectric properties of PLZFNT ceramics	Journal of Alloys and Compounds	2014	601, 207–211	3.133
319	K Kaur, GS Lotey, NK Verma	Structural, magnetic, dielectric and magnetodielectric properties of Gd-doped CdS nanorods	Materials Science in Semiconduct or Processing	2014	19, 6-10	2.359
320	J Singh, NK Verma	Structural, optical and magnetic properties of cobalt-doped CdSe nanoparticles	Bulletin of Materials Science	2014	37 (3), 541-547	0.899
321	Verma, Samiksha; Sharma, Puneet; O.P. Pandey ; Paesano, Andrea, Jr.; Sun, An-Cheng	Structure and Magnetic Properties of Ba _{1-x} LaxFe ₁₂ O ₁₉ Prepared by Ba _{1-x} LaxFe ₂ O ₄	IEEE Trans. Magn.	2014	50 (1)	1.243

322	Panwar, Ranvir Singh; Kumar, Suresh; Pandey, Ratandeep; O.P. Pandey	Study of Non-lubricated Wear of the Al-Si Alloy Composite Reinforced with Different Ratios of Coarse and Fine Size Zircon Sand Particles at Different Ambient Temperatures	Tribology Letters	2014	55(1), 83-92	
323	Kapil Sood, K. Singh , O.P. Pandey	Study of the Effect on Ionic Conductivity and Structural Morphology of the Sr doped Lanthanum Gallate Solid Electrolyte	Solid State Ionics	2014	https://doi.org/10.1142/9789814415040_0050	2.354
324	GS Lotey, NK Verma	Synthesis and characterization of BiFeO ₃ nanowires and their applications in dye-sensitized solar cells	Materials Science in Semiconductor or Processing	2014	21, 206-211	2.359
325	L Khanna, NK Verma	Synthesis, characterization and biocompatibility of potassium ferrite nanoparticles	Journal of Materials Science & Technology	2014	30 (1), 30-36	2.764
326	Kaur, Jagdeep; Sharma, Manoj; O.P. Pandey	Synthesis, characterization, photocatalytic and reusability studies of capped ZnS nanoparticles	Bull. Mater. Sci.	2014	37(4), 931-940	0.899
327	D. Jain, M. K. Sharma , Rajni, Raj Kumar , and R. K. Gupta	Systematic analysis of hot Yb* isotopes using energy density formalism	Eur. Phys. J. A	2014	50, 155	2.833
328	M. Kaur and Manoj K Sharma ,	Systematics of fusion evaporation in 58Ni+54Fe->112Xe reaction around the Coulomb barrier.	Euro J. of Phys A	2014	50 (3), 61	2.833
329	Kaur, Ravneet; Singh, Surinder; O.P. Pandey	UV-vis spectroscopic studies of gamma irradiated lead sodium borosilicate glasses	J. Molecular Structure	2014	1060, 251-255	1.753
330	Mittal, Manish; Sharma, Manoj; O.P. Pandey	UV-Visible light induced photocatalytic studies of Cu doped ZnO nanoparticles prepared by co-precipitation method	Solar Energy	2014	110, 386-397	4.018
331	Kaur, Ravneet; Singh, Surinder; O.P. Pandey	A Comparison of Modifications Induced by Li ³⁺ and Ag ¹⁴⁺ Ion Beam in Spectroscopic Properties of Bismuth Alumino-Borosilicate Glass Thin Films	J. Spectroscopy	2013	391428, 1-11	0.84
332	Chandni ; Andhariya, Nidhi; O.P. Pandey ; Chudasama , Bhupendra	A growth kinetic study of ultrafine monodispersed silver nanoparticles	RSC Advances	2013	3(4), 1127-1136	3.108
333	Singh, Harjinder; O.P. Pandey	A Novel Approach for Direct Synthesis of Nanocrystalline Tungsten Carbide from Milled Scheelite Ore	Metallurgical and Materials Trans B	2013	44(6), 1428-1434	1.642

334	Kaur, Ravneet; Singh, Surinder; O.P. Pandey	Absorption spectroscopic studies on gamma irradiated bismuth borosilicate glasses	J. Molecular Structure	2013	1049, 386-391	1.753
335	Bansod, Babankumar S.; O.P. Pandey	An application of PCA and fuzzy C-means to delineate management zones and variability analysis of soil	Eurasian Soil Sci.	2013	46(5), 556-564	0.576
336	Panwar, Ranvir Singh; O.P. Pandey	Analysis of wear track and debris of stir cast LM13/Zr composite at elevated temperatures	Mater. Characterization	2013	75, 200-213	2.714
337	Bhupinder Kaur, K. Singh, O.P. Pandey	Corrosion study of SiO ₂ -CaO-Al ₂ O ₃ -Na ₂ O-TiO ₂ glass coating on the low carbon steel	Surface Eng.	2013	29, 479-483	1.51
338	Kaur, B.; Singh, K.; O.P. Pandey	Corrosion study of SiO ₂ -CaO-Al ₂ O ₃ -Na ₂ O-TiO ₂ glass coating on steel	Surface Eng.	2013	29(6), 479-483	1.347
339	Gurvinder Kaur and Manoj K. Sharma.	Decay of 150,158Tb* nuclear systems formed in loosely bound 6Li-induced reactions.	Phys. Rev. C	2013	87, 44601	3.82
340	M. Batra, A. Upadhyay	Detailed Balance and Spin Content of Λ using Statistical Model	IJMPA	2013	28 (15), 1350062	1.699
341	Gourav Singla, K. Singh,	Dielectric properties of Ti substituted Bi _{2-x} Ti _x O _{3+x/2} ceramics	Ceramic International	2013	39(2) 1785-1792	2.08
342	R Rani, JK Juneja, S Singh, KK Raina, C Prakash,	Dielectric, ferroelectric, magnetic and magnetoelectric properties of 0.1Ni _{0.8} Zn _{0.2} Fe ₂ O ₄ -0.9Pb _{1-3x/2} Sm _x Zr _{0.65} Ti _{0.35} O ₃ magnetoelectric composites	Ceramics International	2013	39 (7), 7845-7851	2.986
343	S Kumar, NK Verma, ML Singla	Diffuse reflectance and reflective flexible coatings of capped ZnS nanoparticles	Materials Chemistry and Physics	2013	142 (2-3), 734-739	2.084
344	Singh, Harjinder; O.P. Pandey	Direct synthesis of nanocrystalline tungsten carbide from scheelite ore by solid state reaction method	CERAMICS INTERNATIONAL	2013	39(1), 785-790	2.986
345	G. Kaur, D. Jain, R. Kumar and Manoj K Sharma	Dynamics of 66As* formed in exotic proton halo 8B induced reaction at near barrier energies.	Nucl. Phys. A	2013	916, 260-274.	1.916
346	D. Jain. R. Kumar and Manoj K Sharma	Effect of deformation and orientation on interaction barrier and fusion cross-sections using various proximity potentials.	Nucl. Phys. A	2013	915, 106-124	1.916
347	Kumar, Suresh; Panwar, Ranvir Singh; O.P. Pandey	Effect of dual reinforced ceramic particles on high temperature tribological properties of aluminum composites	Ceramics Int.	2013	39(6), 6333-6342	2.986
348	Kumar, Suresh; Pandey, Ratandeep; Panwar, Ranvir Singh; O.P. Pandey	Effect of Particle Size on Wear of Particulate Reinforced Aluminum Alloy Composites at Elevated Temperatures	J. Mater Engg. & Performance	2013	22(11), 3550-3560	1.331

349	Kaur, Jagdeep; Sharma, Manoj; O.P. Pandey	Effect of pH on Photocatalytic Activity of Capped ZnS Nanoparticles	J. Nanosci Nanotech	2013	13(7), 4861-4871	1.483
350	P Kumar, JK Juneja, C Prakash, , KK Raina , S Singh	Effect of Sm on dielectric, ferroelectric and piezoelectric properties of BPTNZ system	Physica B: Condensed Matter	2013	426, 112-117	1.386
351	R. Kaur, S. Singh. K. Singh and O.P. Pandey	Effect of swift heavy ions on structural and optical properties of bismuth based alumino-borosilicate glasses	Radiation Physics and Chemistry	2013	86, 23-30	1.19
352	RK Shukla, KK Raina	Effect of transition metal salt additive on the structural packing and thermal stability of the non-aqueous lyotropic mesophases	Liquid Crystals	2013	40 (11), 1581-1585	1.959
353	O.H. Kwon, B.C. Mohanty , D.H. Yeon, J.S. Yeo, I.H. Cho, K.H. Lee and Y.S. Cho,	Effective Laser Sealing Enabled by Glass Thick Films Containing Carbon Black/Carbon Nanotube	J. Am. Ceram. Soc.	2013	96, 1113-1117	2.841
354	MK Paul, R Kumar, N Chakraborty, KK Raina , NVS Rao	Electro-optic and molecular relaxation behaviour of fluoro substituted achiral unsymmetrical four-ring bent-core mesogen	Liquid Crystals	2013	41 (5), 635-641	1.959
355	R Singh, KK Raina	Electro-optical studies in a ferroelectric liquid crystal mixture	International Journal of Modern Physics b	2013	27 (19), art. no. 1350038	1.006
356	Supreet, S Kumar, KK Raina , R Pratibha	Enhanced stability of the columnar matrix in a discotic liquid crystal by insertion of ZnO nanoparticles	Liquid Crystals	2013	40 (2), 228-236	1.959
357	J Singh, NK Verma	Ferromagnetism in Fe-doped CdSe nanorods prepared by solvothermal route	Journal of Materials Science: Materials in Electronics	2013	24 (11), 4464-4470	2.019
358	N Andhariya, RV Upadhya, RV Mehta, BN Chudasama	Folic acid conjugated magnetic drug delivery system for controlled release of doxorubicin	Journal of Nanoparticle Research	2013	15, 1416-9	2.175
359	G. Kaur, D. Jain, Raj Kumar , and M. K. Sharma	Formation and decay cross sections of $^{66}\text{As}^*$ formed in an exotic proton-halo 8B induced reaction	Nucl. Phys. A	2013	916, 260-274	1.916
360	R. Kumar, K. Sandhu, Manoj K. Sharma and R.K. Gupta	Fusion-evaporation residue and α -decay chains of superheavy element Z=115 formed in $^{243}\text{Am}+^{48}\text{Ca}$ reaction using dynamical cluster decay model.	Phys. Rev. C	2013	87, 054610	3.82
361	Kaur, Ravneet; Singh, Surinder; O.P. Pandey	Gamma ray irradiation effects on the optical properties of BaO-Na ₂ O-B ₂ O ₃ -SiO ₂ glasses	J. Molecular Structure	2013	1048, 78-82	1.753

362	GS Lotey, NK Verma	Gd-doped BiFeO ₃ nanoparticles– A novel material for highly efficient dye-sensitized solar cells	Chemical Physics Letters	2013	574, 71- 77	1.815
363	Kaur, Kamalpreet; O.P. Pandey	High Temperature Sliding Wear of Spray-Formed Solid-Lubricated Aluminum Matrix Composites	J. Mater. Engg. & Performance	2013	22(10), 3101- 3110	1.331
364	Kaur, Ravneet; Singh, Surinder, O.P. Pandey	Influence of CdO and gamma irradiation on the infrared absorption spectra of borosilicate glass	J. Molecular Structure	2013	1049, 409-413	1.753
365	A Chaudhary, P Malik, R Mehra, KK Raina	Influence of ZnO nanoparticle concentration on electro-optic and dielectric properties of ferroelectric liquid crystal mixture	Journal of Molecular Liquids	2013	188, 230- 236	1.684
366	Jen-Hwa Hsu, An- Cheng Sun and Puneet Sharma	Lateral grain size effect on exchange bias in polycrystalline NiFe/FeMn bilayer films	Thin Solid Films	2013	542, 87– 90	
367	GS Lotey, NK Verma	Magnetodielectric properties of rare earth metal-doped BiFeO ₃ nanoparticles	Journal of Materials Science: Materials in Electronics	2013	24 (10), 3723- 3729	2.019
368	GS Lotey, NK Verma	Magnetoelectric coupling in multiferroic BiFeO ₃ nanowires	Chemical Physics Letters	2013	579, 78- 84	1.815
369	GS Lotey, NK Verma	Magnetoelectric coupling in multiferroic Tb-doped BiFeO ₃ nanoparticles	Materials Letters	2013	111, 55- 58	2.572
370	Kaur, Bhupinder; Singh, K.; O.P. Pandey	Microstructural analysis of glass- steel interface	Surface & Coating Tech	2013	217, 156- 161	2.589
371	Kaur, Ravneet; Singh, Surinder; O.P. Pandey	Modifications induced in the structural and optical properties of bismuth sodium borosilicate glass thin films by 120 MeV Ag ⁷⁺ ions	Nucl. Inst. Methods in Physics Res. B	2013	305, 51- 54	1.109
372	GS Lotey, NK Verma	Multiferroic properties of Tb- doped BiFeO ₃ nanowires	Journal of nanoparticle research	2013	15 (4), 1553	2.02
373	GS Lotey, NK Verma	Multiferroism in rare earth metals- doped BiFeO ₃ nanowires	Superlattices and Microstructur es	2013	60, 60-66	2.123
374	Jha, Paramjyot Kumar; O.P. Pandey; Singh, K.	Na ₂ S-P ₂ S ₅ Based Super-Ionic Glasses for Solid Electrolytes	Trans. Of Indian Ceramic Soc.	2013	72(1), 5-9	0.558
375	Neeraj, KK Raina	Nickel nanoparticles doped ferroelectric liquid crystal composites	Optical Materials	2013	35 (3), 531-535	2.238
376	A Chaudhary, P Malik, R Mehra, KK Raina	Observation of memory behaviour in cadmium sulphide nanorods doped ferroelectric liquid crystal mixture	Phase Transitions	2013	86 (12), 1256- 1266	1.006

377	S. Chopra, M. Bansal, Manoj K. Sharma and R. K Gupta	One-neutron and non-compound – nucleus decay contributions in $^{12}\text{C}+^{93}\text{Nb}$ reaction at below barrier energies.	Phys. Rev. C	2013	88, 014615	3.82
378	Bansod, B. S.; O.P. Pandey ; Rajesh, N. L.; Dhatteval, S.	Optimisation of agricultural input application to enhance the crop quality and yield quantity in paddy under precision farming	Quality assurance and safety of crop and food	2013	5(3), 179-185	0.597
379	L Khanna, NK Verma	PEG/CaFe ₂ O ₄ nanocomposite: Structural, morphological, magnetic and thermal analyses	Physica B: Condensed Matter	2013	427, 68-75	1.386
380	M Kaur, NK Verma	Performance of dye-sensitized solar cell fabricated using titania nanoparticles calcined at different temperatures	Materials Science-Poland	2013	31 (3), 378-385	0.533
381	M Kaur, NK Verma	Performance of Eu ₂ O ₃ coated ZnO nanoparticles-based DSSC	Journal of Materials Science: Materials in Electronics	2013	24 (9), 3617-3623	2.019
382	S. M. Lee, B. C. Mohanty , Y. H. Jo, D. H. Yeon and Y. S. Cho,	Phase development, microstructure and optical properties of Cu ₂ ZnSnSe ₄ thin films modified with Pb and Ti	Surf. Coating Technol.	2013	231, 389-393	2.589
383	GS Lotey, NK Verma	Phase-dependent multiferroism in Dy-doped BiFeO ₃ nanowires	Superlattices and Microstructures	2013	53, 184-194	2.123
384	M. Batra, A. Upadhyay	Phenomenology of neutrino oscillation in vacuum and matter,	ISRN-HEP,	2013	206516	1.74
385	D. Jain, Raj Kumar , and M. K. Sharma	Reaction dynamics of Pt* isotopes formed using stable and radioactive Sn beams	Phys. Rev. C	2013	87, 044612	3.82
386	Kumar, R.; Kumar, A.; Singh, S.; O.P. Pandey	Reduction of WO ₃ to WC nanoparticles by the reflux reaction	J. Mater Sci	2013	49(1), 102-109	0.187
387	GS Lotey, J Singh, NK Verma	Room temperature ferromagnetism in Tb-doped ZnO dilute magnetic semiconducting nanoparticles	Journal of Materials Science: Materials in Electronics	2013	24 (9), 3611-3616	2.019
388	L Khanna, NK Verma	Silica/potassium ferrite nanocomposite: Structural, morphological, magnetic, thermal and in vitro cytotoxicity analysis	Materials Science and Engineering: B	2013	178 (18), 1230-1239	2.552
389	Kaur, Gurbinder; Homa, D.; Singh, K. ; O.P. Pandey ; Scott, B.; Pickrell, G.	Simulation of thermal stress within diffusion couple of composite seals with Crofer 22APU for solid oxide fuel cells applications	J. Powder Sources	2013	242, 305-313	6.359

390	Mahajan, Mani; Singh, K.; O.P. Pandey	Single step synthesis of nano vanadium carbide-V8C7 phase	Int. J. Refractory metals and Hard Metals	2013	36, 106-110	2.155
391	Singh, Harjinder; O.P. Pandey	Single step synthesis of tungsten carbide (WC) nanoparticles from scheelite ore	Ceramics Int	2013	39(6), 6703-6706	2.986
392	G Dhir, GS Lotey, P Uniyal, NK Verma	Size-dependent magnetic and dielectric properties of Tb-doped BiFeO3 nanoparticles	Journal of Materials Science: Materials in Electronics	2013	24 (11), 4386-4392	2.019
393	L Khanna, NK Verma	Size-dependent magnetic properties of calcium ferrite nanoparticles	Journal of Magnetism and Magnetic Materials	2013	336, 1-7	2.63
394	C. S. Han, B. C. Mohanty , C. Y. Kang, Y. S. Cho,	Sputter-deposited low loss Mg2SiO4 thin films for multilayer hybrids,	Thin Solid Films	2013	527, 250-254	1.867
395	Alka Upadhyay , M. Batra	Strange Mass Corrections to Hyperonic Semi-Leptonic Decay in Statistical Model	Eur. Phys. J. A	2013	49, 160	2.736
396	Thakur, Samita; O.P. Pandey; Singh, K.	Structural and dielectric properties of Bi1-xSrxMnO3 (0.40 ≤ x ≤ 0.55)	Ceramics Int.	2013	39(6), 6165-6174	2.986
397	Sakshi Gupta, K. Singh,	Structural and optical properties of barium doped bismuth vanadate melt quenched sample	Physica B: Condensed Matter	2013	431, 89-93	1.386
398	M Kaur, NK Verma	Structural and optical properties of Eu 2 O 3 coated TiO 2 nanoparticles and their application for dye sensitized solar cell	Journal of Materials Science: Materials in Electronics	2013	24 (4), 1121-1127	2.019
399	GS Lotey, Z Jindal, V Singhi, NK Verma	Structural and photoluminescence properties of Eu-doped ZnS nanoparticles	Materials Science in Semiconductor Processing	2013	16 (6), 2044-2050	2.359
400	Kaur, Gurbinder; Singh, K.; O.P. Pandey; Homa, D.; Scott, B.; Pickrell, G.	Structural and thermal properties of glass composite seals and their chemical compatibility with Crofer 22APU for solid oxide fuel cells applications	J. Powder Sources	2013	240, 458-470	6.395
401	Singla, Gourav; Singh, K.; O.P. Pandey	Structural and thermal properties of in-situ reduced WO3 to W powder	Powder Technology	2013	237, 9-13	2.942
402	Jha, Paramjyot Kumar; O.P. Pandey; Singh, K.	Structural and thermal properties of Na2S-P2S5 glass and glass ceramics	J. Non-crystalline solids	2013	379, 89-94	2.124
403	R Rani, S Singh, KK Raina , C Prakash	Structural, electrical and magnetic properties of microwave processed Ni0.80Zn0.20Fe2O4	Key Engineering Materials	2013	547, 25-30	0.39

404	R Rani, JK Juneja, S Singh, C Prakash, KK Raina	Structural, electrical, magnetic and magnetoelectric properties of composites	Journal of Magnetism and Magnetic Materials	2013	345, 55-59	2.63
405	K Kaur, GS Lotey, NK Verma	Structural, optical and magnetic properties of cobalt-doped CdS dilute magnetic semiconducting nanorods	Materials Chemistry and Physics	2013	143 (1), 41-46	2.084
406	R Rani, JK Juneja, S Singh, KK Raina , C Prakash	Study of 0.1Ni 0.8Zn 0.2Fe 2O 4-0.9Pb 1-3x/2La xZr 0.65Ti 0.35O 3 magnetoelectric composites	Journal of Magnetism and Magnetic Materials	2013	325, 47-51	2.63
407	Sood, Kapil; Singh, K.; O.P. Pandey	Study of the Structural and Electrical Behaviour of Ca Doped LaInO3 Electrolyte Material	Trans. Of Indian Ceramic Soc.	2013	72(1), 32-35	0.558
408	Panwar, Ranvir Singh; O.P. Pandey	Study of Wear Behavior of Zircon Sand-Reinforced LM13 Alloy Composites at Elevated Temperatures	J. Mater Engg. & Performance	2013	22(6), 1765-1775	1.331
409	Rekha Rani, J.K.Juneja, SangeetaSingh, K.K.Raina , ChandraPrakash	Study of 0.1Ni0.8Zn0.2Fe2O4.9Pb13x/2LaxZr0.65Ti0.35O3magnetoelectr iccomposites	Journal ofMagnetism andMagnetic Materials	2013	325, 47-51	2.63
410	M Kaur, NK Verma	Study on CaCO 3-coated ZnO nanoparticles based dye sensitized solar cell	Journal of Materials Science: Materials in Electronics	2013	24 (12), 4980-4986	2.019
411	S Kumar, NK Verma , ML Singla	Study on reflectivity and photostability of Al-doped TiO 2 nanoparticles and their reflectors	Journal of Materials Research	2013	28 (3), 521-528	1.673
412	Dipti, JK Juneja, S Singh, KK Raina , C Prakash,	Study on structural, dielectric, ferroelectric and piezoelectric properties of Ba doped Lead Zirconate Titanate Ceramics	Physica B: Condensed Matter	2013	431, 109-114	1.386
413	C. S. Han, B. C. Mohanty , H. R. Choi and Y. S. Cho	Surface Scaling Evolution and Dielectric Properties of Sputter-Deposited Low Loss Mg2SiO4 Thin Films,	Surf. Coating Technol	2013	231, 229-233	2.589
414	L Khanna, NK Verma	Synthesis, characterization and in vitro cytotoxicity study of calcium ferrite nanoparticles	Materials science in semiconductor processing	2013	16 (6), 1842-1848	2.359
415	Gudveen Sawhney ,Gurvinder Kaur, Manoj K. Sharma , and Raj K. Gupta	Theoretical study of odd-mass Fr isotopes using the collective clusterization approach of the dynamical cluster-decay model.	Phys. Rev. C	2013	88, 034603	3.82

416	B. C. Mohanty , D. H. Yeon, S. N. Das, J. H. Kwak, K. H. Yoon, and Y. S. Cho,	Unusual near-band-edge photoluminescence at room temperature in heavily-doped ZnO:Al thin films prepared by pulsed laser deposition,	Mater. Chem. Phys.	2013	140, 610-615	2.084
417	Kumar, Suresh; Panwar, Ranvir Singh; O.P. Pandey	Wear Behavior at High Temperature of Dual-Particle Size Zircon-Sand-Reinforced Aluminum Alloy Composite	Metallurgical and Materials Trans A	2013	44(3), 1548-1565	1.642
418	Singla, Gourav; Singh, K.; O.P. Pandey	Williamson-Hall study on synthesized nanocrystalline tungsten carbide (WC)	Appl. Physics A	2013	113(1), 237-242	1.455

**Highlight of the Research Activities of SPMS
(2013-2018)**



Structural and thermal properties of glass composite seals and their chemical compatibility with Crofer 22APU for solid oxide fuel cells applications



Gurbinder Kaur^{a,*}, K. Singh^b, O.P. Pandey^b, D. Homa^a, B. Scott^a, G. Pickrell^a

^aDepartment of Material Science and Engineering, Holden Hall, Virginia Tech, Blacksburg, VA 24060, USA

^bSchool of Physics and Materials Science, Thapar University, Patiala 147004, India

HIGHLIGHTS

- Glass composite seals are prepared by ball-milling different glasses in fixed ratio for 5 h.
- No reactive particle was used in glass matrix to obtain composites.
- The structural characteristics of composites were studied using XRD, particle size and zeta potential.
- The chemical compatibility of these composites was investigated with Crofer 22APU.
- The interface and resulting microstructure was morphologically characterized by using SEM/EPMA.

ARTICLE INFO

Article history:

Received 11 January 2013

Received in revised form

28 February 2013

Accepted 25 March 2013

Available online 3 April 2013

Keywords:

Glass composite

Solid oxide fuel cell (SOFC)

Scanning electron microscopy (SEM)

Chemical interaction

X-ray diffraction (XRD)

Diffusion

ABSTRACT

In the present investigation, glass composite seals have been prepared by mixing the different glass compositions in fixed ratio and then ball milling for 5 h. The main aim of this approach is to investigate the sealing and bonding issues in solid oxide fuel cells (SOFC) without using unreactive particles in glass matrix. The structural and thermal characteristics of these composites were studied using particle size analyzer, zeta potential, dilatometry, differential scanning calorimetry (DSC) and thermogravimetric analysis (TGA). X-ray diffraction has revealed phase formation in all composites after 1000 h heat-treatment at 850 °C. In addition to this, the chemical compatibility of the prepared glass composites with the interconnect Crofer 22APU has been studied using scanning electron microscope (SEM), electron probe microanalysis (EPMA), energy dispersive spectroscopy (EDS) and dot-mapping techniques. The interfacial study has revealed that GG6 and GG7 composites have good adhesion without delamination, cracks or pore formation. Chromate formation occurred in GG3 and GG4 composite couples, though no delamination was observed at the interface of GG4 composite with Crofer 22APU. GG5 could not form a diffusion couple due to its high viscosity and very low coefficient of thermal expansion.

© 2013 Elsevier B.V. All rights reserved.

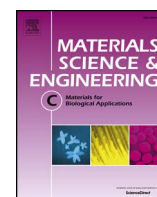
1. Introduction

High temperature solid oxide fuel cells (SOFC) can generate power from a variety of fuels. Their solid geometry, high efficiency along with environment friendly byproducts has lead to a broad range of applications like aeronautics, power generation in automobiles and various electronic devices [1–5]. Usually planar and tubular geometries are the most preferred designs for SOFC operation. The short current path for planar SOFC results in a high power density as compared to the tubular design [6–8]. However,

hermetic seals are required for planar SOFC to bond cell components together, prevent leakage losses and direct combustion of fuel and oxygen. In addition to this, these hermetic seals should fulfill many stringent requirements in order to be a suitable sealing material for SOFC operation [9–13]. The most important requirement is mechanical and chemical compatibility of seals with adjoining components in reducing/oxidizing atmospheres at high temperatures between 600 and 1000 °C for prolonged periods of operation.

The general approaches for sealing include compressive, compliant, rigid bonded and composite [14–16]. Compliant seals do not bond well to SOFC components resulting in hydrogen embrittlement whereas compressive seals require load. Rigid bonded seals like glass and glass ceramics are preferred seals due to their

* Corresponding author. Tel.: +1 540 239 7929.
E-mail address: gkaur82@vt.edu (G. Kaur).



Antimicrobial and bioactive phosphate-free glass–ceramics for bone tissue engineering applications



Praveen Jha^a, Satwinder Singh Danewalia^b, Gaurav Sharma^b, K. Singh^{b,*}

^a State Forensics Science Laboratory, Sagar, Madhya Pradesh 470001, India

^b School of Physics & Materials Science, Thapar University, Patiala 147004, India

ARTICLE INFO

Keywords:

Heat-treatment
In-vitro
Bioactivity
Microhardness
SBF
Microbial test

ABSTRACT

Glasses with composition $55\text{SiO}_2\text{-}10\text{K}_2\text{O}\text{-}(35\text{-}x)\text{CaO}\text{-}x\text{MgO}$ ($x = 5, 10, 15$ up to 35) were prepared via conventional melt-quench technique. The glasses were converted to glass–ceramics by controlled heat-treatment at 850°C . Higher content of MgO instead of CaO prevents the devitrification of the glasses. The in-vitro bioactivity of the glasses/glass–ceramics was evaluated in simulated body fluid (SBF). Glasses exhibited better bioactivity than the glass–ceramics. The weight loss and ions leaching profiles (especially potassium ions) of the samples played crucial role in formation of hydroxyapatite layer and its morphology. Hydroxyapatite had Ca/P ratio close to that for natural bone. However, it could not crystallize within experimental time and exhibited amorphous nature in X-ray diffraction. Microhardness of the glasses/glass–ceramics before and after immersion in SBF is also given. Microbial tests reveal that these glasses/glass–ceramics are effective in inhibiting the growth of fungi and do not affect the normal functioning of the antimicrobial drugs.

1. Introduction

Biomaterials research has expanded beyond its horizon over the past several years. Variety of glass/ceramic based biomaterials is used now days for dental, orthopedic and maxillofacial applications [1]. However, brittle nature and poor mechanical properties of the glasses serve as a barrier that limits their use as load bearing implants [2]. Mechanical properties of the glasses can be improved by growing some crystalline phase(s) within the glassy matrix by controlled heat-treatment. In general, glass–ceramics possess superior mechanical properties as compared to parent glasses [3]. The mechanical properties of the glass–ceramics depend upon microstructure, grain size and volume fraction of the crystalline phases [4–6]. Several glass ceramics like A-W containing crystalline oxoflourapatite, wollastonite, hydroxyapatite and tricalcium phosphate rich phases in glassy matrix for better mechanical compliance have been used in the past [7]; however, crystallization may prove detrimental for the bioactive nature of the glasses [8]. Therefore, controlled crystallization is needed to achieve optimum mechanical properties without compromising bioactivity. Bioactivity of the bioglasses/glass–ceramics is evaluated by their ability to form hydroxyapatite (HAp) layer on their surfaces in contact with the physiological fluids. This is ascribed to open structure of the glass network which leads to the exchange of selective ions with the solutions mimicking body environments known as simulated body fluid (SBF) [9].

Most of the bioactive glasses exhibit four basic constituents i.e. SiO_2 , Na_2O , CaO and P_2O_5 . However, it has been reported that phosphate-free glasses also exhibit good in-vitro bioactivity [10]. The necessary phosphate content is taken from the body fluids itself during the bioactivity evaluation. It has also been found that replacement of Na_2O by K_2O helps to improve the bioactivity of the glasses by modifying their chemical durability [11]. Moreover, MgO based glasses exhibited better mechanical properties along with good bioactivity [12, 13]. Hence, in the present study, we have chosen the $\text{SiO}_2\text{-K}_2\text{O-CaO-MgO}$ glass system. The aim of the present work is to determine the bioactive behavior of the heat-treated glasses/glass–ceramics by exploiting their composition flexibility with CaO/MgO ratio. The effect of structural changes upon heat-treatment on bioactivity and microhardness of the glasses/glass–ceramics is also accessed. Infection and lack of tissue integration are generally two main complications that may be caused by the biomaterials. Certain implants such as external fixation pins are susceptible to infection. Therefore, the possible threat of microbial contamination and microbial growth on the samples in due course of time after implantation has also been studied in the present work.

* Corresponding author.

E-mail address: kusingh@thapar.edu (K. Singh).

<https://doi.org/10.1016/j.msec.2018.01.002>

Received 10 June 2017; Received in revised form 17 October 2017; Accepted 13 January 2018

Available online 31 January 2018

0928-4931/ © 2018 Elsevier B.V. All rights reserved.



Research articles

Effect of thermal aging on stability of transformer oil based temperature sensitive magnetic fluids



Navjot Kaur, Bhupendra Chudasama*

School of Physics and Materials Science, Thapar University, Patiala 147004, Punjab, India

ARTICLE INFO

Article history:

Received 19 June 2017

Received in revised form 5 November 2017

Accepted 20 November 2017

Available online 21 November 2017

Keywords:

Magnetic fluids

Thermal aging

Co-precipitation

Hydrodynamic size

Magnetic properties

ABSTRACT

Synthesizing stable temperature sensitive magnetic fluids with tunable magnetic properties that can be used as coolant in transformers is of great interest, however not exploited commercially due to the lack of its stability at elevated temperatures in bulk quantities. The task is quite challenging as the performance parameters of magnetic fluids are strongly influenced by thermal aging. In this article, we report the effect of thermal aging on colloidal stability and magnetic properties of $Mn_{1-x}Zn_xFe_2O_4$ magnetic fluids prepared in industrial grade transformer oil. As-synthesized magnetic fluids possess good dispersion stability and tunable magnetic properties. Effect of accelerated thermal aging on the dispersion stability and magnetic properties have been evaluated by photon correlation spectroscopy and vibration sample magnetometry, respectively. Magnetic fluids are stable under accelerated aging at elevated temperatures (from 50 °C to 125 °C), which is critical for their efficient performance in high power transformers.

© 2017 Elsevier B.V. All rights reserved.

1. Introduction

Magnetic fluids are colloidal dispersion of magnetic nanoparticles in carrier liquid. It combines both the fluidic and magnetic properties in single domain system. They find variety of applications in diverse field of science and technology, which is ranging from space science to nanomedicine [1]. These fluids are used as a 'liquid seal' in hard drives, as dampers in automobiles and aerospace, as drug carriers in magnetically guided drug delivery and as contrast agents in MRI [2–4]. Another promising application of magnetic fluids is to use them as coolant in heat exchangers and in magnetocaloric energy conversion devices like high power transformers [5]. Heat transfer in oil immersed transformers can be improved significantly if convectional mineral oil is replaced with temperature sensitive magnetic fluid in transformers [6]. In temperature sensitive magnetic fluids; the magnetization of fluid strongly depends on fluid temperature. When exposed to temperature gradient, they exhibits magnetic convection in addition to natural convection caused by the density gradient. This additional drag force enhances the cooling efficiency of the fluid and thus improves their performance in transformers.

In order to use magnetic fluids in heat exchange devices, they should possess large thermomagnetic coefficient and suitable

Curie temperature, which should be matching with the operating temperature of device. Temperature sensitive magnetic fluids suitable for cooling applications in high power transformers should have Curie temperature between 70 °C and 300 °C [7]. Most substituted ferrites used in the preparation of magnetic fluids tend to have Curie temperatures that are too high for practical use in transformers. Curie temperature of mixed metal ferrites lie between 100 °C and 200 °C. Amongst them Mn-Zn ferrite nanoparticles are well suited for thermo-magnetic coolants, because of their moderate saturation magnetization and tunable Curie temperature [8,9].

Magnetic nanoparticles dispersed in transformer oil should be able to withstand the device's operating temperature without any loss in their dispersity [6]. One of the important parameter that effects the stability of the magnetic fluids is the size of nanoparticles and its distribution. Small size of nanoparticles and narrow size distribution is essential to prepare stable magnetic fluids [8]. Arulmurugan et al. have reported synthesis of $Mn_{1-x}Zn_xFe_2O_4$ ($x = 0.1-0.5$) nanoparticles with Curie temperatures from 160 °C to 360 °C. They have observed that Curie temperature of $Mn_{1-x}Zn_xFe_2O_4$ nanoparticles decreases with increasing Zn content [10]. Giri et al. and Mohapatra et al. have reported surface controlled synthesis of MFe_2O_4 ($M = Mn, Fe, Co, Ni$ and Zn) nanoparticles and studied effect of surface ligands on the magnetic properties of MFe_2O_4 nanoparticles [11–13]. Desai et al. have reported synthesis of $Mn_{0.5}Zn_{0.5}Fe_2O_4$ nanoparticles with tunable Curie temperature and saturation magnetization using

* Corresponding author at: Laboratory of Nanomedicine, School of Physics & Materials Science, Thapar University, Patiala 147004, India.

E-mail address: bnchudasama@thapar.edu (B. Chudasama).



Structural, magnetic and microwave properties of barium hexaferrite thick films with different Fe/Ba mole ratio



Samiksha Verma^a, S.K. Dhawan^b, Andrea Paesano Jr^c, O.P. Pandey^a, Puneet Sharma^{a,*}

^a School of Physics and Materials Science, Thapar University, Patiala 147004, India

^b Polymeric & Soft Materials Section, National Physical Laboratory, New Delhi 119912, India

^c Departamento de Física, Universidade Estadual de Maringá, Av. Colombo 5790, Maringá, Brazil

ARTICLE INFO

Article history:

Received 14 June 2015

Received in revised form

11 July 2015

Accepted 11 August 2015

Available online 11 August 2015

Keywords:

Fe/Ba mole ratio

Barium hexaferrite

Screen printing

Magnetic properties

Microwave absorption

ABSTRACT

Barium hexaferrite (BaFe₁₂O₁₉) thick films (~60 μm) with different BaO · xFe₂O₃ mole ratio (x=5.0–6.0) were prepared by screen printing method. X-ray diffraction analysis confirmed the formation of single phase BaFe₁₂O₁₉ (BaM). Preferential site occupation of Fe³⁺ ion at five different crystallographic sites, with varied mole ratio was measured by Mössbauer spectroscopy. Vacancy fraction found to be higher at 4f₁, 4f₂ and 2b sites for mole ratio 5.5 and 5.0 respectively. Magnetic measurement shows that the magnetization (M) and magnetocrystalline anisotropy field (H_a) depends upon mole ratio. M and H_a are found to be maximum for mole ratio 5.5, while the coercivity (H_c) remains constant. Reflection losses (R_L) in the frequency range of 12–18 GHz were also studied. Present investigation demonstrates the effect of mole ratio on structural, magnetic and microwave absorption properties of BaM thick films for microwave device applications.

© 2015 Elsevier B.V. All rights reserved.

1. Introduction

Among the class of M-type hexaferrite, barium hexaferrite (BaFe₁₂O₁₉) possess dominant position due to its high saturation magnetization (M_s), moderate coercivity (H_c) and high uniaxial magnetocrystalline anisotropy (H_a) [1]. Such properties make this materials suitable for commercial permanent magnets [2] and high density magnetic recording [3]. In last decade, BaFe₁₂O₁₉ (BaM) has gained considerable attention for microwave application such as microwave absorbers [4,5], circulators [6], isolators [7] and phase shifter [8] owing to its higher ferromagnetic resonance (FMR) frequencies [9]. The natural FMR frequency (f_R=γH_a) for BaM is 36 GHz [9]. It can be further tuned by applying an external magnetic field or by suitable substitution for Fe cation, which drastically reduces or increases the H_a.

The high H_a in BaM arises due to its hexagonal crystal structure. One unit cell of BaM consists of two formula units, where 24 Fe³⁺ ions occupy five different crystallographic sites, three octahedral sites (12k, 4f₂ and 2a), one tetrahedral (4f₁) and one trigonal bipyramidal (2b) site. The Fe³⁺ ions located at 12k, 2a and 2b sites have up spins and those at 4f₁ and 4f₂ sites have down spins with net magnetic moment of 40 μ_B per unit cell [1].

Various studies have been reported on Fe³⁺ ion substitution for

tuning H_a and M_s of BaM for high frequency applications from 1 to 100 GHz. The substitutions such as Al³⁺ [10] and Ga³⁺ [11] reportedly increase the H_a, while substitutions of Co–Ti [12], Ru–Ti [13] and Zn–Zr [14] ions decrease the magnitude of H_a. Alternatively, magnetic properties can also be tuned by creating Fe³⁺ ion vacancy at five different crystallographic sites, which is not yet been investigated for BaM thick films.

In this work single phase BaM with different fraction of Fe³⁺ ion vacancy is prepared. The vacancy fraction of Fe is controlled by varying BaO · xFe₂O₃ composition, where x=5.0–6.0. Further BaM thick films of ~60 μm thickness has been prepared by screen printing method, considering its possibility for microwave device application with tunable operating frequency. For high frequency applications the film thickness should be higher than 50 μm [15]. In the present work, we have systematically investigated the effect of mole ratio on structural, magnetic and microwave properties of BaM thick films. Obtained magnetic and microwave properties demonstrate that vacant Fe ion site plays a key role in tuning magnetic and microwave absorption properties.

2. Experimental

BaM powder samples with composition BaO · xFe₂O₃ (x=5.0, 5.25, 5.5, 5.75 and 6.0) were prepared by using solid state reaction method. Henceforth the 'x' will be referred as the Fe/Ba mole ratio. High purity BaCO₃ and Fe₂O₃ were weighed in the desired

* Corresponding author.

E-mail address: puneet.sharma@thapar.edu (P. Sharma).

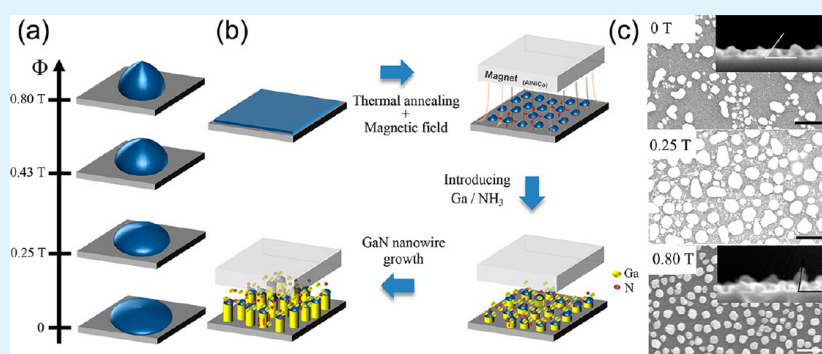
In Situ Magnetic Field-Assisted Low Temperature Atmospheric Growth of GaN Nanowires via the Vapor–Liquid–Solid Mechanism

Jun Sik Kim,^{||,†,‡} Bhaskar Chandra Mohanty,^{||,†,⊥} Chan Su Han,[†] Seung Jun Han,[‡] Gwang Heon Ha,[‡] Liwei Lin,[§] and Yong Soo Cho^{*†}

[†]Department of Materials Science & Engineering, Yonsei University, Seoul 120-749, Korea

[‡]R&D Center, LG Displays Co. Ltd., Paju-si, Gyeonggi-do 413-811, Korea

[§]Department of Mechanical Engineering, University of California at Berkeley, Berkeley, California 94720-1740, United States



ABSTRACT: We report the growth of GaN nanowires at a low temperature of 750 °C and at atmospheric pressure in a conventional chemical vapor deposition (CVD) setup via the vapor–liquid–solid mechanism with remarkable control of directionality and growth behavior by using an in situ magnetic field. Under typical growth conditions, without any magnetic field, the nanowires are severely twisted and kinked, and exhibit a high density of planar stacking defects. With increasing in situ magnetic field strength, the microstructural defects are found to decrease progressively, and quasi-aligned nanowires are produced. At an applied magnetic field strength of 0.80 T, near-vertical aligned straight and several micrometers long nanowires of average diameter of ~40 nm with defect-free microstructure are routinely produced. Photoluminescence measurements show that the relative intensity of the defect-related peaks in the visible region with respect to the near-band-edge emission continuously decrease with increase in the applied in situ magnetic field strength, ascribable to the magnetic field-assisted significant structural improvement of the wires. It is found out that the degree of agglomerative Ni droplet on Si is critically influenced by the surface tension driven by the magnetic force, which in turn determines the eventual properties of the nanowires.

KEYWORDS: GaN, nanowires, chemical vapor deposition, magnetic field, growth mechanism

INTRODUCTION

One-dimensional (1D) semiconducting nanowires have been extensively studied as critical solutions for next generation electronic and optoelectronic devices because of the extraordinary performance of their size/geometry-dependent properties.^{1–4} There have been a lot of examples of promising nanowire-based devices actually showing better performance than the corresponding thin films or bulk materials. Nevertheless, the realization of the full potential of these nanowires has been limited by the difficulty in obtaining high quality growth, specific orientation, and spatial manipulation of nanowires into complex but ordered nanoscale architectures. Even until now, considerable progress has been made in achieving controllable nanowires by using different growth techniques with a concern for the accompanying processing cost.^{5–8} The bottom-up approaches for growing nanowires, including solution growth, chemical vapor deposition (CVD)

via the vapor–liquid–solid (VLS) mechanism, and electrochemical deposition using nanoporous templates, are considered more competitive because of their general lower cost compared to the top-down approaches typically employing lithography techniques.^{5–8} However, the bottom-up approaches generate the random alignment of nanowires with kinks and twists, which must be avoided for actual applications. The post-growth assembly using the inferior nanowires for target configurations has shown the limitation in realizing highly integrated nanodevices.^{9–11} The use of an external magnetic field for the controllable assembly of nanowires presents a noncontact and “easy-to-implement” way that can be successful on a large scale.^{12–17} A few research groups have

Received: July 28, 2013

Accepted: October 11, 2013

Published: October 11, 2013



Interaction Study of Yttria-Based Glasses with High-Temperature Electrolyte for SOFC

V. Kumar^{1,2*}, O. P. Pandey³, K. Singh³, K. Lu^{1*}

¹ Department of Materials Science and Engineering, Virginia Polytechnic Institute and State University, Blacksburg, VA 24061, USA

² Shri Guru Granth Sahib World University, Fategarh Sahib, Punjab 140406, India

³ School of Physics and Materials Science, Thapar University, Patiala 147004, India

Received May 22, 2013; accepted January 30, 2014; published online June 17, 2014

Abstract

The chemical interaction study of $\text{AO-SiO}_2\text{-B}_2\text{O}_3\text{-Y}_2\text{O}_3$ ($A = \text{Ba, Sr}$) (BaY, SrY) glass with high-temperature electrolyte yttria-stabilized zirconia (YSZ 8 mol%) is reported as a function of different heat treatment durations. The as-prepared glass with 10 mol% of yttria shows limited amount of crystallization at 800 °C. Due to this yttria-based glasses BaY and SrY have been chosen to make diffusion couples with high-temperature electrolyte and interconnect material. These diffusion couples have been heat treated at 850 °C, for 100, 200, and 500 h. The heat-treated diffusion couples have been characterized using X-ray diffraction (XRD), scanning electron microscopy (SEM), and energy dispersive spectroscopy (EDS). Microstructural analysis of diffusion couples

shows absence of any undesired oxides and detrimental reaction products at the interface. The glass has shown good bonding characteristics and absence of cracks, pores, or any kind of delamination from YSZ. Apart from this, SrY and BaY glass seals have also shown good adhesion characteristics with Crofer 22 APU, even after 500 h at 850 °C. The morphology and microstructure of the glass matrix suggest limited amount of devitrification in the glass.

Keywords: Crystallization, Solid Oxide Fuel Cells, Glass Sealant, Interaction, Electron Microscopy, EDS Element Mapping, X-Ray Diffraction

1 Introduction

High-temperature solid oxide fuel cells (SOFCs) possess high efficiency, environmental friendly byproducts, fuel flexibility, and variable geometry. Because of rapid technological progress in recent years, SOFCs are now considered a promising alternative to convert chemical energy into electrical energy [1–3]. There are two designs of SOFCs: the tubular and planar. The planar design has higher development potential and already provides higher volumetric and gravimetric power density [3]. However, for a planar SOFC stack, gas-tight seals must be applied along the edges of each cell and between the cell stack and gas manifolds in order to avoid intermixing of fuel gas (on anode side) and air (on cathode side) [4]. The composition of glasses can be tuned to optimize the desired glass transition temperature, softening temperature, and coefficient of thermal expansion (CTE). The “soft state” of seal is the mandatory condition for wetting capability and contact of seal with stack. However, below glass transition temperature (T_g), thermal stresses can lead to crack formation in glass seals [5]. In order to maintain hermeticity

of seal, T_g should be matched properly with cell stack operating temperature so that seals can self-heal under viscous flow above T_g [6]. Among the various criteria required for seal, the most important thermo-mechanical requirement is good adhesion of seal with SOFC components without severe reaction at the interface [7].

Generally, the sealants for SOFC must meet the following requirements: (a) matching CTE with adjoining components (b) high-electrical resistivity to avoid short circuiting between different layers of the stack, (c) good thermo-chemical compatibility with relevant SOFC components (i.e., no harmful reaction with joining components), (d) high-chemical stability and low-vapor pressure in both reducing and oxidizing atmospheres, (e) non-spreading nature to the adjoining fuel cell components at the operating temperature, (f) deformability but certain ability to withstand a slight overpressure, and (g)

[*] Corresponding author, klu@vt.edu; vishal80@vt.edu



Magnetoelectric coupling in multiferroic Tb-doped BiFeO₃ nanoparticles

Gurmeet Singh Lotey*, N.K. Verma

Nano Research Lab, School of Physics & Materials Science, Thapar University, Patiala 147004, India



ARTICLE INFO

Article history:

Received 7 May 2013

Accepted 4 August 2013

Available online 15 August 2013

Keywords:

Nanoparticles

Magnetic materials

Phase transformation

Structural

Sol-gel preparation

Ferroelectrics

ABSTRACT

Bi_{1-x}Tb_xFeO₃ nanoparticles ($x=0, 0.05, 0.10$ and 0.15) of size 30–39 nm, have been synthesized by the sol-gel technique. The effects of nano-size and Tb-doping on structural, magnetic and magnetoelectric coupling (ME) have been reported. Crystallographic analysis reveals the structural transition from rhombohedral (R3c) to orthorhombic (Pn2₁a) phase, i.e. polar-to-polar phase, with Tb-doping. The synthesized nanoparticles exhibit ferromagnetic behavior, and, the 15% Tb-doped BiFeO₃ nanoparticles possess large magnetic saturation, 2.92 emu/g. The dynamic lock-in technique has been used to measure longitudinal ($L-\alpha_{ME}$) and transverse ($T-\alpha_{ME}$) ME coefficients. It has been found that both $L-\alpha_{ME}$ and $T-\alpha_{ME}$ increase quickly with increase in bias magnetic field, and attain maximum value, $L-\alpha_{ME}=11.01, 10.35, 11.92, 13.18$ mV/cm Oe and $T-\alpha_{ME}=6.81, 6.85, 6.88, 7.86$ mV/cm Oe, respectively, for $x=0, 0.05, 0.10,$ and 0.15 . The observed ME effect has been explained on the basis of quantum confinement, exchange interactions, spin-exchange constriction, and magnetostriction effect.

© 2013 Elsevier B.V. All rights reserved.

1. Introduction

Multiferroic materials with strong magnetoelectric coupling (ME) are the most promising materials for future spintronic and nanoelectronic devices [1–9]. The semiconductor-based electronic industry is under threat as we are at the verge of fundamental limit of integration (number of device components such as transistors on integrated circuit). Therefore, for the miniaturization and high performance of electronic devices either new technologies or multifunctional materials are required. BiFeO₃ is one of the scarcest multifunctional multiferroic material, exhibiting simultaneously spontaneous polarization as well as weak ferromagnetism ordering with high Curie ($T_C \sim 830$ °C) and Néel ($T_N \sim 370$ °C) temperatures [1–9]. Therefore, the possibility to integrate multifunctions such as electric and magnetic in BiFeO₃ can be explored in spintronic and nanoelectronic devices [1–9]. The practical applications of bulk BiFeO₃ have been mired because of weak ferromagnetism and very low magnetoelectric coupling; this happens due to spin-spiral incommensurate structure of BiFeO₃ with large cycloidal period of 62 nm [4–12,17–20]. This cycloidal period can be broken, and high magnetoelectric coupling with ferromagnetic behavior can be achieved in BiFeO₃ by reducing its size smaller than cycloidal period, i.e., 62 nm, and simultaneously doping of rare earth ions [9–12]. The nanostructures of BiFeO₃ possess excellent multiferroic properties [9–12,18].

In the present communication, Tb-doped BiFeO₃ nanoparticles have been synthesized by the sol-gel method. The effect of Tb-doping and the smaller size of synthesized nanoparticles on structural, magnetic and magnetoelectric coupling has been studied.

2. Experimental

Materials and synthesis: Bi_{1-x}Tb_xFeO₃ nanoparticles ($x=0, 0.05, 0.10$ and 0.15) have been synthesized by the sol-gel method [10]. The crystallographic analysis has been carried using an X-ray diffractometer of PANalytical X'PertPRO MRD (Cu-K α , $\lambda=1.54060$ Å). Transmission electron microscopy (TEM) has been carried out using Hitachi-H7650. The magnetization versus applied magnetic field ($M-H$) hysteresis loops measurement has been done using SQUID of Quantum Design. The dynamic lock-in technique has been employed to measure the direct magnetoelectric coupling (ME) coefficients [13,14].

3. Results and discussion

Crystallographic and morphological analysis: TEM images of pure and 15% Tb-doped BiFeO₃ nanoparticles (Fig. 1(a) and (b)) reveal that the average particle size of synthesized nanoparticles is 39 and 30 nm, respectively. The nanoparticles are found to be spherical, homogenous in size, well-dispersed and without any agglomeration. Rietveld refinement of XRD patterns has been performed

* Corresponding author. Tel.: +91 175 239 3343; fax: +91 175 236 4498.

E-mail addresses: gslotey1986@gmail.com, gsloteyz@gmail.com (G.S. Lotey).



Effect of Gd-substitution on the ferroelectric and magnetic properties of BiFeO₃ processed by high-energy ball milling



Shiwani Sharma^a, Alok Mishra^a, P. Saravanan^b, O.P. Pandey^a, Puneet Sharma^{a,*}

^a School of Physics and Materials Science, Thapar University, Patiala 147004, Punjab, India

^b Defence Metallurgical Research Laboratory, Hyderabad 500058, India

ARTICLE INFO

Article history:

Received 30 November 2015

Received in revised form

23 February 2016

Accepted 2 March 2016

Available online 3 March 2016

Keywords:

BiFeO₃

High-energy ball milling

Dielectric

Magnetization

ABSTRACT

Multiferroic BiFeO₃ was synthesized by means of high-energy ball milling (HEBM) followed by thermal annealing at various temperatures and the effect of Gd³⁺ substitution ($x=0.0-0.20$) at Bi³⁺ site was investigated in this study. It is found that the Gd-substitution tends to decrease the impurity phases and the crystallization of single phase BiFeO₃ is observed at $x=0.1$. Scanning electron micrograph of Bi_{1-x}Gd_xFeO₃ sintered sample indicated a decrease in particle size and change in shape with increasing x . For all the studied samples, the measured dielectric constant values tend to increase from 110 ($x=0.0$) to 250 ($x=0.10$). The dielectric loss is found to be more for the pure BiFeO₃ as compared to the Bi_{1-x}Gd_xFeO₃. Ferroelectric loops show a maximum polarization of 1.63 $\mu\text{C}/\text{cm}^2$ for the Bi_{0.9}Gd_{0.1}FeO₃. Magnetization (M) versus magnetic field (H) hysteresis loops at 300 K BiFeO₃ and Bi_{0.9}Gd_{0.1}FeO₃ demonstrated non-saturated loops, suggesting the antiferromagnetic nature of the samples. The $M-H$ behavior of the Bi_{1-x}Gd_xFeO₃ at 300 K shows the antiferromagnetic nature of the samples. The estimated magnetization value at 10 kOe for the Bi_{0.9}Gd_{0.1}FeO₃ sample (0.23 emu/g) is found to be higher than that of the pure BiFeO₃ (0.037 emu/g).

© 2016 Elsevier B.V. All rights reserved.

1. Introduction

Multiferroic materials have recently gained a considerable attention due to its multifunctional device applications and underlying new physics. Among the multiferroics, BiFeO₃ is one of the widely investigated materials due to its ferroelectric and magnetic transition temperature well above room temperature (RT) [1,2]. BiFeO₃ is known to possess rhombohedrally distorted perovskite structure that belongs to a space group of $R3c$. The unit cell of BiFeO₃ can be represented as pseudo cubic ($a_c=3.963 \text{ \AA}$); and hexagonal ($a_h=5.587 \text{ \AA}$, $c_h=13.867 \text{ \AA}$) structure, where the pseudo cubic direction $[111]_c$ is considered equivalent to $[100]_h$ [3]. Over the past several years, considerable efforts have been made to achieve both strong ferroelectric (FE) and ferromagnetic (FM) polarizations. Researchers have made a considerable progress on the processing and microstructural aspects of BiFeO₃ [4–6]. Similarly, efforts also have been made to substitute A site and B site of BiFeO₃ by rare earth and transition metal ions, respectively. Effect of metal ion substitution has been thoroughly investigated on the structural, electric and magnetic properties [7–9]. Mathe et al. observed a structural phase transition to orthorhombic at $x=0.6$

and triclinic at $x=0.8$ with La³⁺ substitution at Bi³⁺ site. All the samples showed dispersion in dielectric data. The variation of dielectric constant (ϵ') with temperature shows a broad peak that broadens with change in composition and shifts corresponding to frequency change reflecting relaxor-type behavior [10]. Palkar et al. studied the coexistence of ferroelectricity and ferromagnetism in Bi_{0.9-x}Tb_xLa_{0.1}FeO₃ powder samples ($0 < x < 0.3$) and these samples were found to exhibit high dielectric constant and magneto-electric coupling at RT [11]. The magnetoelectric coupling was evidenced by the increase of the dielectric constant with the increase of applied magnetic field (H). For Bi_{0.75}Ba_{0.25}FeO₃ with $H=8 \text{ kOe}$, the values of $[\epsilon_r(H) - \epsilon_r(0)]/\epsilon_r(0)$ were 1.7% and 1% at 80 and 300 K, respectively [12]. Fanggao et al. showed that substituting Gd³⁺ at Bi³⁺ site eliminates the impurity phases in BiFeO₃ ceramics; also the lattice constants a and c become smaller as the Gd³⁺ content is increased. A strong variation in the dielectric constant and loss has been observed by substitution of Gd [13]. Gd-substitution was found to induce structural phase transition from $R3c$ to $\text{Pn}2_1a$ at $x=0.1$ and further increase in x suppresses the spontaneous polarization (P_s) in Bi_{1-x}Gd_xFeO₃ resulting in a ferroelectric–paraelectric ($\text{Pn}2_1a \rightarrow \text{Pnma}$) phase transition around $0.2 < x < 0.3$ [14,15].

From the above, it is clear that the low level doping of rare earth at Bi³⁺ site can impart changes in the structure and brings a noticeable variation in the magnetic and electrical properties.

* Corresponding author.

E-mail address: puneet.sharma@thapar.edu (P. Sharma).



Self-trapped elliptical super-Gaussian beam in cubic–quintic media



Soumendu Jana^{a,*}, Ajitpal Singh^a, K. Porsezian^b, T. Mithun^b

^a School of Physics and Materials Science, Thapar University, Patiala 147004, India

^b Department of Physics, Pondicherry University, Puducherry 605014, India

ARTICLE INFO

Article history:

Received 21 April 2014

Received in revised form

28 June 2014

Accepted 28 June 2014

Available online 10 July 2014

Keywords:

Elliptical super-Gaussian beam

Cubic–quintic nonlinearity

Self-trapping

Spatial soliton

ABSTRACT

We find self-trapped propagation of elliptical super-Gaussian beam in cubic–quintic nonlinear media. The soliton beam preserves its shape and size during propagation in Kerr media. Both defocusing and focusing quintic nonlinearities are considered. In a cubic (focusing)–quintic (defocusing) media breather like beam propagation with intriguing beam width oscillation is observed. The influence of beam ellipticity, super-Gaussian nature and quintic nonlinearity on self-trapping has been studied. A formula for critical power for self-focusing has been derived and it readily agrees with the results obtained by variational method. In Kerr and focusing quintic media beam collapse occurs quicker for higher order super-Gaussian beam. The critical power of self-focusing in defocusing (focusing) quintic medium prominently increases (decreases) with increasing strength of quintic nonlinearity. This variation rate is greater for higher order super Gaussian beam. A beam with greater ellipticity requires larger power for self-trapping.

© 2014 Elsevier B.V. All rights reserved.

1. Introduction

Nonlinear optical beam propagation and consequent formation of spatial optical soliton has been a fascinating topic of both fundamental and applied research in nonlinear optics [1–4]. This area of research is highly active due to its versatility and potential application in optical communication, all-optical device fabrication and many other fields. Spatial optical solitons are optical beams confined in directions transverse to the propagation axis. In other words, they are optical beams of invariable or periodically fluctuating cross section. Owing to their additional degrees of freedom along transverse dimension spatial solitons are much more versatile over their temporal counterpart. Beyond optics, spatial solitons are familiar in mathematics (in fact, the idea of soliton was conceived from integrable system), mechanical engineering, fluid dynamics, thermodynamics, pattern formation, biology, etc. Even spatial solitons are available in nature. For example, the tsunami waves, sand dunes, some strange cloud formation, namely, ‘morning glory’ cloud or ‘rolling cloud’ [5]. However, the mechanism of such soliton formation is very complicated and topic of fundamental multidisciplinary research. Our topic of interest, i.e., optical spatial soliton, arises due to counter balance of self-diffraction with nonlinearity induced self-focusing in conservative media. They have been studied to address different aspects in various media that ranges from turbulent

atmosphere to media with higher order nonlinearity. Also, a wide variety of beam profile, starting from simple hyperbolic secant to complicated decentered elliptical Hermite–Gaussian beam (DEHGB) has been adopted [6–11]. Generally, Kerr media supports (1+1) D stable soliton of hyperbolic secant profile that encouraged the early stage research to adopt the aforesaid profile or more convenient Gaussian profile. However, soliton of similar forms can be expected for higher dimension too. Attempts have been made to explore the possibility of soliton formation with more complex beam profiles. Sinusoidal-Gaussian and hyperbolic–sinusoidal-Gaussian beam propagation has been studied in quadratic nonlinear media [6]. The propagation properties of cosh-Gaussian beams [7], Hermite cosh-Gaussian beams [8], elegant Hermite–cosh-Gaussian beams [9], Hermite cosine-Gaussian beams [10] and off-axial Hermite–cosh-Gaussian beams [11] have been widely studied. Self-focusing of necklace beams [12], self-trapped vector waves [13] and self-trapping, compression and decompression of Bessel beams has been studied in Kerr media [14]. A sinh-Gaussian beam propagating through Kerr medium eventually converts into sin-Gaussian type beam at low and moderate initial power [15]. Also transformation from cosh-Gaussian to flat-top beam has been achieved in cubic–quintic nonlinear media [16].

Laguerre–Gaussian (LG) beam Propagation has been studied in a local cubic–quintic nonlinear medium, using the variational approach [17]. Generation and propagation of two-dimensional vortex solitons, has been studied in presence of nonlocal focusing nonlinearity, where the nonlocality stabilizes the dynamics of an otherwise unstable vortex beam [18]. Stable spatiotemporal spinning solitons with internal vorticity in a bimodal system has also

* Corresponding author.

E-mail address: soumendu.jana@yahoo.com (S. Jana).



Size-dependent magnetic properties of calcium ferrite nanoparticles

Lavanya Khanna*, N.K. Verma

Nano Research lab, School of Physics and Materials Science, Thapar University, Patiala-147004, India

ARTICLE INFO

Article history:

Received 31 May 2012

Received in revised form

8 January 2013

Available online 19 February 2013

Keywords:

Nanotechnology

Nanocrystalline particles

Calcium ferrite

Nanocapsules

Magnetic behaviour

ABSTRACT

The union of nanotechnology with the other fields of science heralds the influx of many newer and better technologies, with the capability to revolutionize the human life. In the present work, calcium ferrite nanoparticles were synthesized by conventional sol–gel method and were characterised by X-ray diffraction, Transmission electron microscope, Vibrating sample magnetometer and Fourier transform infrared spectroscope. The synthesized nanoparticles were calcined at different temperatures and their magnetic behaviour was studied. The synthesized nanoparticles calcined at 900 °C were formed in the shape of capsules and exhibited mixed characteristics of ferrimagnetic and paramagnetic grains with magnetic saturation of 0.85 emu/g whereas nanoparticles calcined at 500 °C were spherical in shape and exhibited superparamagnetic characteristics with saturation magnetization of 37.67 emu/g.

© 2013 Elsevier B.V. All rights reserved.

1. Introduction

Ferrites are iron based oxides with technologically fascinating magnetic properties, making them a prominent category in magnetic materials. The ferrite particles in nano-regime with significant change of physical properties provide more advantages over the bulk ferrites [1]. With regards to the rapidly mounting field of nanotechnology, ferrite nanoparticles have been the core of extensive research pertaining to their widespread applications, be it biomedical, technological or industrial. Nanocrystalline particles of magnetic materials show substantially enhanced magnetic properties. The magnetic behaviour of ferrites is strongly influenced by the particle size [2]. As the particle size decreases below the critical diameter, the coercivity decreases due to thermal effects, which become dominant enough to demagnetize a previously saturated assembly of particles [3]. Ferrite nanocrystallites of Mn, Co, Ni, Mg, Zn, K, Ca have been synthesized by reverse micelle [4–7,2], co-precipitation method [8,9], sol–gel auto combustion [1], thermal decomposition [10] and polymeric precursor method [11].

The synthesis and formation mechanism of Ca-ferrite compounds in bulk form have been carried out using different methods such as polymeric precursor method [11], under controlled oxygen potentials [12], thermolysis [13] and with different molar ratios of precursors under varying temperatures [14]. Moreover, it has been reported that the phase transition in Ca-ferrite is related to Fe⁺³ high-spin/low-spin transition [15–18]. Ca-ferrite compounds so far have extensively been explored in the optical memory devices,

steel making industry (as deoxidizer, desulfuration, and dephosphorization) [14], pigment [11] and absorbent of hydrogen sulphide (H₂S) [12]. All the above mentioned studies have been carried out on bulk Ca-ferrites. Till date and to the best of our knowledge no report is available on the size-dependent properties of Ca-ferrite at nanoscale.

It is well known that reduction in size leads to drastic changes in properties of materials. Therefore, the structure and size of ferrite nanoparticles are the important parameters to study their magnetic behaviour. In this communication, we report the synthesis of Ca-ferrite nanoparticles by sol–gel method. The morphology, structure and magnetic properties of Ca-ferrites at nanoscale have been studied in order to gain information regarding their formation mechanism in the nano regime. Further, the effects of different calcination temperatures on their morphology, structure and magnetic properties have also been reported.

2. Materials and methods

2.1. Materials

All the chemicals used for synthesis were of analytical grade. Calcium nitrate (Ca (NO₃)₂ · 4H₂O), Ferric nitrate (Fe (NO₃)₃ · 9H₂O), and citric acid (C₆H₈O₇ · H₂O), were purchased from Loba Chemie, India and ethylene glycol was purchased from sdfine chemicals, India and were used without any further purifications.

2.2. Synthesis

Conventional sol–gel method was employed for the synthesis of calcium ferrite nanoparticles [11]. Metallic citrate polymerization using ethylene glycol is the basis of this process [11]. 1 M solution

* Corresponding author. Tel.: +91 175 239 3513;

fax: +91 175 236 4498/239 3002.

E-mail addresses: lavanshya@yahoo.co.in,

lavanya.khanna@thapar.edu (L. Khanna), nkverma@thapar.edu (N.K. Verma).



Gd-doped BiFeO₃ nanoparticles – A novel material for highly efficient dye-sensitized solar cells

Gurmeet Singh Lotey*, N.K. Verma

Nano Research Lab, School of Physics & Materials Science, Thapar University, Patiala 147 004, India

ARTICLE INFO

Article history:

Received 17 March 2013
In final form 19 April 2013
Available online 6 May 2013

ABSTRACT

This communication reports a novel idea on dye-sensitized solar cells (DSSCs) fabricated using Gd-doped BiFeO₃ nanoparticles with particle size between 26 and 30 nm. The effect of Gd-doping and smaller size of synthesized nanoparticles on the structural, morphological, optical and photo-electrochemical properties have been investigated. The high energy-conversion efficiency, 3.85%, has been achieved for 12% Gd-doped BiFeO₃ DSSCs, which is more than 100% higher than the undoped BiFeO₃. The possible origin of the observed performance of DSSCs has been explained on the basis of smaller size of the synthesized nanoparticles, doping of Gd and structural transformation with doping in BiFeO₃.

© 2013 Elsevier B.V. All rights reserved.

1. Introduction

The supply of clean, green and environment friendly energy to our society is a matter of great concern for the scientific communities, as the non-renewable resources such as gas, coal and oil are limited and for sure will run out with time [1,2]. Solar energy is one of the most promising alternative energy resources. Therefore, today much attention has been paid on dye-sensitized solar cells (DSSCs) in the both academic and industrial platforms as an alternative clean and green energy resource precisely because of their relatively high energy conversion efficiency, low production cost, low manufacturing toxicity, ease of fabrication and flexibility [2–9]. Advances in this field have been achieved by improving the energy conversion efficiency, by extensively studying the mechanism to enhance electron generation, injection or transfer to semiconductors and reduction in the charge recombination processes [2–6,9–20]. Nanostructured TiO₂ and ZnO are the most widely used photo-anode material for DSSCs [2–6,9,10]. The lots of efforts had paid to develop alternative new photo-anode materials such as ZnO [10,11], SnO₂ [12], Nb₂O₅ [13], BaTiO₃ [14]. The charge recombination at the electrode/electrolyte interface, low efficiency, stability and reproduction of results are the challenges [10–14]. Different approaches such as, coating of insulating layer or higher band gap materials [15,16], doping of secondary species [17,19], plasmonics [4,20], polymers [21] based have been employed to improve the electronic structure of semiconductors, which reduces electron–hole recombination rate and enhances efficiency [2–21]. The main passion for above said research activities is to develop

alternative photo-electrode materials with improve overall energy conversion efficiency [2–6,8–21].

BiFeO₃ is direct energy band-gap (2.2–2.8 eV) semiconductor, chemically stable with high electron mobility and non-toxic [22–27]. It is well known multiferroic material possessing simultaneously ferroelectricity, ferromagnetism or ferroelasticity in a single phase [22]. Recently, it has been reported that BiFeO₃ thin film based-diode showing photovoltaic effects [28–30]. More, importantly BiFeO₃ nanostructures are possessing interesting photocatalytic activity in the visible region [22–27]. Joshi et al. suggested that BiFeO₃ nanostructures can be used as photo-electrode material for DSSCs [24]. The above said properties, photocatalytic behavior and Joshi et al. [24] suggesting superior photo-voltaic properties of BiFeO₃ nanostructures. This has been the motivation for the present study, to utilized rare earth-doped BiFeO₃ nanostructures as photo-anode material in DSSCs.

In this communication, thus, for the first time, we introduce Gd-doped BiFeO₃ nanoparticles – a novel material employed as a photo-anode for developing efficient DSSCs. Synthesis of Gd-doped BiFeO₃ nanoparticles has been done by sol–gel method. The effect of Gd-doping and smaller size of synthesized nanoparticles on structure, optical and photo-electrochemical properties have been studied.

2. Experimental

2.1. Materials and synthesis

Undoped and Gd-doped BiFeO₃ nanoparticles (Bi_{1-x}Gd_xFeO₃ with $x = 0, 0.04, 0.08, \text{ and } 0.12$) have been synthesized by sol–gel method [31,32]. In typical synthesis procedure, the analytical grade Bi(NO₃)₂·5H₂O, Fe(NO₃)₃·9H₂O and Gd(NO₃)₃·3H₂O, in

* Corresponding author. Fax: +91 175 236 4498.

E-mail addresses: gslotey1986@gmail.com, gsloteyz@gmail.com (G.S. Lotey).



Room temperature investigations on optical and magnetic studies of $\text{Co}_x\text{Zn}_{1-x}\text{S}$ nanorods

Sunil Kumar^{a,b,*}, N.K. Verma^a

^a Nano Research Lab, School of Physics and Material Science, Thapar University, Patiala-147004, Punjab, India

^b Department of Physics, Indus International University, Una-174301, Himachal Pradesh, India



ARTICLE INFO

Article history:

Received 13 June 2014

Received in revised form

12 August 2014

Available online 16 September 2014

Keywords:

Nanorods

Dilute magnetic semiconductors

Blue-shift

Ferromagnetism

ABSTRACT

In this report, structural optical and magnetic properties of $\text{Co}_x\text{Zn}_{1-x}\text{S}$ ($x=0, 0.01, 0.05$ and 0.1) nanorods have been investigated at room temperature. The average diameter and length of as synthesized nanorods, analyzed using transmission electron microscopy (TEM), are ~ 10 nm and ~ 100 nm, respectively. The crystal structure of $\text{Co}_x\text{Zn}_{1-x}\text{S}$ nanorods, studied using X-ray diffraction (XRD), indicates wurtzite structure with lattice parameters, $a=3.84$ Å and $c=6.25$ Å for $\text{Co}_x\text{Zn}_{1-x}\text{S}$ ($x=0$) nanorods which are found decreased with increased Co concentration in ZnS lattice. The band gap of Co-doped ZnS nanorods has been found to be blue shifted as compared to the undoped counterpart. Emission spectra indicate two peaks at 422 nm and 485 nm. Emission intensity increases in case of $\text{Co}_x\text{Zn}_{1-x}\text{S}$ ($x=0.01, 0.05$) nanorods, and quenches in $\text{Co}_x\text{Zn}_{1-x}\text{S}$ ($x=0.1$) nanorods. The ferromagnetization has been observed in case of Co-doped ZnS nanorods, whereas, undoped ZnS nanorods exhibit mixed diamagnetic-ferromagnetic behavior. The magnetization increases with increased Co concentration.

© 2014 Elsevier B.V. All rights reserved.

1. Introduction

In the recent times, there has been a tremendous interest in the research on transition metals doped chalcogenide nanomaterials. The new kinds of materials developed are more popularly known as dilute magnetic semiconductors (DMS). DMS materials exhibit optical and magnetic behavior due to charge and spin controllability [1]. These materials exhibit unique optical as well as magnetic properties at nanoscale. Due to its wide band gap, ZnS has been an attractive material as it acts as a good host for transition metals. The transition metals doped ZnS nanostructures have wide variety of applications in area of spintronics, solar cells, light emitting diodes, magnetic resonance imaging (MRI), lasers [2–7] etc. Bhargawa et al., attempted first time with Mn-doped ZnS nanocrystals to explore the optical properties of ZnS based DMS nanostructures [8]. Since then, a lot of research has been focused on the structural, optical and magnetic studies of transition metals doped ZnS nanostructures. The one dimensional (1-D) nanostructures or nanorods can be specifically used in variety of applications due to unique quantum confinement effects. Generally, the properties of materials are size and shape dependent; hence transition metals doped 1-D nanostructures can be useful as fundamental building blocks for fabricating the advanced nanoscale inter connecting electronic and optoelectronic devices. Various studies on

photoluminescence and magnetic properties [9–14] of transition metals-doped ZnS nanostructures are available in literature, however, very few reports have been found on Co-doped ZnS nanorods. Lu et al. [15] reported the structural and magnetic behavior of Co-doped ZnS nanowires. It was observed that the Co-doped ZnS nanowires exhibit ferromagnetism at room temperature and ferromagnetism increases as the Co concentration is increased. Sambavisham et al. [16] reported temperature dependent induced magnetism in Co-doped ZnS nanoparticles at room-temperature. In this study, magnetic hysteresis was observed at room temperature and the magnetization reduces with increased Co concentration. Patel et al. have reported the grain boundaries induced magnetization at room temperature in Co-doped ZnS thin films [17]. Synthesizing high quality ZnS nanorods using ethylenediamine (EN), a bidentate ligand, is a difficult task as it leads to the formation of ZnS-EN complex [18]. Hence, to synthesize high quality ZnS nanorods a mixture of water and EN (1:1) is used.

In this report we have tried to analyze the structural, optical and magnetic behavior induced in Co-doped ZnS nanorods.

2. Experimental details

2.1. Synthesis

All the chemicals are of analytical grade and were used without any further purification. Zinc acetate was used as a source of Zn, thiourea as a source of sulphur, and cobalt chloride as source of Co. A mixture of water and EN as solvent (1:1) has been used as solvent. For

* Corresponding author at: Nano Research Lab, School of Physics and Material Science, Thapar University, Patiala-147 004, Punjab, India. Tel.: +91 175 239 3039.
E-mail address: skt_nano@yahoo.co.in (S. Kumar).



Swift heavy ion induced modifications of single walled carbon nanotube thin films



Vishalli ^{a,*}, K.K. Raina ^b, D.K. Avasthi ^c, Alok Srivastava ^d, Keya Dharamvir ^a

^a Department of Physics, Panjab University, Chandigarh 160014, India

^b Materials Research Laboratory, School of Physics and Materials Science, Thapar University, P.O. Box 32, Patiala 147004, Punjab, India

^c Materials Science Group, Inter University Accelerator Centre, Aruna Asaf Ali Marg, P.O. Box 10502, New Delhi 110067, India

^d Department of Chemistry, Panjab University, Chandigarh 160014, India

ARTICLE INFO

Article history:

Received 28 November 2015

Received in revised form 8 January 2016

Accepted 15 February 2016

Available online 1 March 2016

Keywords:

Single walled carbon nanotubes

Langmuir Blodgett method

Ion irradiation

Raman spectroscopy

Optical absorption spectroscopy

ABSTRACT

Thin films of single walled carbon nanotubes (SWCNTs) were prepared by Langmuir–Blodgett method and irradiated with swift heavy ions, carbon and nickel each of energy 60 MeV. The ion beams have different electronic energy loss (S_e) values and the samples were exposed to various irradiation doses. The irradiated films were characterized using Raman and optical absorption spectroscopy. Raman spectroscopy results indicate the competing processes of defect creation and healing (annealing) of SWCNTs at lower fluences, while at higher fluences defect creation or damage dominates. In UV–Vis–NIR spectroscopy we find that there is decrease in the intensity of characteristic peaks with every increasing fluence, indicating decrease in the optically active states with irradiation.

© 2016 Elsevier B.V. All rights reserved.

1. Introduction

Carbon nanotubes (CNTs) have some remarkable physical properties which make them potential candidates for applications in various fields [1–3]. They are sensitive to various kinds of radiation, and have been proposed for different applications. CNTs can be used in nanosensors and nanodevices [4,5] in high radiation environment, such as in outer space. Due to their radiation stability, CNTs can also be used as radiation shields in nuclear reactors [6]. Irradiation causes defects on the surface of CNTs which give rise to various types of structural modifications such as welding and bending [7,8], formation of nanocompartments [9], transformation of single walled nanotubes to multi-walled carbon nanotubes [10], reordering, healing of the system [10–14].

In recent times the effect of swift heavy ions (SHIs; heavy ions with energy of the order of MeV/nucleon) on the CNTs has been extensively studied [14–16]. The SHIs lose energy mainly to the electronic subsystem, which leads to excitation or ionization of atoms in the material. This huge amount of energy in small cylindrical volume surrounding the ion trajectory leads to various kinds of structural modifications in the materials. These structural changes alter their electrical, magnetic and optical properties

[17,18]. Thus irradiation by SHIs can also be used as a tool to tailor the structure as well as other related properties.

In the present study, investigations have been made upon the changes in thin films of single walled carbon nanotubes (SWCNTs) irradiated by SHIs. Uniform thin films of SWCNTs were deposited on quartz substrate by Langmuir Blodgett (LB) method. In this method deposition is done in a layer by layer manner. By using this method we have attempted to get a uniform thin film. The deposited films were irradiated with carbon and nickel ion beams each of energy 60 MeV. A systematic detailed analysis of Raman spectroscopy of these films has been carried out. The effect on the optical absorption properties has also been studied. The characterization results for both the beams have been compared.

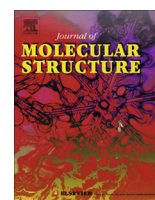
2. Experimental

2.1. Preparation of the samples

SWCNTs functionalized with octadecylamine (ODA) (Sigma Aldrich; diameter = 2–10 nm; length = 0.5–2 μm) have been used for this study. The long chain ODA gets attached to the ends and defect sites of SWCNTs, which helps in the exfoliation of bundled nanotubes to individual ones by overcoming the Van der Waals forces between them [19,20]. Thin films of SWCNTs were deposited on quartz substrate by Langmuir Blodgett (LB) method [21]. Using

* Corresponding author.

E-mail address: vishalli_2008@yahoo.com (Vishalli).



Structural and optical properties of $\text{Bi}_{1-x}\text{A}_x\text{FeO}_3$ (A = Sr, Ca; $0.40 \leq x \leq 0.55$)



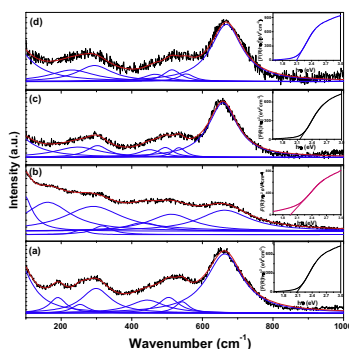
Samita Thakur, O.P. Pandey, K. Singh*

School of Physics & Materials Science, Thapar University, Patiala 147004, India

HIGHLIGHTS

- $\text{Sr}^{2+}/\text{Ca}^{2+}$ substituted BiFeO_3 are synthesized and characterized.
- Substitution has profound effect on structural and optical properties.
- $\text{Bi}_{0.45}\text{Sr}_{0.55}\text{FeO}_3$ exhibits lowest optical band gap.

GRAPHICAL ABSTRACT



ARTICLE INFO

Article history:

Received 28 January 2014

Received in revised form 25 May 2014

Accepted 26 May 2014

Available online 9 June 2014

Keywords:

Raman spectroscopy
Iodometric titration
Oxygen vacancies
Optical properties

ABSTRACT

The effect of Sr^{2+} and Ca^{2+} cation substitution on BiFeO_3 -type ($\text{Bi}_{1-x}\text{A}_x\text{FeO}_3$; A = Sr, Ca; $0.40 \leq x \leq 0.55$) ceramics are investigated for structural and optical properties. X-ray diffraction patterns confirmed that $\text{Ca}^{2+}/\text{Sr}^{2+}$ substitution facilitates the formation of tetragonal phase instead of rhombohedral phase as observed in undoped BiFeO_3 (BFO). The iodometric titration results show that substitution of Sr^{2+} has higher tendency to form oxygen vacancies than Ca^{2+} substituted samples. On the other hand, Ca^{2+} substitution shows opposite trend. The FT-IR and Raman spectra show shift in the peak positions towards higher wavenumber and diffused bands with the increasing concentration of substituent. The parameters like band gap energy, Urbach energy has been calculated from the UV-visible spectra. Sr^{2+} substituted samples show higher structural distortion and low optical band gap values which can be correlated to the higher oxygen vacancies and low Fe^{4+} content as compared to Ca^{2+} substituted samples.

© 2014 Elsevier B.V. All rights reserved.

Introduction

Among various multi-ferroic materials, undoped and doped BiFeO_3 (BFO) is widely studied compound due to simultaneous existence of ferro-electricity with Curie temperature of 830 °C and anti-ferromagnetism with Neel's temperature of 370 °C [1–3]. In addition to multi-ferroic properties, BFO can also be used in variety of devices because of its interesting optical and photocat-

alytic properties [4,5]. However, undoped BFO exhibits secondary phase as an impurity which restricts its applications. The formation of secondary phase can be suppressed by proper doping at A and B or both the sites of BiFeO_3 (ABO_3) [6,7]. Thus, the main focus of most studies is on the use of dopants such as rare earth metals, transition metals and alkaline earth metals to improve the different properties of BFO. Doping at both sites (A and B sites) gives rise to oxygen non-stoichiometry and conversion of Fe^{3+} into $\text{Fe}^{2+}/\text{Fe}^{4+}$ to maintain the charge neutrality of the system. The aliovalent substitution such as Ba^{2+} , Pb^{2+} , Sr^{2+} and Ca^{2+} at bismuth site creates oxygen vacancies and transforms Fe^{3+} to Fe^{4+} . It will affect the

* Corresponding author. Tel.: +91 1752393130; fax: +91 1752393005.

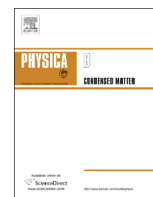
E-mail address: kusingh@thapar.edu (K. Singh).



ELSEVIER

Contents lists available at [SciVerse ScienceDirect](http://SciVerse.ScienceDirect.com)

Physica B

journal homepage: www.elsevier.com/locate/physb

PEG/CaFe₂O₄ nanocomposite: Structural, morphological, magnetic and thermal analyses

Lavanya Khanna*, Narendra K. Verma

Nano Research Lab, School of Physics and Materials Science, Thapar University, Patiala, Punjab 147004, India

ARTICLE INFO

Article history:

Received 1 December 2012

Received in revised form

9 May 2013

Accepted 29 May 2013

Available online 18 June 2013

Keywords:

Calcium ferrite nanoparticles

PEG

PEG coated calcium ferrite nanoparticles

Nanocomposite

Superparamagnetic

ABSTRACT

The coating of Polyethylene Glycol (PEG) on calcium ferrite (CaFe₂O₄) nanoparticles has been reported in the present study. The X-ray diffraction pattern revealed the formation of orthorhombic structure of bare CaFe₂O₄ nanoparticles, which was also retained after the PEG coating, along with additional characteristic peaks of PEG at 19° and 23°. The rings of CaFe₂O₄ nanoparticles were identified by the selected area electron diffraction pattern. The characteristic bands of PEG as observed in its Fourier transform infrared spectrum were also present in PEG coated CaFe₂O₄ nanoparticles, hence confirming its presence. In the thermal gravimetric studies, the complete thermal decomposition of PEG occurred in a one step process, but in case of PEG coated CaFe₂O₄ nanoparticles, the decomposition took place at a higher temperature owing to the formation of covalent bonds of PEG with CaFe₂O₄ nanoparticles. The presence of PEG on CaFe₂O₄ nanoparticles, spherical formation of PEG coated CaFe₂O₄ nanoparticles and reduced agglomeration in the CaFe₂O₄ nanoparticles were revealed by high resolution transmission electron microscope, transmission electron microscope and scanning electron microscope studies, respectively. In vibrating sample magnetometer analysis, both bare as well as coated CaFe₂O₄ nanoparticles exhibited superparamagnetic behavior. However, a drop in the magnetic saturation value was observed from 36.76 emu/g for CaFe₂O₄ nanoparticles to 6.74 emu/g for PEG coated CaFe₂O₄ nanoparticles, due to the formation of magnetically dead layer of PEG. In ZFC and FC analyses, superparamagnetic behavior with blocking temperature for bare and coated nanoparticles has been observed at ~40 K and ~60 K, respectively. The increase in the blocking temperature is attributed to the increase in the particle size after PEG coating.

© 2013 Elsevier B.V. All rights reserved.

1. Introduction

The research on magnetic nanoparticles is proceeding at an accelerated pace owing to their distinctive optical, electronic, surface and magnetic properties, leading to various inter-disciplinary technological applications ranging from information storage, materials science to biomedicine [1]. In context to biomedical applications, Fe₃O₄ [2–4], NiFe₂O₄ [2,5,6], MnFe₂O₄ [7,8], CoFe₂O₄ [1,9,10], and ZnFe₂O₄ [2] nanoparticles have been studied. The ferrites of Ni, Mn, Co, Zn although possess good magnetic properties, their inherent toxicity diminishes their credibility. This elevates concerns on their biocompatibility and further on their effectiveness for biomedical applications. Ferrites of calcium are expected to be more biocompatible since calcium is inherently non-toxic. In our earlier work, the formation of calcium ferrite nanoparticles at different calcination temperatures has been studied [11]. In literature, the reports on calcium ferrite compounds in bulk form are available, where they have been explored in the optical memory devices, steel making industry (as deoxidizer, desulfuration, and dephosphorization) [12], as

pigment [13] and absorbent of hydrogen sulfide (H₂S) [14]. Not much has been explored about calcium ferrite in the nano-regime.

There are some other major factors that influence the fate of the nanoparticles. Pertaining to high surface energy and magnetic interactions of the magnetic nanoparticles, they have the tendency to agglomerate. When the nanoparticles agglomerate, they adsorb plasma proteins and are quickly cleared by the macrophages in the Reticuloendothelial system (a part of the immune system of the human body) before reaching the target cells [15]. The body instead of allowing them to work efficiently recognizes them as a foreign entity and removes them. This reduces the circulation time of nanoparticles in the blood stream. Polymer coating reduces agglomeration and so helps in evading the Reticuloendothelial system. The agglomeration results in clogging of the capillaries, this can be avoided by polymer coating of the nanoparticle surface. The surface inertness of nanoparticles restricts the number of molecules to be bio-conjugated with them [16,17]. The polymer coating facilitates the selective binding of the biological entities, thus enables more functional groups to be attached to the ferrite surface. The corrosion of the ferrite surface is prevented by coating and makes it more biocompatible. Also, the polymer coating effectively shields the surface charge of nanoparticles to disperse them in suspensions.

In the light of the above, the formation of magnetic polymer nanocomposite (magnetic core with a polymer coating on its surface

* Corresponding author. Tel.: +91 175 2393513x3343;

fax: +91 175 2364498, +91 175 2393002.

E-mail addresses: lavanshya@yahoo.co.in, lavanya.khanna@thapar.edu (L. Khanna), nkverma@thapar.edu, nkverma.thapar@gmail.com (N.K. Verma).



Surface scaling evolution and dielectric properties of sputter-deposited low loss Mg₂SiO₄ thin films



Chan Su Han, Bhaskar Chandra Mohanty^{*}, Hong Rak Choi, Yong Soo Cho^{**}

Department of Materials Science and Engineering, Yonsei University, Seoul 120-749, Republic of Korea

ARTICLE INFO

Available online 3 August 2012

Keywords:

Mg₂SiO₄
Magnetron sputtering
Dielectrics
Surface scaling

ABSTRACT

The evolution of surface roughness and dielectric properties of sputter-deposited Mg₂SiO₄ thin films have been studied. Analysis of height–height correlation function and power spectrum densities of the atomic force microscope images revealed that the growth surface experiences a difference in short-range and global roughening, indicating an anomalous scaling (super-rough) behavior. The growth exponent $\beta = 0.9$ suggests that the growth instability due to the shadowing far outweighs the effects of a high substrate temperature (700 °C). The dielectric loss tangent showed a pronounced dependence on deposition time, while dielectric constant remained unchanged at the bulk value; the changes in the grain structure via the evolution of surface scaling are suggested as a contributing factor.

© 2012 Elsevier B.V. All rights reserved.

1. Introduction

In recent years, nonconventional dielectric thin films have received significant attention for their potential in upcoming high frequency applications such as high speed LAN, intelligent transport systems, point-to-point telecommunication, etc. [1,2]. The key requirements for such applications include high frequency selectivity and stability, low power dissipation, and reduced delay time of electronic signal transmission, which has demanded engineering of thin films with exceptionally low dielectric loss ($\tan \delta$) as well as low dielectric constant (ϵ). Among the few candidates, α -Mg₂SiO₄ (forsterite) offers unique advantages from its low electrical conductivity, competitive dielectric properties and high tunability, as evidenced from the recent report of a Qf value as high as 270,000 GHz for the bulk forsterite [3–5]. In thin films, however, the dielectric properties can be substantially different from that of the bulk counterpart, arising due to various aspects of microstructure, interface between the electrode and thin film, residual stress, etc. [6–8]. Typically, thickness of the dielectric thin films has been identified to significantly affect all of the above features, and thus the values of both ϵ and $\tan \delta$ [8,9].

On the other hand, the increase in film thickness leads to an evolution of surface roughness during growth of the films [10]. The surface roughening process is quite predominant in the initial stages of film growth (extending up to several hundred nanometers of thickness, which is of practical interest) and affects various, for example, electrical, optical, and tribological properties of the films. The kinetic roughening

of the surface growth front follows from the competition between various roughening and smoothing mechanisms depending upon the process parameters [10]. Therefore, from a study of the surface roughness evolution versus deposition time (thickness), one can gain insight into growth mechanisms appropriate to the deposition process, and their influence on various properties of the films. Thus, such a study has tremendous technological implications and forms the basis of this work. The present study aims at understanding the evolution of the surface roughness and the dielectric properties of the Mg₂SiO₄ thin films grown by RF magnetron sputtering. We show that the surface width scaled differently at short-range and long range scales (anomalous scaling behavior). Concurrently and more importantly, the dielectric loss showed a pronounced dependence on the deposition time, while the dielectric constant remained surprisingly constant.

2. Experimental

The Mg₂SiO₄ thin films were grown on Pt(111)/Ti/SiO₂/Si(100) substrates at 700 °C by rf magnetron sputtering from a two-inch α -Mg₂SiO₄ ceramic target of purity 99.99% (LTS Chemical Inc.). The substrates were tilted by an angle of $\sim 45^\circ$ with respect to the target normal and the distance between the centers of substrate and the target was ~ 6 cm. The substrates were rotated at 7 RPM about their axes during sputtering. Prior to loading into the deposition chamber, the substrates were ultrasonic-cleaned sequentially with acetone, isopropyl alcohol, and ethyl alcohol anhydrous each for 10 min. The sputtering chamber was evacuated to a base pressure of 5×10^{-6} Torr using a turbomolecular pump backed by a rotary pump and a constant working pressure of 10 mTorr was maintained by allowing an argon–oxygen gas mixture (Ar/O₂: 30/10) through mass-flow controllers. Films of different growth times (15–150 min) were deposited at a rf power of 200 W.

^{*} Corresponding author.

^{**} Corresponding author. Tel.: +82 2 2123 5848; fax: +82 2 365 5882.

E-mail addresses: bhaskarmohanty@gmail.com (B.C. Mohanty), ycho@yonsei.ac.kr (Y.S. Cho).



Lateral grain size effect on exchange bias in polycrystalline NiFe/FeMn bilayer films

Jen-Hwa Hsu^a, An-Cheng Sun^b, Puneet Sharma^{c,*}

^a Department of Physics, National Taiwan University, Taipei, 106, Taiwan

^b Department of Chemical Engineering & Materials Science, Yuan Ze University, Chung-Li, 32003, Taiwan

^c School of Physics and Materials Science, Thapar University, Patiala, 147004, India

ARTICLE INFO

Article history:

Received 23 August 2012

Received in revised form 19 June 2013

Accepted 20 June 2013

Available online 2 July 2013

Keywords:

Exchange bias

Interfacial grain size

Thin films

ABSTRACT

This study explores the effect of lateral grain size on the exchange bias in the magnetron sputtered NiFe(5 nm)/FeMn(20 nm) bilayer films. The thicknesses of ferromagnetic (NiFe) and antiferromagnetic (FeMn) layers were kept constant in the study. The lateral grain size variation was induced by increasing Ta buffer layer thickness. The cross-sectional transmission electron microscopy revealed that bilayers deposited on thicker Ta buffer layers have larger lateral grain diameter. Grain-to-grain epitaxy from buffer layer controls lateral grain size at NiFe/FeMn interface. A large increase in exchange bias field was observed with increasing thickness of Ta buffer layer, which is attributed to the enhanced ferromagnetic/antiferromagnetic coupling originated from larger interface lateral grain area.

© 2013 Elsevier B.V. All rights reserved.

1. Introduction

The characteristics feature of exchange coupling between ferromagnetic (FM)/antiferromagnetic (AFM) layers is the shift of hysteresis loop from the centre, known as exchange bias (EB) effect [1]. For about two decades, there has been considerable interest in exchange-biased FM films because the shift can be utilized in controlling the magnetization in spin-valve devices, which sense changing magnetic fields through the giant magnetoresistance effect [2].

Among various exchange-coupled systems, the exchange-coupled polycrystalline FM/AFM bilayer films are the most widely studied [3,4]. Since the EB is considered to be interface phenomenon, the immediate questions that prompt in polycrystalline bilayer films are the influence of grain size, morphology, and orientation on the EB. All these factors, however, show strong dependence on the FM/AFM thicknesses and the deposition conditions. To understand the effect of aforementioned parameters several experimental studies were carried out and various theoretical models have been invoked [5–13]. However, the microscopic origin is not yet clear. One of the unresolved issue is the effect of grain size, which strongly affects the EB. It is reported that the EB is large for smaller grain size and vice versa [13,14].

The established approaches to vary grain size are by varying the FM and AFM layer thickness, deposition conditions etc. However, due to interdependence of thickness, grain size, texture and roughness, it is difficult to separate out the individual effect. Reviewing the previous works on the thickness variation of FM layer, the large

EB was found in 3–7 nm thick films [4]. The EB was found to decrease for any further increase in the thickness of FM layer EB. In contrast to the effect of FM layer thickness, EB initially increases with the AFM thickness and then become constant [5]. This effect of thickness variation on EB is considered as grain size effect as it varies with thickness. Since exchange bias is considered as an interface phenomenon therefore, the lateral grain size may affect EB. Indeed increasing FM/AFM film thickness increases the grain size, however the film texture, grain orientation, and interface roughness simultaneously varies and affects the EB.

In order to understand the grain size effect, lateral grain size variation is imparted in identical NiFe(5 nm)/FeMn(20 nm) bilayers films by depositing on Ta underlayer with different grain sizes. Larger Ta grain may promote larger lateral grain area at NiFe/FeMn interface and the interface coupling.

2. Experimental details

In the present investigation, Ta(t nm)/NiFe(5 nm)/FeMn(20 nm) film with varying Ta thickness ($t_{Ta} = 5–50$ nm) were deposited on glass substrate by conventional direct current magnetron sputtering. The root mean square surface (RMS) roughness of the glass substrates were 0.20 ± 0.02 nm. Prior to deposition the base pressure was less than 7×10^{-5} Pa. Ar gas pressure was maintained at 0.27 Pa. To achieve the uniform film thickness, the substrate holder was rotating at ten revolutions per minute during deposition. The deposition rates for all layers were set at ≈ 0.1 nm/s. In order to produce unidirectional anisotropy, a magnetic field of $300(10^3(4\pi)^{-1}) \text{ Am}^{-1}$ was applied during deposition. No post deposition field annealing was carried out.

* Corresponding author. Tel.: +91 1752393116.

E-mail address: puneet.sharma@thapar.edu (P. Sharma).



Study of $0.1\text{Ni}_{0.8}\text{Zn}_{0.2}\text{Fe}_2\text{O}_4 - 0.9\text{Pb}_{1-3x/2}\text{La}_x\text{Zr}_{0.65}\text{Ti}_{0.35}\text{O}_3$ magnetoelectric composites

Rekha Rani ^{a,d}, J.K. Juneja ^{b,*}, Sangeeta Singh ^c, K.K. Raina ^d, Chandra Prakash ^{e,1}

^a Electroceramics Research Laboratory, GVM Girls College, Sonapat 131001, India

^b Department of Physics, Hindu College, Sonapat 131001, India

^c Department of Physics, GVM Girls College, Sonapat 131001, India

^d School of Physics and Material Sciences, Thapar University, Patiala 147004, India

^e Directorate of ER&IPR, DRDO, DRDO Bhawan, New Delhi 110105, India

ARTICLE INFO

Article history:

Received 5 July 2012

Received in revised form

21 July 2012

Available online 15 August 2012

Keywords:

Dielectric properties

Electric polarization

Magnetization

Poling

Magnetoelectric composite

ABSTRACT

Magnetoelectric composites of nickel zinc ferrite (NZF) and La substituted lead zirconate titanate (PLZT) having representative formula $0.1\text{Ni}_{0.8}\text{Zn}_{0.2}\text{Fe}_2\text{O}_4 - 0.9\text{Pb}_{1-3x/2}\text{La}_x\text{Zr}_{0.65}\text{Ti}_{0.35}\text{O}_3$ ($x=0, 0.01, 0.02$ and 0.03) were synthesized by a conventional solid state route. X-ray diffraction analysis was carried out to confirm the coexistence of individual phases. Scanning electron microscope micrographs were taken for microstructural study of the samples. Dielectric properties were studied as a function of temperature and frequency. To study ferroelectric and magnetic ordering in composite samples, $P-E$ and $M-H$ hysteresis loops were recorded respectively. $M-H$ hysteresis loops were taken for electrically poled and unpoled samples to confirm magnetoelectric coupling between the two phases (NZF and PLZT). La substitution results in significant improvement in dielectric, ferroelectric and piezoelectric properties of composite samples.

© 2012 Elsevier B.V. All rights reserved.

1. Introduction

The area of magnetoelectric (ME) materials has attracted many researchers from both groups (ferroelectricity and magnetism) because these materials exhibit ferroelectric and ferromagnetic/ferrimagnetic properties of matter. These materials have potential applications in many multifunctional devices such as magnetic field sensors, multiple state memory elements, transducers, electro-optic devices, filters, oscillators and phase shifters [1–6]. The ME effect in these materials is defined as an induced electric polarization in external magnetic field or an induced magnetization in external electric field. These materials are classified into two groups: single phase and two phase (composites). Single phase ME materials have coexistence of ferroelectric and magnetic orders in single phase and exhibit direct ME coupling. Though the experimental evidences of ME effect in single phase systems were observed during the first half of 20th century the materials showing ME coupling were found to be rare due to some limiting factors which restrict the coexistence of ferroelectricity and magnetism in a single phase [7,8]. Two phase systems exhibit indirect coupling between ferroelectricity and magnetism. This indirect coupling takes place via stress and results in magnetostriction induced deformation and the generation of piezoelectric charge [9–12] i.e. one phase should be magnetostrictive or

piezomagnetic and other should be piezoelectric or electrostrictive. The most widely studied systems that have been reported correspond to substituted NiFe_2O_4 , CoFe_2O_4 , MnFe_2O_4 , ZnFe_2O_4 , Terfenol, etc. with substituted PZT, PMN-PT, PVDF and BaTiO_3 [13].

For the present work, bulk composites of Ni–Zn ferrite and La substituted PZT with general formula $0.1\text{Ni}_{0.8}\text{Zn}_{0.2}\text{Fe}_2\text{O}_4 - 0.9\text{Pb}_{1-3x/2}\text{La}_x\text{Zr}_{0.65}\text{Ti}_{0.35}\text{O}_3$ ($x=0, 0.01, 0.02$ and 0.03) were synthesized by a conventional solid state reaction route. The presented composites are ferroelectric rich ferrite–ferroelectric composites with small content (10%) of the ferrite phase. The reason is that composites with higher ferrite content show lossy $P-E$ loops due to high conductivity of ferrite phase as compared to that for ferroelectric phase and are also difficult to pole. Higher value of ferrite content also results in lower ME output due to the leakage charges developed in the ferroelectric grains which reduces the charges generated during the ME effect [14,15]. Further, La content (x) in ferroelectric phase was selected from 0 to 0.03 which can be attributed to the fact that for higher La content in PZT, the disordering effect of La becomes important, resulting in considerable decrease in values of remanant polarization (P_r) and saturation polarization (P_s) [16,17].

2. Experimental work

2.1. Material synthesis

The ferrite phase was prepared using AR grade NiO, ZnO and Fe_2O_3 . The powder mixture was ball milled, dried and then

* Corresponding author. Tel.: +919416260242.

E-mail addresses: jk_juneja@yahoo.com (J.K. Juneja), cpakash@hqr.drdo.in (C. Prakash).

¹ Tel.: +91 11 2300 7350; fax: +91 11 2301 7582.



Estimation of particle magnetic moment distribution for antiferromagnetic ferrihydrite nanoparticles



Chandni Rani, S.D. Tiwari*

School of Physics and Materials Science, Thapar University, Patiala 147004, India

ARTICLE INFO

Article history:

Received 21 March 2014

Received in revised form

2 February 2015

Accepted 21 February 2015

Available online 23 February 2015

Keywords:

Nanoparticle

Superparamagnetism

Magnetization

Susceptibility

ABSTRACT

Magnetization as a function of applied magnetic field at different temperatures for antiferromagnetic nanoparticles of ferrihydrite is measured and analyzed considering a distribution in particle magnetic moment. We find that the magnetization of this nanoparticle system is affected by the presence of particle magnetic moment distribution. This particle magnetic moment distribution is estimated at different temperatures.

© 2015 Elsevier B.V. All rights reserved.

1. Introduction

People have been working on small particles of magnetic materials for last several decades due to their potential applications and interesting behavior [1–3]. One of the properties that makes the magnetic nanoparticles unique is superparamagnetism. Sufficiently small particles of ferro and ferrimagnetic materials are expected to show the superparamagnetic behavior [2]. Long back Néel suggested that small particles of antiferromagnetic materials should also exhibit magnetic properties such as superparamagnetism [3]. The magnetization of a bulk antiferromagnetic crystal is expected to be zero in absence of any external magnetic field at 0 K. However if the surface to volume ratio, which increases with decreasing particle size, for an antiferromagnetic particle is made sufficiently large then it can have a nonzero net magnetic moment due to an imperfect cancellation of atomic moments near the surface of the particle. A lot of work have been reported on the magnetic behavior of small particles of ferro and ferrimagnetic materials. Nanoparticles of antiferromagnetic materials have also gained sufficient attention from researchers mainly due to surprising and unusual behavior exhibited by them. Among different antiferromagnetic nanoparticle systems, NiO [4–9], ferritin [10–12] and ferrihydrite [13–17] are comparatively more interesting and well-studied systems.

The magnetization of ferro and ferrimagnetic nanoparticles can be described by the Langevin function [2]. However the

magnetization of antiferromagnetic nanoparticles can not be described by this function. In fact, it can be described by an altered form, known as the modified Langevin function, of this function [6,10,11,13]. People have been using the modified Langevin function to estimate the value of particle magnetic moment. Fitting the magnetization data of 5 nm NiO particles to the modified Langevin function gives a value of about $2000 \mu_B$ for the particle magnetic moment [6,7]. Such values for the particle magnetic moment are very large in comparison to the expected values. Any real sample of nanoparticles always has some distribution in particle size. This particle size distribution gives rise to a particle magnetic moment distribution for a system of magnetic nanoparticles. Recently, it has been shown that the ignorance of the particle magnetic moment distribution is the reason for the strange behavior of NiO nanoparticles [18]. Reasonable value of about few hundred Bohr magnetons for the particle magnetic moments is obtained, if the modified Langevin function is used to fit the magnetization data considering a distribution in the particle magnetic moment for 5 nm NiO particles. However, it is still not clearly understood whether this observation is a characteristic of NiO nanoparticles only or a general behavior applicable for all magnetic nanoparticle systems. For this the effect of particle magnetic moment distribution on the magnetization of few more nanoparticle systems should be studied. This motivated us to study the effect of particle magnetic moment distribution on the magnetization of antiferromagnetic ferrihydrite nanoparticles. During this study the particle magnetic moment distribution in a sample of 2 nm ferrihydrite particles is estimated.

Ferrihydrite is a nanocrystalline material and found in nature in

* Corresponding author.

E-mail address: sdtiwari@thapar.edu (S.D. Tiwari).

Effects of Thickness Ratio of Co to Pt Layer on Magnetic Properties and Microstructure of $[\text{Co/Pt}]_n$ Multilayer Films

Tsu-Ching Yang¹, Yu-Shen Chen¹, Yin-Cheng Ju¹, Yu-Ting Lin¹, Chuan-Fa Huang¹,
Hsi-Chuan Lu², Sea-Fue Wang², Puneet Sharma³, and An-Cheng Sun¹

¹Department of Chemical Engineering and Materials Science, Yuan Ze University, Zhongli 32003, Taiwan

²Department of Materials and Mineral Resources Engineering, National Taipei University of Technology, Taipei 10608, Taiwan

³School of Physics and Materials Science, Thapar University, Patiala 147004, India

$[\text{Co/Pt}]_n$ multilayer films were deposited on a glass substrate with a Pt underlayer by an alternative sputtering method. The effect of overall multilayer $[\text{CoPt}]_n$ thickness and the relative thickness of Co to Pt layers on the structural and magnetic properties were investigated. First, the thickness ratio of Co to Pt layers (Co:Pt = 4:3, 1:1, and 3:4) in $[\text{Co/Pt}]_n$ multilayer films was varied. Higher coercivity and out-of-plane squareness were found for the $[\text{Co}_1 \text{ nm}/\text{Pt}_{0.75} \text{ nm}]_n$ and $[\text{Co}_1 \text{ nm}/\text{Pt}_1 \text{ nm}]_n$ multilayer films. The total thickness of multilayers was varied from 3.5 to 8 nm. When the Co to Pt layers thickness ratio was changed to 3:4, the magnetic performance was declined. Furthermore, the thickness ratio of Co to Pt layers was kept constant to 1:1, and the Co and Pt layer thickness in $[\text{Co}_x \text{ nm}/\text{Pt}_x \text{ nm}]_n$ film was varied. The highest coercivity of 2.1 kOe was obtained in the $[\text{Co}_{0.5}/\text{Pt}_{0.5}]_4$ film. The magnetic properties were decreased with further increase in the Co and Pt layer thickness. In this paper, we demonstrated that $[\text{Co/Pt}]_n$ multilayer films with the suitable thickness ratio of Co to Pt layers are beneficial to prepare CoPt thin films with perpendicular magnetic anisotropy.

Index Terms—CoPt thin films, magnetic properties, magnetic recording media, multilayer.

I. INTRODUCTION

FOR ultrahigh magnetic recording media, $L1_0$ FePt thin film is regarded as a great potential magnetic material, owing to its large coercivity (H_c), huge magnetocrystalline anisotropy constant (K_u), and high chemical stability [1]. However, its higher ordering temperature (~ 500 °C) for soft magnetic $A1$ FePt to transform into hard magnetic $L1_0$ FePt induces a costly fabrication process, coarsened magnetic grains, and serious interlayer diffusion [2], [3]. $L1_1$ CoPt phase with rhombohedral lattice could be an alternative magnetic material [4]. The unit cell of $L1_1$ CoPt phase is constructed with the alternating close-packed atomic layers of Co and Pt along the $[111]$ direction [5]. The higher perpendicular magnetic anisotropy (PMA), large K_u (similar to $L1_0$ FePt), and very low ordering temperature (less than $L1_0$ FePt about 200 °C) make $L1_1$ CoPt film a great opportunity to apply in recording media and spintronic devices [6]. Usually, the method adopted to obtain $L1_1$ CoPt film is the codeposition of Co and Pt atoms, which causes the mixing of Co and Pt atoms prior to the deposition on the substrates [7], [8]. Therefore, the atoms incompletely occupy superlattice sites and induce a disordered phase with poor magnetic performance. In order to improve the magnetic properties of $L1_1$ CoPt superstructure, alternative stacking of Co and Pt atomic planes were sputtered, owing to its special way of layer-by-layer deposition and a controllable diffusion length between layers [9]. In this paper, we systematically studied the variation of Co to Pt thickness

ratio (Co:Pt = 4:3, 1:1, and 3:4) and the total thickness of $[\text{Co/Pt}]_n$ multilayers (1.75–20 nm). The results showed that the higher H_c and PMA were found in the Co to Pt thickness ratios of 4:3 and 1:1. Furthermore, fine tuning of $[\text{Co}_x \text{ nm}/\text{Pt}_x \text{ nm}]_n$ multilayer thickness resulted in maximum H_c at $x = 0.5$ and $n = 4$. Furthermore, Co to Pt layers with thickness ratio 3:4 showed poor magnetic performance. In this investigation, the correlation between the magnetic properties and the microstructures of $[\text{Co/Pt}]_n$ multilayer films were studied.

II. EXPERIMENT

The $[\text{Co}_1 \text{ nm}/\text{Pt}_{0.75} \text{ nm}]_n$, $[\text{Co}_1 \text{ nm}/\text{Pt}_1 \text{ nm}]_n$, and $[\text{Co}_{0.75} \text{ nm}/\text{Pt}_1 \text{ nm}]_n$ multilayer films were deposited on glass substrates in an ultrahigh vacuum magnetron sputtering chamber. Before sputtering the $[\text{Co/Pt}]_n$ multilayer, a 20 nm-thick textured Pt(111) was deposited on a glass substrate. The thickness of Co and Pt layers were changed from 0.75 to 1 nm in order to make the thickness ratio of Co to Pt layers to be 4:3, 1:1, and 3:4. n is the repetition of $[\text{Co/Pt}]$ films, which ranged the total thickness of $[\text{Co/Pt}]_n$ multilayer film from 1.75 ($n = 1$) to 21 nm ($n = 12$). The background pressure was better than 5×10^{-9} Torr, and the working pressure of Ar gas was fixed to 10 mTorr. The deposition temperature of $[\text{Co/Pt}]$ multilayer films was fixed to 350 °C. The film thickness was identified by atomic force microscopy. Magnetic properties were measured by the polar magneto-optical Kerr effect with the maximum applied field of 16 kOe. The phase structures of $[\text{Co/Pt}]_n$ multilayer films were characterized by X-ray diffraction (XRD). The surface morphology and the microstructure of the films were observed by scanning electron microscopy (SEM) and transmission electron microscopy (TEM), respectively.

Manuscript received March 20, 2015; revised June 4, 2015; accepted June 6, 2015. Date of publication August 4, 2015; date of current version October 22, 2015. Corresponding author: A.-C. Sun (e-mail: acsun@saturn.yzu.edu.tw).

Color versions of one or more of the figures in this paper are available online at <http://ieeexplore.ieee.org>.

Digital Object Identifier 10.1109/TMAG.2015.2464321

Structure and Magnetic Properties of $\text{Ba}_{1-x}\text{La}_x\text{Fe}_{12}\text{O}_{19}$ Prepared by $\text{Ba}_{1-x}\text{La}_x\text{Fe}_2\text{O}_4$

Samiksha Verma¹, Puneet Sharma¹, O.P. Pandey¹, Andrea Paesano², Jr., and An-Cheng Sun³

¹School of Physics and Materials Science, Thapar University, Patiala 147004, Punjab, India

²Departamento de Física, Universidade Estadual de Maringá, Maringá, Brazil

³Department of Chemical Engineering and Materials Science, Yuan Ze University, Chung-Li 32003, Taiwan

M-type Barium hexaferrite ($\text{BaFe}_{12}\text{O}_{19}$) with substitution of Ba^{2+} by rare earth metal La^{3+} were prepared by solid state synthesis method from as-prepared powder of barium monoferrite ($\text{Ba}_{1-x}\text{La}_x\text{Fe}_2\text{O}_4$) ($x = 0.0, 0.1$ and 0.2). The structural and magnetic properties of $\text{Ba}_{1-x}\text{La}_x\text{Fe}_{12}\text{O}_{19}$ were investigated by X-ray diffraction (XRD), vibrating sample magnetometer (VSM) and Mössbauer spectroscopy. The refined XRD patterns suggests the formation of single phase hexaferrite. With increased La substitution (x), the saturation magnetization increased and reached maximum at $x = 0.1$ and decreased at $x = 0.2$, without any noticeable change in coercivity. Fitted Mössbauer spectra of $\text{Ba}_{1-x}\text{La}_x\text{Fe}_{12}\text{O}_{19}$ showed increase in hyperfine field and a transition from Fe^{3+} ion to Fe^{2+} ion at 2b site. The present work demonstrates a new methodology for two stage substitution.

Index Terms—Barium hexaferrite, barium monoferrite, magnetic properties.

I. INTRODUCTION

AMONG the M-type hexaferrites, barium hexaferrite ($\text{BaFe}_{12}\text{O}_{19}$) is of particular interest due to its applications in high density magnetic recording media as well as in permanent magnets [1]. High uniaxial magneto crystalline anisotropy, self-biasing nature, low eddy current losses and low microwave losses, i.e., narrow ferromagnetic resonance line width, make hexagonal ferrites possible material solutions for microwave and millimeter devices [2][3]. Recently, spin canonical structure of M-type hexaferrite makes them a promising candidate for high T_c multiferroic materials [4].

The structure of the $\text{BaFe}_{12}\text{O}_{19}$ is derived from a stacking of close packed oxygen and barium layers along the hexagonal c -axis with an ordering sequence of spinel “S” block $(\text{Fe}_6\text{O}_8)^{2+}$ and three layer “R” blocks $(\text{BaFe}_6\text{O}_{11})^{2-}$. The combination of RS gives the building block of the magnetoplumbite structure for M type hexaferrite [5]. One unit cell of $\text{BaFe}_{12}\text{O}_{19}$ contains two formula units. The 24 Fe^{3+} ions per unit cell occupy five different crystallographic sites. Sixteen Fe^{3+} ions are in three octahedral sites ($2a$, $12k$, and $2b$) which have upward spin, whereas the remaining eight Fe^{3+} ions spinning downward are located in the tetrahedral and trigonalbipyramidal site ($4f_1$ and $4f_2$). So the net magnetic moment per unit cell for $\text{BaFe}_{12}\text{O}_{19}$ is $40 \mu_B$ [6].

Several techniques were adopted to prepare $\text{BaFe}_{12}\text{O}_{19}$ which include chemical coprecipitation [7]–[9], sol-gel [10], hydrothermal method [11], solid state synthesis and high energy ball milling [12][13]. To further improve the intrinsic magnetic properties various cations were substituted at Fe or Ba sites [14]–[19]. Substitution of Ba^{2+} with trivalent rare earth ions showed enhancement in magnetic properties [20]–[24]. It is reported that the Ba^{2+} site replaced by a rare earth substitution ions create a valence charge Fe^{3+} to Fe^{2+} ion on 2a site, which

increases the magneto crystalline anisotropy. Higher saturation magnetization (M_s) results from increased super exchange interaction due to lower ionic radii of rare earth ions as compared to Ba^{2+} ion. However, it is also observed that higher substitution amount reduces the saturation magnetization due to presence of residual hematite [23]. In all reported studies it is observed that rare earth ions are directly substituted during the calcination. Until now no studies have been reported in which substituted hexaferrite were prepared by other substituted phases.

The objective of this work is to investigate a new technique to developed La substituted barium hexaferrite ($\text{Ba}_{1-x}\text{La}_x\text{Fe}_{12}\text{O}_{19}$) from as-substituted barium monoferrite ($\text{Ba}_{1-x}\text{La}_x\text{Fe}_2\text{O}_4$). The effect of La^{3+} substitution on structural and magnetic properties is analyzed by using X-ray diffraction (XRD), vibrating sample magnetometer (VSM) and Mössbauer spectroscopy. These two stages substituted $\text{BaFe}_{12}\text{O}_{19}$ show enhanced saturation magnetization without any remarkable change in coercivity. This new method could lead to a novel way to prepare substituted hexaferrite from substituted monoferrite.

II. EXPERIMENT

$\text{Ba}_{1-x}\text{La}_x\text{Fe}_{12}\text{O}_{19}$ has been prepared by solid state synthesis from substituted $\text{Ba}_{1-x}\text{La}_x\text{Fe}_2\text{O}_4$, ($x = 0.0, 0.1$ and 0.2). The starting materials used in this study were laboratory grade BaCO_3 (purity 99.0% Loba Chemicals), Fe_2O_3 (purity 99.0% Sigma-Aldrich grade) and La_2O_3 (purity 99.0% Sigma-Aldrich grade). The process consists of two main steps: In the first step, $\text{Ba}_{1-x}\text{La}_x\text{Fe}_2\text{O}_4$ was prepared by wet mixing equimolar composition of raw materials together using planetary ball milling and a ball to charge ratio of 2:1 was chosen. The milling intensity was 120 rotations per minute (r/min). The as-mixed powder was dried and calcined for 2 hours at 1000°C in a muffle furnace. The heating and cooling rate were fixed to $5^\circ\text{C}/\text{min}$. In the second step, $\text{Ba}_{1-x}\text{La}_x\text{Fe}_{12}\text{O}_{19}$ was prepared by wet mixing of as-prepared $\text{Ba}_{1-x}\text{La}_x\text{Fe}_2\text{O}_4$ and Fe_2O_3 with 1:5 molar compositions in planetary ball milling for 3 hours with speed rotation 120 r/min. The calcination temperature and holding time was fixed to 1250°C and 3 hours respectively.

Manuscript received April 29, 2013; revised July 25, 2013; accepted August 07, 2013. Date of current version December 23, 2013. Corresponding author: P. Sharma (e-mail: puneet.sharma@thapar.edu).

Color versions of one or more of the figures in this paper are available online at <http://ieeexplore.ieee.org>.

Digital Object Identifier 10.1109/TMAG.2013.2278373



Biocompatibility and superparamagnetism in novel silica/CaFe₂O₄ nanocomposite

Lavanya Khanna*, N.K. Verma

Nano Research Lab, School of Physics and Materials Science, Thapar University, Patiala 147004, India

ARTICLE INFO

Article history:

Received 18 July 2013

Accepted 26 April 2014

Available online 5 May 2014

Keywords:

Silica–CaFe₂O₄ nanoparticles

Magnetic materials

Nanocomposites

Superparamagnetic

Biocompatible

ABSTRACT

Calcium ferrite nanoparticles (CaFe₂O₄ NPs) have been successfully passivated by silica coating. The particle size distribution was observed in the narrow range of 3–6 nm, without any agglomeration, suggesting the stabilization of high surface energy and magnetic interaction on the nanoparticles' surface, due to silica. Presence of amorphous silica resulted in less peak intensities of the orthorhombic CaFe₂O₄ core. The characteristic IR bands of silica confirmed its coating thereby making the nanocomposite viable for bio-conjugation (active silanol groups in the silica layer covalently attach to biomolecules). The nanocomposite exhibited superparamagnetic behavior ($M_s=8.55$ emu/g) and high biocompatibility below 500 μ g/ml. The nanosized, superparamagnetic and highly biocompatible synthesized nanocomposite finds potential applications in biomedical hybrids.

© 2014 Elsevier B.V. All rights reserved.

1. Introduction

Magnetic nanoparticles (MNPs) have attracted a great deal of attention in biomedical field [1], but, there are some limitations associated with them. Their surface inertness restricts the number of molecules that can be bonded to the surface [2]. Also, their tendency to agglomerate due to high surface energy and magnetic interactions lead to increase in size. This results in clogging of the capillaries and adsorption of plasma proteins leading to quick clearance by the macrophages in the Reticuloendothelial system in the body, before reaching the target cells [2]. So, it is highly desired that the synthesized nanomaterial be agglomeration-free and biocompatible. Surface stabilization of the MNPs serves both these purposes. It is obtained by passivating the surface of MNPs with the most employed stabilizer i.e. silica. It screens the magnetic dipolar interaction between MNPs, thus preventing their aggregation and favouring their dispersion in liquid media. It protects leaching of MNPs in an acidic environment, eliminates protein adsorption and facilitates bio-conjugation [2,4,5].

In addition, high inherent toxicity of transition metals (Ni, Co, Mn) in ferrites raises concern on their biocompatibility [3]. Ferrites of calcium are more biocompatible since calcium is inherently non-toxic. A novel, agglomeration-free and highly biocompatible nanocomposite composed of inherently non-toxic, superpara-

magnetic calcium ferrite nanoparticles and biocompatible silica is reported in this work. Their structural, morphological, magnetic properties and biocompatibility have been studied.

These find applications in magnetic cell-separation of biological entities, therapeutic drug delivery vehicles, contrast enhancement agents in magnetic resonance imaging (MRI) and magnetic biosensing.

2. Experiment

Silica coating on calcium ferrite nanoparticles was done by the modified Stober process [5]. Briefly, 150 ml ethanol, 3 ml water, 5.1 ml ammonium hydroxide and 900 μ l TEOS were added in a beaker and kept at 40 °C, while stirring. After 20 min, 6 ml aqueous solution of calcium ferrite nanoparticles with the concentration of 4 mg/ml was added and the reaction was allowed to proceed for 5 h. Nanoparticles were magnetically separated, washed and dried to obtain silica coated calcium ferrite nanoparticles.

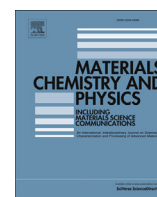
The structure and morphology were studied by X-ray diffraction (XRD; X'PERT PRO Panalytical, MRD ML) and Transmission Electron Microscope (TEM; Hitachi (H-7500)), respectively. FT-IR spectrum was recorded on Perkin Elmer-Model RZX. The magnetic property was determined by vibrating sample magnetometer (VSM; Princeton Applied Research Model 151/155). The viability of synthesized nanocomposite on T cell lines (Jurkat cells) was investigated by MTT (3-(4, 5-Dimethylthiazol-2-yl)-2, 5-diphenyl-tetrazolium bromide, a tetrazole) colorimetric assay at 5, 25, 50,

* Corresponding author. Tel.: +91 0175 2393343; fax: +91 0175 2364498/2393002.

E-mail addresses: lavanshya@yahoo.co.in, lavanya.khanna@thapar.edu (L. Khanna).

<http://dx.doi.org/10.1016/j.matlet.2014.04.168>

0167-577X/© 2014 Elsevier B.V. All rights reserved.



Sr doped BiMO₃ (M = Mn, Fe, Y) perovskites: Structure correlated thermal and electrical properties



Samita Thakur^{a, b, *}, K. Singh^a, O.P. Pandey^a

^a School of Physics and Materials Science, Thapar University, Patiala 147004, India

^b School of Basic Sciences, Arni University, Kathgarh, India

HIGHLIGHTS

- (BiSr)MO₃ (M = Mn, Fe, Y) was synthesized by solid state reaction method.
- The B-site cation highly affect the generation of defects in perovskites.
- The structural and electrical properties strongly depend upon the B-site cation.

ARTICLE INFO

Article history:

Received 27 April 2016

Received in revised form

14 October 2016

Accepted 27 November 2016

Available online 28 November 2016

Keywords:

Rietveld refinement

Raman spectroscopy

X-ray photoelectron spectroscopy

Iodometric titration

ABSTRACT

Sr²⁺ substituted BiMnO_{3-δ} (BSM), BiFeO_{3-δ} (BSF) and BiYO_{3-δ} (BSY) perovskites structured samples have been investigated for their structural, thermal and electrical properties. These samples are characterized by X-ray diffraction, X-ray photoelectron spectroscopy (XPS), iodometric titration, Raman spectroscopy, thermogravimetric analysis (TGA) and conductivity. Rietveld refinement confirms that BSY sample has cubic (*Fm-3m*) symmetry with limited solid solubility of Sr²⁺ as compared to tetragonal symmetry (*p4mm*) of BSM and BSF samples. X-ray photoelectron spectroscopy study confirms the presence of Mn⁴⁺ and Fe⁴⁺ content in BSM and BSF samples. The amount of Mn³⁺, Fe⁴⁺ and oxygen vacancies in these systems are calculated by iodometric titration. The highest oxygen vacancies are found in BSF sample. The BSM system exhibit the highest conductivity followed by BSF and BSY samples due to the presence of Mn⁴⁺ content and moderate oxygen vacancies in this particular sample.

© 2016 Elsevier B.V. All rights reserved.

1. Introduction

Perovskite materials are one of the most important multifunctional compounds. These compounds with small structural changes can generate an incredibly wide array of phases with variable properties. The structural diversity in these compounds arises due to extreme flexibility of their structures in regard to cation and anion replacements and also their tolerance to adjust distortion created by different substituents [1]. Among different perovskite compounds, bismuth containing perovskites are categorized differently because of their different electrical, magnetic and multi-ferroic properties [2–4]. As an important multifunctional material, bismuth containing oxides have shown potential applications in photovoltaic cells, memory devices, non linear

* Corresponding author. School of Physics and Materials Science, Thapar University, Patiala 147004, India.

E-mail address: samitasthakur@gmail.com (S. Thakur).

optical glasses, fuel cells, oxygen sensors and catalysis for industrial selective oxidation reactions [1,5,6]. Bi³⁺ has an electronic configuration [Xe]4f¹⁴5d¹⁰6s². Hybridization of 6s and 6p orbitals and the resulting lone electron pair yields some very interesting stereochemistry and steric related properties [7]. Generally, bismuth is replaced by aliovalent cation (Sr²⁺, Ca²⁺, Ba²⁺ and Pb²⁺) to improve its electrical properties [8–10]. When A site cation is replaced by an aliovalent cation, the neutrality in the system is compensated either by the formation of oxygen vacancies unless the B-site cation does not change its oxidation state or by the change in valency of B-site cation and creation of oxygen vacancies if B-site cation is a transition element. Existence of multiple valence states at B-sites enable movement of electrons in the crystal lattice. Some of the perovskites having transition elements exhibit metallic, superconducting or mixed conducting behavior. Usually, the absence of transition elements at B-site in aliovalent doped ABO₃ leads to good ionic conductivity due to the high possibility to have oxide ion vacancies [11–14]. So, the B-site

Large magnetoelectric response in modified BNT based ternary piezoelectric [72.5(Bi_{1/2}Na_{1/2}TiO₃)-22.5(Bi_{1/2}K_{1/2}TiO₃)-5(BiMg_{1/2}Ti_{1/2}O₃)]-magnetostrictive (NiFe₂O₄) particulate (0-3) composites

Mintu Tyagi,¹ Mukesh Kumari,² Ratnamala Chatterjee,² and Puneet Sharma^{1,a)}

¹School of Physics and Materials Science, Thapar University, Patiala-147004, Punjab, India

²Magnetics and Advanced Ceramics Laboratory, Department of Physics, Indian Institute of Technology, Delhi-110016, India

(Received 11 February 2015; accepted 8 May 2015; published online 20 May 2015)

Lead free ternary solid solution 72.5(Bi_{1/2}Na_{1/2}TiO₃)-22.5(Bi_{1/2}K_{1/2}TiO₃)-5(BiMg_{1/2}Ti_{1/2}O₃) with effective piezoelectric coefficient (d_{33}) of 180 pC/N has been prepared. Further, particulate composites consisting of (1-x)[72.5(BNT)-22.5(BKT)-5(BMgT)]-xNiFe₂O₄ (NFO) (x=0, 0.1, 0.2, 0.3) were synthesized, and its structural, magnetoelectric (ME), magnetostrictive, magnetic, and ferroelectric properties were studied. Large ME voltage coefficient, (α_E) ~ 73 mV/cmOe accompanied by high d_{33} ~ 125 pC/N, and magnetostrictive strains, (λ_{11}) ~ -18 × 10⁻⁶, were obtained for x=0.2 composite. The present study demonstrates an environmental-friendly ME particulate composite for future applications. © 2015 AIP Publishing LLC. [<http://dx.doi.org/10.1063/1.4921521>]

Due to scarcity of single phase multiferroic magnetoelectric (ME) materials with large room temperature (R-T) ME response, the focus of researchers has shifted towards the development of ME composites.^{1,2} Several investigations based on piezoelectric-ferrite particulate ME composite have been reported. The principal combinations include PbZrTiO₃(PZT) and BaTiO₃(BT) as the piezoelectric constituents and CoFe₂O₄(CFO) and NiFe₂O₄(NFO) as the magnetostrictive constitute.³⁻⁶ However, high piezoelectric coefficient (d_{33} ~ 600 pm/V) and high electromechanical coupling coefficient (k_p ~ 0.7) of PZT is difficult to match with other non lead based piezoelectric materials.⁷ ME composite based on PZT has shown the largest ME coupling coefficient (α_E) values from 0.040-4.7 V/cmOe.⁸ Aarti *et al.* have reported the α_E values of 122 mV/cmOe for particulate PZT-CFO system.⁹ However, due to the toxic nature of Pb, the non lead based ME composites were also studied.^{5,6,10} The largest α_E value of 252 mV/cmOe was reported for BT-NFO particulate composites.¹⁰

Among the other alternatives of non-lead based piezoelectric oxides, Bi_{0.5}Na_{0.5}TiO₃ (BNT) is one of the widely studied piezoelectric material possessing high curie temperature (T_c) ~ 320 °C and large remnant polarization (P_r) ~ 38 μ C/cm².¹¹ However, its high coercivity (E_c ~ 73 kV/cm) makes it difficult to pole and thus has a smaller piezoelectric coefficient (d_{33} ~ 80 pC/N). It has been reported that the solid solution of rhombohedral BNT and tetragonal perovskites with morphotropic phase boundary (MPB) exhibit piezoelectric properties.¹² Therefore, to improve its piezoelectric properties, BNT has been modified with solid solutions of BaTiO₃(BT), (Bi_{0.5}K_{0.5})TiO₃ (BKT), (K_{0.5}Na_{0.5})NbO₃ (KNN), and Bi(Mg_{0.5}Ti_{0.5})O₃ (BMgT).¹¹⁻¹⁴ Recently, Jarupoom *et al.* reported d_{33} values greater than 500 pm/V in ternary 72.5BNT-22.5BKT-5BMgT based solid solution.¹⁵ Hence, this modified ternary solid solution could be a potential candidate for lead free particulate ME composites. The studies on

BNT based particulate composite are very scarce; few reported studies on BNT-CFO and BNT-NFO based particulate composites have shown evidence of magnetoelectric response.^{16,17} However, no report is available in literature on the modified BNT based particulate composites. In this work, sol-gel assisted (1-x)[72.5BNT-22.5BKT-5BMgT]-x NFO (x=0, 0.1, 0.2, 0.3) particulate composite series have been prepared, and their structural, magnetic, ferroelectric magnetoelectric, and magnetostrictive properties have been investigated.

Aldrich (99.99%) was used as metal precursors for synthesis. 2-methoxyethanol and citric acid were used as solvents. To prepare 72.5BNT-22.5BKT-5BMgT, the solutions for BNT, BKT, and BMgT were prepared separately by dissolving stoichiometric proportion of metal precursors into 2-methoxyethanol and citric acid. The prepared precursor solutions were mixed together in desired volume ratio of 72.5:22.5:5 using Hamilton microliter microsyringe to get precursor solution of 72.5BNT-22.5BKT-5BMgT. A 10 mol. % excess bismuth nitrate was used to compensate for the volatile Bi loss during sintering process. The 72.5BNT-22.5BKT-5BMgT solution was stirred and heated on magnetic hot plate at 80 °C till the solution turned into yellowish gel. The gel was further heated into furnace at 250 °C, and dried foam was formed. The obtained precursor was ground in agate mortar and calcined at 700 °C in muffle furnace. To prepare the NFO, cobalt nitrate hexahydrate (Co(NO₃)₂·6H₂O) and iron nitrate nonahydrate (Fe(NO₃)₃·9H₂O) of Sigma Aldrich (99.99%) were dissolved in 2-methoxyethanol and citric acid with molar ratio of 1:2. The solution is continuously stirred at 80 °C using magnetic hot plate to form dark reddish gel. The obtained gel was dried at 250 °C and subsequently calcined at 700 °C in furnace. To prepare (0-3) particulate composite, the powders of BNT-BKT-BMgT and NFO were taken in desired weight ratio of x=0, 0.1, 0.2, 0.3 and thoroughly mixed in acetone media for 4 h using planetary ball mill. Further, the as mixed powder was pressed into cylindrical pellets of 10 mm diameter at a pressure of 200 MPa. The pellets

^{a)}Email: puneet.sharma@thapar.edu

Analysis of strong decays of charmed mesons $D_2^*(2460)$, $D_0(2560)$, $D_2(2740)$, $D_1(3000)$, $D_2^*(3000)$, and their spin partners $D_1^*(2680)$, $D_3^*(2760)$, and $D_0^*(3000)$

Pallavi Gupta and A. Upadhyay

School of Physics and Materials Science, Thapar University, Patiala—147004 Punjab, India

 (Received 16 September 2017; published 25 January 2018)

Using the effective Lagrangian approach, we examine the recently observed charm states $D_J^*(2460)$, $D_J(2560)$, $D_J(2740)$, $D_J(3000)$, and their spin partners $D_J^*(2680)$, $D_J^*(2760)$, and $D_J^*(3000)$ with J^P states $1P_{\frac{3}{2}}2^+$, $2S_{\frac{1}{2}}0^-$, $1D_{\frac{3}{2}}2^-$, $2P_{\frac{3}{2}}1^+$, and $2S_{\frac{3}{2}}1^-$, $1D_{\frac{3}{2}}3^-$, $2P_{\frac{3}{2}}0^+$ respectively. We study their two body strong decays, coupling constants and branching ratios with the emission of light pseudo-scalar mesons (π, η, K). We also analyze the newly observed charm state $D_2^*(3000)$ and suggest it to be either $1F(2^+)$ or $2P(2^+)$ state and justify one of them to be the most favorable assignment for $D_2^*(3000)$. We study the partial and the total decay width of unobserved states $D(1^1F_3)$, $D_s(1^1F_3)$ and $D_s(1^1F_2)$ as the spin and the strange partners of the $D_2^*(3000)$ charmed meson. The branching ratios and the coupling constants g_{TH} , \tilde{g}_{HH} , g_{YH} , \tilde{g}_{SH} , and g_{ZH} calculated in this work can be confronted with the future experimental data.

DOI: 10.1103/PhysRevD.97.014015

I. INTRODUCTION

The excitation spectrum of ($c\bar{q}$) heavy-light charmed mesons have received considerable theoretical and experimental attention, as it provide opportunities to study the QCD properties within the context of different models. Recently, LHCb collaboration have used the Dalitz plot analysis to study the resonant substructures $B^- \rightarrow D^+\pi^-\pi^-$ decays in the pp collision at a center-of-mass energy 7 TeV. The masses and the widths of charm resonances with spins 1, 2 and 3 at high $D^+\pi^-$ masses are determined [1]. The study gives indication that, these resonances are mainly coming from the contribution of the $D_2^*(2460)$, $D_1^*(2680)$, $D_3^*(2760)$, and $D_2^*(3000)$ charmed mesons. The measured Breit-Wigner masses and widths of these charmed mesons are

$$D_2^*(2460): M = 2463.7 \pm 0.4 \pm 0.4 \pm 0.6 \text{ MeV},$$

$$\Gamma = 47.0 \pm 0.8 \pm 0.9 \pm 0.3 \text{ MeV}, \quad (1)$$

$$D_1^*(2680): M = 2681.1 \pm 5.6 \pm 4.9 \pm 13.1 \text{ MeV},$$

$$\Gamma = 186.7 \pm 8.5 \pm 8.6 \pm 8.2 \text{ MeV}, \quad (2)$$

$$D_3^*(2760): M = 2775.5 \pm 4.5 \pm 4.5 \pm 4.7 \text{ MeV},$$

$$\Gamma = 95.3 \pm 9.6 \pm 7.9 \pm 33.1 \text{ MeV}, \quad (3)$$

$$D_2^*(3000): M = 3214 \pm 29 \mp 33 \mp 36 \text{ MeV},$$

$$\Gamma = 186 \pm 38 \pm 34 \pm 63 \text{ MeV} \quad (4)$$

In 2010 and 2013, a great achievement have been made by *BABAR* and LHCb collaboration. LHCb collaboration observed two natural parity resonances $D_J^*(2650)^0$, $D_J^*(2760)^0$ and two unnatural parity resonances $D_J(2580)^0$ and $D_J(2740)^0$ by studying the $D^+\pi^-$, $D^0\pi^+$, and $D^{*+}\pi^-$ invariant mass spectra [2]. Along with these states, LHCb has also observed $D_J(3000)^0$ in the $D^{*+}\pi^-$ final state and $D_J^*(3000)^+$ and $D_J^*(3000)^0$ in the $D^0\pi^+$ and $D^+\pi^-$ mass spectra respectively. *BABAR* collaboration in 2010, observed $D_J(2560)^0$, $D_J(2600)^0$, $D_J(2600)^+$, $D_J(2750)^0$, $D_J^*(2760)^+$, and $D_J^*(2760)^0$ in the inclusive $e^+e^- \rightarrow c\bar{c}$ interaction [3]. Masses and the widths of charm states predicted by *BABAR* and LHCb are so close, that they are considered to be in the same J^P state. Masses and widths of these charm states observed by various collaborations are presented in Table I.

It is very crucial to assign a proper J^P to the heavy-light system in a given spectra, as large amount of experimental information like decay width, branching ratios, and hyperfine splitting are based on their J^P . Various theoretical models have suggested different J^P states to the observed charm mesons. In this paper, we analyze the available theoretical and experimental data on the excited charm states and specify their proper J^P . In our analysis, we mentioned $D_2^*(2460)$ to be the well-established state having $J^P = 2^+$ in the charm spectra [4]. The information provided by *BABAR* (2010) and LHCb (2013) for the states $D_J^*(2680)$ and $D_J^*(2760)$ were

Published by the American Physical Society under the terms of the Creative Commons Attribution 4.0 International license. Further distribution of this work must maintain attribution to the author(s) and the published article's title, journal citation, and DOI. Funded by SCOAP³.

Structure induced tunable magnetic properties of Zn substituted $\text{Mn}_{1-x}\text{Zn}_x\text{Fe}_2\text{O}_4$ ($x = 0-1$) NPs

Navjot Kaur¹, Bhupendra Chudasama² ✉

¹Laboratory of Nanomedicine, Thapar University, Patiala 14700, India

²School of Physics and Materials Science, Thapar University, Patiala 14700, India

✉ E-mail: bnchudasama@gmail.com

Published in Micro & Nano Letters; Received on 1st September 2016; Accepted on 14th November 2016

$\text{Mn}_{1-x}\text{Zn}_x\text{Fe}_2\text{O}_4$ nanoparticles (MZ NPs) owing to their Zn content dependent tunable magnetic properties have potential applications in energy conversion devices and in nanomedicine. It is a well-recognised fact that magnetism of MZ NPs has critical dependence on degree of Zn substitution at tetrahedral sites. In addition, the role of cation distribution between the tetrahedral and octahedral sites for a particular degree of Zn-substitution, i.e. the degree of inversion (δ) also influences their magnetic characteristics. However, the exact correlation between distribution of bivalent metal ions between tetrahedral and octahedral sites and corresponding magnetic characteristics is not well understood. In order to explore this structural dependence of magnetic characteristics of MZ NPs, a series of $\text{Mn}_{1-x}\text{Zn}_x\text{Fe}_2\text{O}_4$ ($x = 0-1$) nanoparticles have been synthesized by chemical co-precipitation method. Saturation magnetisation and Curie temperature of MZ NPs are strongly correlated with the degree of inversion and exchange interactions between the magnetic ions, while the coercivity and remanence is independent of it and only depends on crystallite size. Both saturation magnetisation and Curie temperature decreases with increasing Zn substitution into spinel matrix. This could be attributed to the weakening of strong (A-B) inter lattice super exchange interaction instead partial substitution of Zn at octahedral Mn sites.

1. Introduction: In recent years, $\text{Mn}_{1-x}\text{Zn}_x\text{Fe}_2\text{O}_4$ ($x = 0-1$) nanoparticles (MZ NPs) have attracted considerable interest because of their technological importance in magnetic hyperthermia, magnetic resonance imaging, data storage, spintronics, sensors [1, 2] etc. They are also used in power transformers: choke coils, noise filters and recording heads [3]. It is also being considered as one of the promising candidate for the preparation of magnetic fluids for heat transfer and energy conversion devices [4, 5]. MZ NPs possess interesting magnetic properties such as high magnetic permeability and low core losses in addition to strong zinc (Zn)-content dependent saturation magnetisation and Curie temperature. Magnetism in MZ NPs largely depends on the degree of Zn substitution in spinel lattice, synthesis method used and the conditions of preparation. MZ NPs are being synthesised by various bottom-up techniques such as hydrothermal [6], sol-gel [7], microemulsion [8], co-precipitation [9] etc. each showing different magnetic characteristics, the origin of which always remained unsettled [6-9].

MZ NPs are ferrimagnetic. They possess cubic spinel structure with general formula AB_2O_4 , where A and B refer to the tetrahedral and octahedral cation sites, respectively. Type of cations and their distribution between the two interstitial sites in the spinel unit cell determine their intrinsic magnetic properties [10, 11]. This cation distribution depends on the ionic radii of the cation [12]. ZnFe_2O_4 (i.e. $x = 0$) has normal spinel structure, where Zn^{2+} occupies the tetrahedral sites due to its affinity for sp^3 bonding with oxygen anions, leaving all the ferric ions at the octahedral sites. Owing to this the only possible interaction between the ferric ions is intra-lattice (B-B) exchange interaction. Since (B-B) exchange interaction is very weak, ZnFe_2O_4 NPs are paramagnetic at room temperature [13]. On the other hand, MnFe_2O_4 has mixed spinel structure with degree of inversion, $\delta \approx 0.2$. In this case manganese (Mn) and ferric ions occupy both the tetrahedral A-sites and octahedral B-sites. It was previously reported that MZ NPs possess mixed spinel structure as cations Me^{2+} and Fe^{3+} occupy both the interstitial sites [14-16]. Attia [17] has reported the cation distribution in MZ NPs. In MZ NPs, Zn ions always occupy the A-sites while Fe and Mn ions are distributed between

A- and B-sites. This distribution of Mn and Fe ions depends on the degree of inversion and the Zn-content at A-site. Xuan *et al.* [18] have reported increase in saturation magnetisation of MZ NPs for small Zn substitution at A-sites followed by a decrease in their saturation magnetisation for higher Zn substitution. However, they could not reveal the strong magnetisation dependence of MZ NPs on Zn-content at interstitial sites and role of cation distributions. Rath *et al.* have also reported that the particle size, lattice parameter and magnetic properties of MZ NPs depends on cation distribution. They have denoted decrease in particle size and lattice parameter with increase in Zn concentration in terms of the transformation from mixed spinel to normal spinel structure; however, they failed to provide any experimental evidence for it. In addition, they could not explain the observed magnetisation dependence of MZ NPs on degree of zinc (Zn) substitution in the spinel matrix [19]. Gopalan *et al.* have reported the impact of Zn substitution on the structural and magnetic properties of chemically derived nanosized MZ ($x = 0-1$). They have observed increase in magnetisation of MZ NPs for $x = 0.2-0.4$ followed by a decrease; however, they could not correlate it with the corresponding structural changes taking place in the spinel matrix of MZ NPs due to variation in the Zn substitution at interstitial sites [20]. Varshney *et al.* [21] have studied the effect of site occupancy and cation ordering on structural and vibrational properties of $\text{Zn}_x\text{Mn}_{1-x}\text{Fe}_2\text{O}_4$, but no study on their magnetic properties have been conducted.

From the literature survey it has been found that the role of cations vis-a-vis their occupancies at tetrahedral and octahedral sites are not clear as regards to their influence in deciding the overall magnetic properties of MZ NPs is concern. It is in this context a study of structural dependence of magnetic properties of MZ NPs with varying degree of Zn substitution assume significance. This Letter probes the influence of Zn substitution on magnetic properties (magnetisation, coercivity, remanence and Curie temperature) of chemically co-precipitated MZ NPs and their correlation with structural changes in the unit cell caused by varying cation distribution between tetrahedral and octahedral interstitial sites.

Effect of Ca substitution on structural, magnetic and dielectric properties of BiFeO₃

Samita Thakur, O.P. Pandey and K. Singh*

School of Physics & Materials Science, Thapar University, Patiala, India

(Received 7 September 2013; accepted 26 December 2013)

Bi_{1-x}Ca_xFeO₃ ($x = 0.40, 0.50$) compounds are synthesized by conventional solid-state reaction method. The effect of Ca²⁺ substitution is investigated on structural, dielectric and magnetic properties. Rietveld refinement confirms that crystal structures of both the samples are tetragonal with *P4mm* symmetry. The highest values of remnant magnetization (M_r) and coercive field (H_c) are 0.002 emu/g and 0.23 kOe, respectively, for $x = 0.50$. The electric modulus formalism is used to distinguish and separate out the relaxation process which is dominated by the transport phenomenon. The relaxation process has activation energy ~ 0.32 eV which is found to be related to both the hopping mechanisms, i.e. electronic and oxide ions.

Keywords: Rietveld refinement; magnetic properties; dielectric spectroscopy; electric modulus

1. Introduction

Multiferroic materials exhibit ferroelectric and ferromagnetic properties simultaneously. The presence of ferromagnetism and ferroelectricity in the same material is difficult to achieve because most of ferromagnetic oxides possess a center of symmetry in their crystal structure and do not allow electric polarization.[1–3] In contrast to this, most of ferroelectric compounds have only diamagnetic transition metal ions. Centrosymmetry of crystal structures can be disturbed by the introduction of stereochemically active lone pairs such as 6s² lone pair of Bi³⁺ cations, whereas, super exchange interactions between Fe³⁺ ions determine magnetic ordering in this material.[4–6]

BiFeO₃ (BFO) is one of the few multiferroic materials that can function at room and elevated temperatures due to its high Neel's temperature (380 °C) and Curie temperature (830 °C). In spite of some advantageous properties, BFO has some inherent problems due to spatially modulated spin structure which does not allow net magnetization and inhibits the observation of a notable linear magnetoelectric effect.[7–9] This problem can be solved by substitution of rare earth lanthanide ions (La³⁺, Nd³⁺ or Sm³⁺) or divalent ions (Ca²⁺, Sr²⁺, Ba²⁺, Pb²⁺) at the A site of BFO [10–15] or other ions (Nb⁵⁺, Mn⁴⁺, Cr³⁺, Ti⁴⁺) at B site.[16–18] Substitution on A site is more important as it reduces the number of Bi³⁺ ions which will further reduce the 6s² lone pairs in the system. To overcome charge imbalance created by divalent cations, oxygen vacancies will be created which will affect the degree of centrosymmetry of FeO₆ octahedra and thus also dielectric and magnetic properties of BFO.[19]

*Corresponding author: Email: kusingh@thapar.edu

Structural, Dielectric and Magnetoelectric Properties of $x \text{Co}_{0.8}\text{Ni}_{0.2}\text{Fe}_2\text{O}_4 + (1-x) \text{PbZr}_{0.55}\text{Ti}_{0.45}\text{O}_3$ Composites

DIPTI,^{1,4} J. K. JUNEJA,² SANGEETA SINGH,³ K. K. RAINA,⁴ R. K. KOTNALA,⁵ AND CHANDRA PRAKASH^{6,*}

¹Electroceramics Research Lab, G.V.M. Girls College, Sonapat-131001, India

²Department of Physics, PG Hindu College, Sonapat-131001, India

³Department of Physics, G.V.M. Girls College, Sonapat 131001, India

⁴School of Physics & Materials Science, Thapar University, Patiala-147004, India

⁵National Physical Laboratory, Dr. K.S. Krishnan Marg, New Delhi-110012, India

⁶Solid State Physics Laboratory, Lucknow Road, Delhi-110054, India

Communicated by Professor Amar S. Bhalla
(Received in final form February 19, 2015)

In this paper, we are reporting structural, dielectric, ferroelectric and magnetic properties of polycrystalline composites (ferrite and ferroelectric) of PZT ($\text{PbZr}_{0.55}\text{Ti}_{0.45}\text{O}_3$) + CNFO ($\text{Co}_{0.8}\text{Ni}_{0.2}\text{Fe}_2\text{O}_4$). The sample with composition $x \text{CNFO} + (1-x) \text{PZT}$ ($x = 0.00, 0.05, 0.10, 0.15$ and 1.00) were prepared using the solid state double sintering method. Here the ratio $x: (1-x)$ of two components is by weight. X-ray diffraction (XRD) studies show that lattice constant and tetragonality decreases with increasing ferrite content. Dielectric constant was found to decrease with increase in amount of CNFO. The value of tangent loss ($\tan\delta$) was reasonably low (< 0.04) for all the samples. Ferroelectric and ferrimagnetic behavior was confirmed by observing P-E and M-H hysteresis loop, respectively. The room temperature magnetoelectric coupling coefficient ($\alpha = dE/dH$) was measured as a function of applied DC magnetic field. The value of α was observed to be maximum ($855 \mu\text{V}/(\text{cm.Oe})$) at DC magnetic field of 1.7 kOe for sample with 5% CNFO. Value of piezoelectric coefficient ' d_{33} ' decreases from 133 to 60 pC/N.

Keywords Ferroelectrics; magnetoelectrics; ferrites; PZT; ME effect

Introduction

Magnetoelectric materials are the potential candidates for technological applications such as magnetic field sensors, transducers, memory devices, oscillators, phase shifters, microwave devices [1–6]. The main problem with these materials is their dielectric loss. In comparison to single phase multiferroics, a much stronger ME-coupling has been realized in two

*Corresponding author.; E-mail: cprakash2014@gmail.com

Color versions of one or more of the figures in the article can be found online at www.tandfonline.com/gfel.

SCIENTIFIC REPORTS

OPEN

Agricultural wastes as a resource of raw materials for developing low-dielectric glass-ceramics

Satwinder Singh Danewalia¹, Gaurav Sharma¹, Samita Thakur² & K. Singh¹

Received: 04 December 2015

Accepted: 30 March 2016

Published: 18 April 2016

Agricultural waste ashes are used as resource materials to synthesize new glass and glass-ceramics. The as-prepared materials are characterized using various techniques for their structural and dielectric properties to check their suitability in microelectronic applications. Sugarcane leaves ash exhibits higher content of alkali metal oxides than rice husk ash, which reduces the melting point of the components due to eutectic reactions. The addition of sugarcane leaves ash in rice husk ash promotes the glass formation. Additionally, it prevents the cristobalite phase formation. These materials are inherently porous, which is responsible for low dielectric permittivity i.e. 9 to 40. The presence of less ordered augite phase enhances the dielectric permittivity as compared to cristobalite and tridymite phases. The present glass-ceramics exhibit lower losses than similar materials synthesized using conventional minerals. The dielectric permittivity is independent to a wide range of temperature and frequency. The glass-ceramics developed with adequately devitrified phases can be used in microelectronic devices and other dielectric applications.

Agricultural wastes could be used as resource materials in many engineering applications. In general, silica is a major constituent of the agricultural waste ash. It varies from 98–36 wt% in ash of rice husk, sugarcane leaves and corn husk etc¹. In addition to silica, other metal oxides like CaO, MgO and K₂O are also present along with some trace elements². Rice husk after burning in air, produces highly reactive silica particles (usually nanosized)³. During this process, about 20% of biomass remains as ash, which contains different minerals⁴. These minerals can be amorphous or crystalline depending upon the conditions in which rice husk is burnt. On the other hand, sugarcane leaves ash (SCLA) have silica along with alkali and alkaline earth metal oxides as the major constituents⁵. Silica, derived from the waste, can be utilized as raw materials to form different high performance materials, such as glasses, refractories, capacitors, glass sealants, bioceramics, fibres and optical cavities, etc^{6–8}. In addition to this, silica can also be converted to silicon after heating in the presence of activated charcoal. The formed silicon, after refinement, can be used in solar energy production and electronic chips⁹.

Formation of glasses and glass-ceramics from the agriculture waste have many benefits. It is environment friendly, economical and renewable source of high content silica. Moreover, it could be better and effective way to manage huge agricultural waste for producing different engineering materials. Additionally, during melt-quench process, the organic contents present in the waste materials convert in various gasses. These by-product gasses can be collected for further applications. Moreover, these gasses act as *in-situ* foaming agents and enhance the inherent porosity in the glasses and glass-ceramics. Inherent porosity in the glasses and glass-ceramics decreases the thermal conductivity, dielectric permittivity and density. On the other hand, it enhances the sensing and absorption of sound waves¹⁰. So, these glasses and glass-ceramics can readily find applications in the microelectronic devices, such as band-pass filters, dielectric resonant antennas and oscillators etc. For these applications, the material should have dielectric permittivity ~10 or above at room temperature with good thermal and mechanical stability. It also must have temperature and frequency independent behaviour in the microwave frequency region¹¹. Silica and silicate based glasses could meet these requirements. High silica glasses are required for thermophotovoltaic system due to their good resistance to heat and thermal shock¹². The disadvantage of the glasses and glass-ceramics derived from the agricultural wastes is the inability to vary the amount of different oxides, which prevents to tailor the properties according to the need and applications. This problem can be addressed by using different agricultural waste materials, which have different SiO₂ content along with other

¹School of Physics and Materials Science, Thapar University, Patiala-147004, India. ²Department of Physics, School of Basic Sciences, Arni University, Kathgarh-176401, India. Correspondence and requests for materials should be addressed to K.S. (email: kusingh@thapar.edu)

Multiferroic properties of Tb-doped BiFeO₃ nanowires

Gurmeet Singh Lotey · N. K. Verma

Received: 18 August 2012 / Accepted: 28 February 2013 / Published online: 12 March 2013
© Springer Science+Business Media Dordrecht 2013

Abstract Nanoscale, multifunctional, multiferroic materials possess strong magnetoelectric coupling (ME), open exciting multitudinous ways for designing future nanoelectronic and spintronic device applications. Bulk nanowires (100 nm), pure, and Tb-doped BiFeO₃ multiferroic nanowires (20 nm) have been synthesized by colloidal dispersion template-assisted technique. The effects of Tb-doping and size of synthesized nanowires on structural, electrical, magnetic, dielectric, and magnetodielectric properties have been investigated. X-ray diffraction study reveals that doping of Tb in BiFeO₃ nanowires leads to structural transformation from rhombohedral to orthorhombic. X-ray photoemission analysis confirms the +3 oxidation state of Fe and high purity of samples. Bulk nanowires exhibit antiferromagnetic characteristics, whereas the Tb-doped BiFeO₃ nanowires show ferromagnetic character. Moreover, with increase in Tb concentration, the saturation magnetization increases. Temperature-dependent magnetization study suggests their size-dependent ferro and ferri-magnetic behavior. Polarization versus electric field (P–E) study reveals that pure BiFeO₃ nanowires possess elliptical loop; however, doping of Tb results in rectangular loop—portentous good ferroelectric properties. All synthesized samples exhibit frequency-dependent dielectric

constant which decreases with increase in frequency and remains fairly constant at higher frequencies. Leakage current density decreases with increase in Tb concentration, and has been found to be three orders of magnitude less than those of bulk BiFeO₃ nanowires. The ME coupling in synthesized nanowires was estimated by measuring magnetodielectric. A very high value of ME, 7.2 %, has been found for 15 % Tb-doped BiFeO₃ nanowires. In this communication, we, for the first time, report new cue on size-dependent Tb-doped BiFeO₃ nanowires, which may be further used to explore its technological device applications.

Keywords Nanowires · Ferroelectricity · Multiferroics · Spin spiral cycloid · Magnetoelectric effect

Introduction

Multifunctional oxide nanostructures such as nanowires, nanotubes are the demand of future technology. These are the building blocks for future nanoelectronic devices for the development of miniaturization and high-density data storage system. It is highly desirable to integrate multifunctions in a single material. Multiferroic materials, with strong coupling [magnetoelectric (ME) coupling] among different orders of ferroics such as electric and magnetic, meet the necessary requisites and are the most promising materials for data storage, spintronics, and nanoelectronics (Eerenstein et al. 2006).

G. S. Lotey (✉) · N. K. Verma
Nano Research Lab, School of Physics and Materials
Science, Thapar University, Patiala 147004, India
e-mail: gslotey1986@gmail.com; gslotey@thapar.edu

Effective Laser Sealing Enabled by Glass Thick Films Containing Carbon Black/Carbon Nanotubes

Oh Hyeon Kwon,[‡] Bhaskar Chandra Mohanty,[‡] Deuk Ho Yeon,[‡] Jong-Seok Yeo,[§] Kyoungho Lee,[¶] and Yong Soo Cho^{‡,†}

[‡]Department of Materials Science & Engineering, Yonsei University, Seoul 120-749, Korea

[§]School of Integrated Technology, Yonsei University, Songdo 406-840, Korea

[¶]Department of Display Materials Engineering, Soonchunhyang University, Asan 336-745, Korea

An effective way of providing complete sealing of glass using an 810 nm diode laser was investigated for longer lifetime of glass panel-based devices. Small amounts (<5 wt%) of laser-absorbing materials such as carbon black (CB) or carbon nanotubes (CNT) were added to a bismuth zinc borate glass paste for instantaneous adhesion between glass substrates without interfacial cracks or severe pores. A higher laser power was required for a lower content of carbon for the laser-assisted sealing of glass. As optimal compositions, the addition of 1.0 wt% CB or 0.5 wt% CNT led to complete densification of glass with higher optical transmittance. Higher absorption coefficients calculated in the CNT case, e.g., $\sim 536.4 \text{ cm}^{-1}$ for the 0.5 wt% CNT sample compared to $\sim 277.6 \text{ cm}^{-1}$ for the 0.5 wt% CB sample, are believed to be responsible for the effective sealing even with a lower content of CNT.

I. Introduction

As in the case of many other currently active electronic and photonic devices, long-term stability has been a critical issue for the glass panel-based modules and devices including displays and photovoltaic applications. However, the reliable technology of sealing glass panels has been very limited even though the glass sealant has been recognized as one of the most promising choices due to the hermetic capability and chemical inertness of glass itself.^{1–3} This limitation comes mainly from the fact that glass needs to be fully densified at a minimum temperature of $\sim 450^\circ\text{C}$ – 500°C as exemplified for the current glass sealing technology for plasma display panels.⁴ This high-temperature processing can be critically detrimental as many electronic and optical devices contain volatile organics or temperature-sensitive constituents.^{5,6}

Laser transmission welding (or joining), which is a viable alternative to thermal welding, has been recently developed for polymer-based panels containing laser-absorbing materials such as carbon black (CB), carbon nanotube (CNT), or other pigments.^{7–10} In this technique, the laser energy transmitted through the first joint partner made of a laser-transparent polymer heats up the joining interface with the assistance of the laser-absorbing components. The local generation of effective heat happens by energy transfer from the laser source into the limited periphery of a few tens of micrometers around the absorbing components. In the case of glass, the utilization of femtosecond laser pulses has been

reported primarily for multiphoton absorption, melting, and limited welding, but has not been recognized as an effective alternative of sealing due to the induced pores and cracks at interfaces.^{11,12}

In this work, the effect of adding laser-absorbing materials such as CB and CNT to a potential low softening glass sealant is reported for the first time for complete laser sealing of glass plates without interfacial damages and entrapped pores. Absorption coefficient and penetration depth according to the content of carbon materials are discussed as major parameters for explaining the sealing capability of glass with excellent microstructural evidences.

II. Experimental Procedure

A commercially available Bi_2O_5 – ZnO – B_2O_3 glass-based frit (BSP780; DAION Co., Incheon, Korea) was used in this work. The frit has a softening point of $\sim 385^\circ\text{C}$ and an average particle size of $\sim 3 \mu\text{m}$. Carbon black powder (High Purity Chemical, Tokyo, Japan) or multiwalled CNT (CM-95; Hanhwa Nanotech, Incheon, Korea; ~ 10 – 15 nm in diameter and $\sim 20 \mu\text{m}$ in length) was added as a laser-absorbing material up to 5 wt% of the glass weight. Viscous ink paste was prepared by admixing the glass frit and carbon materials with organic binder vehicles composed of ethyl cellulose (Kanto Chemical Co., Ltd, Tokyo, Japan), α -terpineol (90%; Aldrich, Milwaukee, WI) and lauric acid (98%; Aldrich, Milwaukee, WI) using a commercial paste mixer (PDM-150; Daewha Tech, Yongin, Korea). For the primary adhesion evaluation, the resultant paste was screen printed three times using a 250 mesh screen on soda lime silicate (SLS) glass substrates to obtain a dried film thickness of $\sim 30 \mu\text{m}$. The screen printed paste was dried at 120°C and then pre-fired at 370°C for 1 h. The pre-firing was conducted mainly for organic burnout.

A diode laser having $\lambda = 810 \text{ nm}$ (Koryeo Semiconductor System, Bucheon, Korea) was used for irradiation. The irradiation was performed by scanning a laser beam of $\sim 1.0 \text{ mm}$ in diameter onto the surface of the pre-fired thick films at various laser powers in the range of 3–40 W. The incident and transmitted intensity of laser radiation was measured by an energy meter (Field Max II; Coherent, Santa Clara, USA). The actual sealing experiment was additionally conducted by placing another glass substrate onto the pre-fired thick films and then by irradiating through one side of the laser-transparent SLS substrate using the laser, as demonstrated in the schematic of Fig. 1. The sandwiched structure was evaluated in terms of the degree of sealing basically from microstructural features. For the sealing experiment, the screen printing of the glass paste was repeated seven times to have a thicker fired thickness of $\sim 40 \mu\text{m}$.

Surface and cross-sectional microstructure of the laser-irradiated samples were observed by an optical microscope

B. Derby—contributing editor

Manuscript No. 32223. Received October 23, 2012; approved January 31, 2013.
[†]Author to whom correspondence should be addressed. e-mail: ycho@yonsei.ac.kr

Nuclear fusion as a probe for octupole deformation in ^{224}Ra

Raj Kumar,^{*} J. A. Lay,[†] and A. Vitturi

*Dipartimento di Fisica e Astronomia "Galileo Galilei", Università di Padova, via Marzolo, 8, I-35131 Padova, Italy
and INFN, Sezione di Padova, via Marzolo, 8, I-35131 Padova, Italy*

(Received 21 January 2015; revised manuscript received 2 June 2015; published 5 November 2015)

Background: Nuclear fusion has been shown to be a useful probe to study the different nuclear shapes. However, the possibility of testing octupole deformation of a nucleus with this tool has not been fully explored yet. The presence of a static octupole deformation in nuclei will enhance a possible permanent electric dipole moment, leading to a possible demonstration of parity violation.

Purpose: To check whether static octupole deformation and octupole vibration in fusion give different results so that both situations could be experimentally disentangled.

Method: Fusion cross sections are computed in the coupled-channel formalism making use of the ingoing-wave boundary conditions (IWBC) for the systems $^{16}\text{O} + ^{144}\text{Ba}$ and $^{16}\text{O} + ^{224}\text{Ra}$.

Results: Barrier distributions of the two considered schemes show slightly different patterns. In the case of ^{144}Ba , the difference between them is negligible. For the ^{224}Ra case, perceptible differences are found in correspondence with its larger octupole deformation. However, the possibility of disentangling both schemes is not guaranteed and it will depend on the available experimental accuracy and the strength of the octupole deformation.

Conclusions: The measurement of barrier distributions could be a complementary probe to support the presence of octupole deformation.

DOI: [10.1103/PhysRevC.92.054604](https://doi.org/10.1103/PhysRevC.92.054604)

PACS number(s): 25.60.Pj, 24.10.Eq, 25.70.Jj

I. INTRODUCTION

The search of octupole deformations in nuclei is experiencing a revival thanks to its impact in a possible permanent atomic electric dipole moment (EDM) [1,2]. A nonzero EDM will indicate a time-reversal (or equivalently charge-parity) violation. The magnitude or the experimental maximum limit to it can constrain the different suggested extensions to the standard model [3]. The presence of a static octupole deformation in an odd nucleus will generate enhanced nuclear Schiff moments, which contributes to the atomic EDM so that it can be improved by several orders of magnitude [4].

Therefore, the experimental focus is set on the search for permanent octupole deformations in some of the regions where different theoretical approaches predict strong octupole correlations [5,6] with the help of continuous development of radioactive beam facilities. In the present work we will focus on ^{144}Ba and ^{224}Ra as representative of two different regions where possible static deformations have been predicted.

In [1,7], Coulomb excitation was used to measure the different electric transition probabilities. This tool provides quadrupole and octupole transition probabilities with good accuracy. Smaller dipole electric transition probabilities will carry larger error bars, even though this problem is experimentally affordable and they were able to provide some measurements. It should be kept in mind that large octupole transitions can be found also for dynamic octupole vibrations. In addition, the coupling between quadrupole deformation and octupole vibrations can lead to enhanced dipole moments [5].

Therefore, we would like to propose here a complementary experimental probe for static octupole deformation. A traditional experimental tool for the study of nuclear structure is provided by subbarrier fusion. It is well known that fusion at energies around the Coulomb barrier is driven by the dynamical couplings to the internal degrees of freedom of the fusing counterparts [8,9]. The absence or presence of octupole and dipole moments in one of the fusing partners will have a certain impact in the final subbarrier fusion cross section. This fact could suggest, if the minimum accuracy is reached, the possibility of distinguishing between static octupole deformation and the corresponding dynamical vibration.

The work is structured as follows. In Sec. II we recall the reaction formalism for studying nuclear fusion including deformations and/or vibrations. We apply this framework in Sec. III to the reactions $^{16}\text{O} + ^{144}\text{Ba}$ and $^{16}\text{O} + ^{224}\text{Ra}$ considering quadrupole deformations for ^{144}Ba and ^{224}Ra looking for the differences between adding an octupole vibration or deformation to the previous quadrupole deformation. Finally, in Sec. IV the main results of this work are summarized.

II. REACTION FRAMEWORK

Fusion probabilities are calculated by solving the corresponding coupled-channel equations under ingoing-wave boundary conditions (IWBC). The coupled-channel formalism for direct reaction processes given by Austern [10] expands the total wave function in terms of the wave function for the internal state of the projectile ϕ_β and the radial wave functions χ_β that account for the relative motion between projectile and target. This leads to a set of coupled equations for the radial

*rajkumarfzr@gmail.com

†lay@pd.infn.it

Room Temperature Magnetism in Co-Doped ZnS Nanoparticles

Sunil Kumar · N. K. Verma

Received: 23 June 2014 / Accepted: 26 September 2014
© Springer Science+Business Media New York 2014

Abstract Cobalt (0, 1, 5, and 10 %)-doped ZnS nanoparticles have been synthesized via low-temperature solvothermal technique. The resultant nanoparticles have been analyzed using transmission electron microscope (TEM), electron dispersive spectroscope (EDS), X-ray diffraction (XRD), and UV-visible (UV-Vis.) and photoluminescence (PL) spectrophotometer. Magnetic studies have been carried out using a vibrating sample magnetometer (VSM). The average size of nanoparticles has been found to be ~ 9 nm. The XRD spectra indicated cubic phase of the undoped and Co-doped ZnS nanoparticles. The band gap of doped nanoparticles, 4.80 eV, has been found to be blueshifted as compared to its undoped counterpart, 4.59 eV. Room-temperature emission spectra exhibited blue and green lines. Magnetic studies indicated diamagnetic and ferromagnetic character at lower Co concentrations, 0 and 1 %, and ferromagnetic and paramagnetic character at higher Co concentrations, 5 and 10 %.

Keywords Dilute magnetic semiconductors · Nanostructures · Blue emission · Ferromagnetism

1 Introduction

Semiconducting materials doped appropriately with magnetic materials, such as transition metals or rare-earth metals, are known as dilute magnetic semiconductors (DMS). In the recent times, there has been a tremendous interest in the research on transition metal-doped chalcogenide nanostructures. The new kind of DMS materials exhibit optical and magnetic behaviors due to charge and spin controllability [1]. Due to its wide band gap, ZnS has been an attractive material, as it acts as a good host for transition metals. The transition metal-doped ZnS nanostructures have a wide variety of applications in the area of spintronics, solar cells, light-emitting diodes, magnetic resonance imaging (MRI), lasers [2–7], etc. Bhargava et al., in 1994, attempted for the first time with Mn-doped ZnS nanocrystals to explore the optical and magnetic properties of ZnS-based DMS nanostructures [8]. Since then, a lot of research has been focused on the structural, optical, and magnetic studies of transition metal-doped ZnS nanostructures. The nanostructures can be specifically used in a variety of applications due to its unique quantum confinement effects. Generally, the properties of materials are size and shape dependent; hence, when doped appropriately with transition metals or rare-earth metals, these ZnS nanostructures can be useful as fundamental building blocks for fabricating the advanced nanoscale electronic and optoelectronic devices. Various studies on photoluminescence and magnetic studies [9–12, 14, 16] of transition metal-doped ZnS nanostructures are available in literature. But very few reports have been found on Co-doped ZnS nanostructures. Lu et al. [15] reported the structural and magnetic behavior of Co-doped ZnS nanowires. It was observed that the Co-doped ZnS nanowires exhibit ferromagnetism at room temperature and ferromagnetism increases as the Co concentration

S. Kumar (✉) · N. K. Verma
Nano Research Lab, School of Physics and Material Science,
Thapar University, Patiala, Punjab 147004, India
e-mail: skt.nano@gmail.com

S. Kumar
Department of Physics, Indus International University,
Una, Himachal Pradesh 174301, India



Seedless co-surfactant-based dimensional and optical tunability of gold nanorods with simultaneous pH regulation

Parveer Kaur¹ and Bhupendra Chudasama^{1,*}

¹Laboratory of Nanomedicine, School of Physics and Materials Science, Thapar University, Patiala 147004, India

Received: 24 March 2017

Accepted: 24 June 2017

Published online:
5 July 2017

© Springer Science+Business
Media, LLC 2017

ABSTRACT

Intense electromagnetic fields generated by the gold nanorods (GNRs) owing to their strong plasmon resonance make them promising candidate for applications in cancer diagnostics, photothermal therapy, single-molecule detection, drug delivery, etc. Use of GNRs in these applications as plasmon resonance probes depends on the extent to which their plasmon resonance band can be tuned into NIR region. In this study, we propose a facile seedless approach to synthesize GNRs in a cetyltrimethylammonium bromide (CTAB)–benzyltrimethylhexadecylammonium chloride (BDAC) co-surfactant system with simultaneous pH regulation that yields GNRs with tunable plasmon resonance in tissue transparent NIR region. The role of binary co-surfactants, pH of the growth solution, and influence of the volume of the reducing agent on GNRs growth has been studied. Under optimized conditions, the longitudinal plasmon resonance band of GNRs can be tuned from 780–1300 nm by regulating the pH of the growth solution from 2.5 to 1.3. The role of co-surfactants and pH in the regulation of dimensions and thus plasmonic properties of GNRs synthesized by single-step seedless approach has been evaluated.

Introduction

Collective excitation of conduction band electrons on the surface of metal nanoparticles under the influence of incident electromagnetic radiation of appropriate frequency causes strong absorption of electromagnetic radiations. This optical property of metal nanoparticles is known as ‘surface plasmon resonance’ [1]. Owing to their tunable plasmonic

properties, gold nanorods (GNRs) have evolved deep interest in the field of bio-imaging, chemical sensing, plasmon resonance spectroscopy, photonics, optoelectronics, therapeutics, diagnosis, etc. [2–4]. The extent to which the longitudinal surface plasmon resonance (LSPR) band of GNRs can be tuned depends on the size and shape of the nanoparticles as well as on the dielectric constant of the surrounding medium [5]. LSPR band of GNRs red shifts into the NIR region when their aspect ratio increases beyond

Address correspondence to E-mail: bnchudasama@gmail.com

Dynamics of Db isotopes formed in reactions induced by ^{238}U , ^{248}Cm , and ^{249}Bk across the Coulomb barrier

Gurjit Kaur,¹ Kirandeep Sandhu,² Amandeep Kaur,¹ and Manoj K. Sharma^{1,*}

¹*School of Physics and Materials Science, Thapar Institute of Engineering and Technology, Patiala-147004, India*

²*Department of Physics, GSSDGS Khalsa College, Patiala-147001, India*



(Received 27 February 2018; published 3 May 2018)

The dynamical cluster decay model is employed to investigate the decay of $^{265}\text{Db}^*$ and $^{267}\text{Db}^*$ nuclei, formed in the $^{27}\text{Al} + ^{238}\text{U}$, $^{18}\text{O} + ^{249}\text{Bk}$, and $^{19}\text{F} + ^{248}\text{Cm}$ hot fusion reactions at energies around the Coulomb barrier. First, the fission dynamics of the $^{27}\text{Al} + ^{238}\text{U}$ reaction is explored by investigating the fragmentation and preformation yield of the reaction. The symmetric mass distribution of the fission fragments is observed for $^{265}\text{Db}^*$ nucleus, when static β_{2i} deformations are used within hot optimum orientation approach. However, the mass split gets broaden for the use of β_{2i} -dynamical hot configuration of the fragments and becomes clearly asymmetric for the cold-static-deformed approach. Within the application of cold orientations of fragments, a new fission channel is observed at mass asymmetry $\eta = 0.29$. In addition to ^{238}U -induced reaction, the work is carried out to address the fission and neutron evaporation cross sections of $^{267}\text{Db}^*$ nucleus formed via $^{19}\text{F} + ^{248}\text{Cm}$ and $^{18}\text{O} + ^{249}\text{Bk}$ reactions, besides a comprehensive analysis of fusion and capture processes. Higher fusion cross sections and compound nucleus formation probabilities (P_{CN}) are obtained for the $^{18}\text{O} + ^{249}\text{Bk}$ reaction, as larger mass asymmetry in the entrance channel leads to reduced Coulomb factor. Finally, the role of sticking (I_S) and nonsticking (I_{NS}) moments of inertia is analyzed for the $4n$ and $5n$ channels of $^{267}\text{Db}^*$ nuclear system.

DOI: [10.1103/PhysRevC.97.054602](https://doi.org/10.1103/PhysRevC.97.054602)

I. INTRODUCTION

The investigation of the reaction dynamics involving the evolution of odd- Z superheavy nuclei is essential to examine the unexplored region of the nuclear chart. The existence of unpaired nucleons in the odd- Z nuclei effect the structure and reaction dynamics to a reasonable extent, which could be investigated through the dynamical study of the superheavy nuclei [1]. Therefore, an attempt is made to investigate the decay paths of dubnium ($Z = 105$) nucleus formed in different hot fusion reactions. This nucleus has been of great interest for past few decades and its first signature was reported by the Joint Institute for Nuclear Research in the analysis of the $^{22}\text{Ne} + ^{243}\text{Am}$ reaction [2]. Subsequently, various isotopes of Db were synthesized in hot and cold fusion reactions. The excitation functions for the $1n$ and $2n$ exit channels of the $^{208}\text{Pb}(^{51}\text{V}, xn)^{259-x}\text{Db}$ and $^{209}\text{Bi}(^{50}\text{Ti}, xn)^{259-x}\text{Db}$ reactions were measured at Lawrence Berkeley National Laboratory [3]. In addition to this, the capture and fusion processes were also obtained for $^{259}\text{Db}^*$ and $^{265}\text{Db}^*$ nuclear systems, respectively formed in the $^{50}\text{Ti} + ^{209}\text{Bi}$ [4] and $^{27}\text{Al} + ^{238}\text{U}$ [5] reactions. To have a comprehensive knowledge about the decay of Db nuclei, recently the $^{248}\text{Cm}(^{19}\text{F}, xn)^{267-x}\text{Db}$ and $^{249}\text{Bk}(^{18}\text{O}, xn)^{267-x}\text{Db}$ reactions were compared by Haba *et al.* [6] for the production of Db isotopes through $4n$ and $5n$ emissions, and the same are tested here in the framework of the dynamical cluster decay model (DCM) [7–12]. The individual excitation functions for ^{263}Db and ^{262}Db nuclei are evaluated across

the Coulomb barrier energies. The channel cross sections are calculated for both sticking and nonsticking moments of inertia (I_S and I_{NS} , respectively), by including the quadrupole (β_{2i}) deformations and “hot-optimum” orientations. The $4n$ channel could be addressed via I_S and I_{NS} approaches, whereas nonsticking (I_{NS}) approach seems favorable to address the $5n$ cross sections, particularly for the $^{18}\text{O} + ^{249}\text{Bk}$ reaction.

In addition to the addressal of the evaporation residue cross sections, the separation between the capture and fusion events is the main quest to handle the superheavy reaction dynamics. The origin of the noncompound nuclear processes, such as quasifission, quasielastic, and deep-inelastic events, always hinder the superheavy compound nucleus formation [13], hence the fusion cross sections generally have lower magnitude as compare to the capture cross sections. The reason lies in the fact that the fusion of two heavy nuclei is governed through various factors such as excitation energy, Coulomb interactions, entrance channel mass asymmetry, deformation parameters, and barrier characteristics of the reaction partners, etc. Keeping this in mind, the fusion mechanism of the $^{19}\text{F} + ^{248}\text{Cm} \rightarrow ^{267}\text{Db}^*$ and $^{18}\text{O} + ^{249}\text{Bk} \rightarrow ^{267}\text{Db}^*$ reactions is analyzed through the Wong model [14], using the barrier characteristics such as barrier height (V_B), barrier position (R_B), curvature ($\hbar\omega$), etc. In addition to the above reactions, the uranium-induced hot fusion reaction leading to $^{265}\text{Db}^*$ nucleus is also investigated within the framework of the DCM model [7–12]. Within this methodology, the symmetric mass distribution of the fission fragments is governed through the hot-optimum orientations of the fragments, suggesting that fusion-fission is a main decay mode for $^{265}\text{Db}^*$ and $^{267}\text{Db}^*$ nuclei. However, the contribution of the symmetric fission

*msharma@thapar.edu



Cite this: *RSC Adv.*, 2016, 6, 51046

Combined and individual doxorubicin/vancomycin drug loading, release kinetics and apatite formation for the $\text{CaO-CuO-P}_2\text{O}_5\text{-SiO}_2\text{-B}_2\text{O}_3$ mesoporous glasses†

Gurbinder Kaur,^{*a} O. P. Pandey,^a K. Singh,^a Bhupendra Chudasama^a and V. Kumar^b

The novel mesoporous glass series based on $(25 - x)\text{CaO} - x\text{CuO} - 10\text{P}_2\text{O}_5 - 5\text{B}_2\text{O}_3 - 60\text{SiO}_2$ ($x = 2.5, 5, 7.5, 10$) has been prepared using the sol-gel technique. The pore size of the prepared mesoporous bioactive glasses (MBG) lies between 6.1 and 9.1 nm, whereas the surface area varies from 281 to 418 $\text{m}^2 \text{g}^{-1}$. The pH variation, zeta potential, Fourier transform infra-red (FTIR) spectroscopy and simulated body fluid (SBF) studies indicated the *in vitro* bioactivity of all the MBGs. The MBGs were loaded with the anticancerous and antibacterial drugs, doxorubicin and vancomycin, respectively. The increasing copper content predominantly influenced the bioactive properties as well as the drug loading and release kinetics of the doxorubicin and vancomycin drugs. In addition to the individual loading of drugs in the MBG, both the drugs were also loaded together in the MBG to investigate the effect of combined loading on the release capability of the MBGs.

Received 15th March 2016
Accepted 16th May 2016

DOI: 10.1039/c6ra06829d

www.rsc.org/advances

1. Introduction

The most striking feature of bioactive glass (BG) is its ability to induce the formation of a hydroxyapatite layer on its surface upon contact with biological fluids (especially simulated body fluid, SBF).¹⁻³ Usually, for enhanced bioactive behavior, the glasses are prepared by the sol-gel technique as it yields higher surface area and porosity along with a uniform distribution of the particle size.⁴⁻⁶ The higher bioactivity of a material implies a greater ability of the material to deposit apatite on its surface *via* a series of biochemical and biophysical reactions at the site of the material-biological fluid interface. Bioactive glasses are biocompatible, bioresorbable, osteoconductive and possess controllable degradation rate. These features make BG excellent carriers/vehicles for the delivery of therapeutic drugs, bioactive molecules, proteins and growth factors.⁷⁻¹¹ Drug loaded BG enhance the osteogenesis, bone regeneration and proliferation by releasing the osteoconductive factors like growth factors, hormones, peptides, chemotherapeutic agents, anti-inflammatory drugs and antiestrogens. The targeted/local drug delivery system exhibits 'zero premature release', so that the loss of activity of drugs shall not take place before reaching the target tissue.¹²⁻¹⁵ Hence, for the effective treatment of the target, the biodistribution and

pharmacokinetics of the associated drug with the BG must be controlled such that sufficient dose of drug is provided.

Bioactive glasses have been a boon in curing the bone related diseases. The bone degradation usually occurs due to the non-traumatic malignant bone tumours, osteomyelitis and post-surgical infections. The targeted tumour therapy of bone promotes bone healing along with killing bone cancer cells. Though, bone tissue grafts have been implied as allografts, but they may result in immunological problems or viral/bacterial contaminations. In order to treat the infected bones without any adverse reactions such as chronic inflammations/infections, the bioactive glass drug vehicle must be loaded with the anti-cancer drugs and broad-spectrum drugs simultaneously.

By adding certain co templates and structure directing agents like cetyltrimethyl ammonium bromide (CTAB), F127 (EO106-PO70-EO106) and P123 (EO20-PO70-EO20) into the glass structure, mesoporous bioactive glasses (MBG) can be obtained.¹⁴⁻¹⁹ P123 and F127 are triblock copolymers with chemical formula $\text{HO}(\text{CH}_2\text{CH}_2\text{O})_{20}(\text{CH}_2\text{CH}(\text{CH}_3)\text{O})_{70}(\text{CH}_2\text{CH}_2\text{O})_{20}\text{H}$ (molecular weight ≈ 5800 Da) and $\text{HO}(\text{CH}_2\text{CH}_2\text{O})_{106}(\text{CH}_2\text{CH}(\text{CH}_3)\text{O})_{70}(\text{CH}_2\text{CH}_2\text{O})_{106}\text{H}$ (molecular weight ≈ 12500 Da), respectively.¹⁶⁻¹⁹ The mesoporous glasses have mesochannels and act as excellent source for drug delivery. The drugs can be loaded into the channels without chemical bonding. Apart from MBGs, mesoporous silica material has also received wide attention for the drug delivery whereas cell encapsulation technology is the preferred system for transplantation as it can treat multiple diseases in the absence of immunosuppression.²⁰⁻²² Microencapsules consist of biologically active

^aSchool of Physics and Materials Science, Thapar University, Patiala-147004, India. E-mail: gkapds@gmail.com; Tel: +91-9888372281

^bShri Guru Granth Sahib World University, Fatehgarh Sahib, 140406, India

† Electronic supplementary information (ESI) available. See DOI: 10.1039/c6ra06829d

Study on Structural, Multiferroic, Optical and Photocatalytic Properties of Ferroelectromagnetic Nanoparticles: $\text{Bi}_{0.9}\text{Ba}_{0.1}\text{Fe}_{0.8}\text{Ti}_{0.2}\text{O}_3$

Manpreet Kaur¹ · Poonam Uniyal¹

Received: 25 July 2016 / Accepted: 16 August 2016
© Springer Science+Business Media New York 2016

Abstract Ferroelectromagnetic nanoparticles ($\text{Bi}_{0.9}\text{Ba}_{0.1}\text{Fe}_{0.8}\text{Ti}_{0.2}\text{O}_3$) have been successfully fabricated for multifunctional applications and photocatalytic degradation of an industrial dye. X-ray diffraction of $\text{Bi}_{0.9}\text{Ba}_{0.1}\text{Fe}_{0.8}\text{Ti}_{0.2}\text{O}_3$ nanoparticles suggested the pure phase formation with tetragonal structure. The average particle size was found to vary in the range of 10–15 nm. An anomaly in dielectric constant was observed in the vicinity of antiferromagnetic transition temperature. Also, impedance spectroscopy measurements clearly indicated a non-Debye-type relaxation phenomenon in $\text{Bi}_{0.9}\text{Ba}_{0.1}\text{Fe}_{0.8}\text{Ti}_{0.2}\text{O}_3$ ceramic. The resistivity of the $\text{Bi}_{0.9}\text{Ba}_{0.1}\text{Fe}_{0.8}\text{Ti}_{0.2}\text{O}_3$ ceramic was of the order of $10^7 \Omega$ and was found to decrease with an increase in temperature. The remnant polarization (P_r) value of $9.77 \mu\text{C}/\text{cm}^2$ and weak ferromagnetic properties with a magnetization value of 0.025 emu/g were induced. The appropriate energy bandgap of nanoparticles ($E_g = 2.161 \text{ eV}$) makes it suitable for the degradation of azo-dye in the visible region. The absorption peak intensity of azo-dye gradually decreased with the addition of $\text{Bi}_{0.9}\text{Ba}_{0.1}\text{Fe}_{0.8}\text{Ti}_{0.2}\text{O}_3$ nanoparticles. Finally, the nanoparticles degrade the azo-dye at approximately 94 % after 80 min in acidic medium.

Keywords Nanoparticles · Multiferroic properties · Impedance analysis · Optical property · Photocatalytic activity

1 Introduction

Presently, the development in the field of wireless communication technology requires miniaturization of highly efficient electronic devices, especially on multilayer/multidoped components. This implies a design of novel ceramics, which can be sintered at lower temperature and exhibit excellent electrical properties. The most promising ceramic for such application is polycrystalline ferrite, which shows superior electric and magnetic properties. This ceramic material is easy to fabricate, cost-effective, and stable, and offers a wide range of technological applications in the cores of transformers, semiconductors, frequency circuits, filters, operating devices, etc. [1–3].

Literature evidences that BiFeO_3 is the only natural material that possesses high intrinsic polarization ($100 \mu\text{C}/\text{cm}^2$ in the $(111)_{pc}$ direction) and offers both ferroelectric and antiferromagnetic properties, above room temperature [4, 5]. In addition, the multiferroic BiFeO_3 gains more attention in fundamental understandings due to its ability of converting light into electrical, mechanical, and chemical energies and also helpful in attaining application goals as these are proficient in photovoltaic, phototransduction, and photocatalytic devices [6]. Industrial effluent is also becoming a serious challenge for society as they damage water courses, endangering human life as well as wildlife. At that point, BiFeO_3 contributes as a proficient semiconductor photocatalyst to remove environment pollutants. The most known and extensively studied semiconductor for photocatalysis is titanium dioxide (TiO_2) because of its adequate stability, low cost, and suitable band edge positions, but the large energy bandgap (3.2 eV) degrades its efficacy in visible light resulting in inadequate utilization of solar energy [7–9]. Even the modified TiO_2 may be activated in the presence of visible light, they also show weak activity as well as

✉ Poonam Uniyal
uniyalpoonam@gmail.com; poonam.uniyal@thapar.edu

¹ Smart Materials Lab, School of Physics and Materials Science, Thapar University, Patiala 147 004, Punjab, India

Effect of Tb³⁺ ion substitution on structural, optical and magnetic properties of CdS nanoparticles

Shivani Jindal¹ · Kamaldeep Kaur¹ · N. K. Verma¹ · Puneet Sharma¹

Received: 7 June 2017 / Accepted: 20 September 2017
© Springer Science+Business Media, LLC 2017

Abstract Cd_{1-x}Tb_xS ($x=0.00, 0.05, 0.10, 0.15$) nanoparticles were synthesized by hydrothermal technique. The effect of Tb-doping on structural, optical and magnetic properties were studied. The X-ray diffraction (XRD) confirmed wurtzite phase without any impurity. HR-TEM micrographs revealed the particle size of ~18 nm with spherical morphology. Band gap calculated from UV-Visible absorption spectra showed an initial decrease from 2.49 eV ($x=0$) to 2.45 eV ($x=0.10$). Further, increasing Tb-doping to $x=0.15$ band gap increased to 2.54 eV. Photoluminescence emission spectra showed peaks at 430 and 490 nm for $x=0$ and 0.05 which corresponds to blue emission. Further increase in Tb doping, peaks found to be quenched. Peak at 530 nm is due to green emission and shifted to higher wavelength with Tb-doping. Magnetic analysis confirmed ferromagnetism in both undoped and Tb-doped nanoparticles. Saturation magnetization found to decrease upto $x=0.10$ and increased for $x=0.15$.

1 Introduction

Rare earth or transition metal doped group IV-VI, III-V and II-VI semiconductors are known as dilute magnetic semiconductors (DMS). These DMS materials are promising candidates for spintronic applications, in which they allow the manipulation of carrier spins [1]. These materials possess unique electronic and magnetic properties as compared to their bulk counterparts due to quantum effect at nanoscale

[2, 3]. The origin of ferromagnetism in nanomaterials is a controversial topic and is still under investigation [4]. The observed ferromagnetism were explained by various types of exchange interactions i.e. double-exchange, RKKY and super-exchange in these materials [5, 6]. It is also attributed to the reduction of one or more dimensions at nanoscale that decreases the atomic coordination number. This reduces the hopping tendency of electrons and hence increases coulomb interaction to bandwidth ratio which increases the magnetic tendency [7]. Whereas, secondary phases or defects are also found responsible for their magnetic behaviour [8, 9]. In the recent years, the observation of ferromagnetic ordering at room temperature (*RT*) accompanied by high Curie temperature in II-VI and III-V semiconductors has gained a significant attention for future device applications.

Among various II-VI semiconductors, CdS is of greater interest due to its wide band gap (E_g) of 2.42 eV with high electronic transport, high mobility as well as its good magneto-optical properties [10]. Therefore, it is considered to be a promising host material for application in solar cell, light emitting diodes, photocatalysis and photo detectors [11-14]. Recently, II-VI semiconductor materials doped with rare earth ions are in focus as they are potential candidates for optical display devices [15]. These ions have partially filled 4fⁿ shells due to which they exhibit longer fluorescence lifetime, large excitation emission separation and very narrow intense emission lines [16]. There are various reports on rare earth (Gd, Pr, Eu, Ce) doped CdS nanoparticles [17-20]. However, there are few reports on Tb-doped CdS nanoparticles that focused to their fluorescence and photoluminescence properties but not on their magnetic properties [21, 22]. In this communication, we systematically investigated the structural, optical and magnetic properties of Tb-doped CdS nanoparticles.

✉ Puneet Sharma
puneet.sharma@thapar.edu

¹ School of Physics and Materials Science, Thapar University, Patiala 147004, India

SCIENTIFIC REPORTS

OPEN

Dynamics of surface evolution in semiconductor thin films grown from a chemical bath

Indu Gupta & Bhaskar Chandra Mohanty

Received: 25 May 2016
Accepted: 22 August 2016
Published: 12 September 2016

Dynamics of surface evolution in CdS thin films grown by chemical bath deposition technique has been studied from time sequence of atomic force micrographs. Detailed scaling analysis of surface fluctuation in real and Fourier space yielded characteristic exponents $\alpha_{loc} = 0.78 \pm 0.07$, $\alpha = 2.20 \pm 0.08$, $\alpha_s = 1.49 \pm 0.22$, $\beta = 0.86 \pm 0.05$ and $\beta_{loc} = 0.43 \pm 0.10$, which are very different from those predicted by the local growth models and are not related to any known universality classes. The observed anomalous scaling pattern, characterized by power law scaling dependence of interface width on deposition time differently at local and global scale, with rapid roughening of the growth front has been discussed to arise as a consequence of a nonlocal effect in the form of diffusional instability.

Recent developments in scaling invariance and universality have led to a growing interest in kinetic roughening theory with special attention being paid to studies on roughness evolution in thin films grown under far-from-equilibrium conditions^{1–4}. The study of evolving surfaces provides insight to the fundamental growth dynamics and enables one to control the roughness of the films. Such a study is of high technological relevance in that roughness of thin films in multilayer structures affects electrical, optical, mechanical and catalytic properties, and hence, determines the eventual performance of devices^{5–7}.

Typically roughness of a surface evolves as a consequence of simultaneous atomic scale processes such as direct addition of atoms on the growing surface from the surrounding, removal of atoms from the surface and motion of atoms along the surface or diffusive mass transport due to an existing or increasing chemical potential gradient⁸. The surfaces in many non-equilibrium growth models such as random surface recrystallization in the Eden model or ballistic aggregation are self-affine fractal which are described by the Kardar–Parisi–Zhang (KPZ) equation⁹

$$\frac{\partial h(x, t)}{\partial t} = \nu \nabla^2 h(x, t) + \frac{\lambda}{2} |h(x, t)|^2 + \eta \quad (1)$$

where ν accounts for the surface tension, λ is an “excess velocity” in the growth, and η is white noise. The self-affine patterns that the film surfaces develop into can be analyzed by the scaling properties of the surface fluctuations¹⁰. A number of applications of the KPZ equation were suggested based on the comparison of scaling exponents of surface roughness¹.

The self-affine roughness is widely characterized by engaging it to a dynamic scaling form wherein the root mean square of the fluctuations of the surface height i.e. the interface width w defined as $w(r, t) = \langle (h(\vec{r}, t) - \langle h(\vec{r}, t) \rangle)^2 \rangle_{\vec{r}}^{1/2}$, where h is the surface height and $\langle \dots \rangle_{\vec{r}}$ is spatial averaging in a system of size L and $r \leq L$, evolves following a simple dynamic scaling known as Family–Vicsek relation:

$$w(r, t) = t^\beta f\left(\frac{r}{t^{\beta\alpha}}\right) \quad (2)$$

where the scaling function behaves as $f(u) = \text{constant}$ and u^α for $u \gg 1$ and $u \ll 1$, respectively, α and β are the roughness and growth exponents respectively. The set of exponents corresponds to a specific universality class and is suggestive of the underlying mechanism that governs the evolution of roughness. Equation (2) suggests that for small r (i.e. $r \ll t^{\beta\alpha}$), w is independent of deposition time t and scales as r^α , and independent of r for large r when it scales as t^β . The crossover between these two behaviors occurs at $r = \xi$, the lateral correlation length,

School of Physics and Material Sciences, Thapar University, Patiala–147004, India. Correspondence and requests for materials should be addressed to B.C.M. (email: bhaskar@thapar.edu)

Improved photovoltaic and grain boundary characteristics of single elementary target-sputtered $\text{Cu}_2\text{ZnSnSe}_4$ thin films by post sulfurization/selenization process

Yeon Hwa Jo^{1,3}, Jin Woo Jang^{1,3}, Bhaskar Chandra Mohanty², Han Byul Kang¹ and Yong Soo Cho¹

¹ Department of Materials Science & Engineering, Yonsei University, Seoul 120-749, Korea

² School of Physics and Materials Science, Thapar University, Patiala 147004, India

E-mail: ycho@yonsei.ac.kr

Received 20 February 2015, revised 27 April 2015

Accepted for publication 1 May 2015

Published 22 May 2015



Abstract

A potential way to improve the quality of $\text{Cu}_2\text{ZnSnSe}_4$ absorber thin film by a one step process of sputtering using a single elementary target is proposed for thin film solar cells. As critical parameters, different S/Se ratios and grain boundary characteristics are achieved by adjusting sequential sulfurization and selenization post-treatment. The simple sulfurization of as-deposited film at 530 °C in H_2S is not effective in raising the performance but the additional Se annealing at a shorter duration of 5 min improves conversion efficiency from 0.12 to 3.21% with a drastic increase of the open circuit voltage. Positively-charged grain boundaries with narrow potential peaks seem to play a critical role for effective exciton separation and higher efficiency. The improvement is also understood as related to well-defined microstructures and the variable optical band gap.

Keywords: $\text{Cu}_2\text{ZnSnSe}_4$, sputtering, thin film solar cells, grain boundary, sulfurization

(Some figures may appear in colour only in the online journal)

1. Introduction

As a promising absorber candidate, $\text{Cu}_2\text{ZnSn}(\text{S,Se})_4$ (CZTSSe) has attracted great attention in recent years. CZTSSe is an earth-abundant and non-toxic material, which has emerged as an alternative to overcome the scarcity and toxicity issue of current $\text{Cu}(\text{In,Ga})\text{Se}_2$ (CIGS) and CdTe materials. CZTSSe has a controllable band gap of 0.9–1.5 eV, which can be determined by the relative content of S to Se, with considerably high absorption coefficients above 10^4 cm^{-1} . Such characteristics make the material very attractive as an alternative absorber for thin film solar cells [1–3].

The highest efficiency of ~12.6% has been reported for the CZTSSe absorber obtained by the spin-coating of the particle-containing hydrazine precursor and then by annealing [2].

The promising cell prefers a higher content of Se than S in CZTSSe, despite the fact that the sulfur-rich CZTSSe has a larger optimal band gap of ~1.4 eV. The co-existence of selenium and sulfur seems to be beneficial in producing better conversion efficiency even though excessive sulfur may cause a high defect density in the absorber, which creates recombinations [4]. Even though some studies on the sequential sulfurization have been reported so far, there is no correlative conclusion demonstrating the direct effect of sulfurization on the performance of CZTSSe [5]. On the other hand, the sputtering process for the absorber has been reported to have the highest efficiency of 9.7% when the multilayer approach using several targets was utilized [6]. It is known to be very difficult to achieve a desirable absorber layer by using a single target, presumably due to the difficulty in controlling the sputtering yield of each element and thus obtaining the intended stoichiometry [7, 8].

³ Equally contributed.

Dynamics of $^{47}\text{V}^*$ formed in $^{20}\text{Ne} + ^{27}\text{Al}$ reaction in view of fusion-fission and DIC mechanism

Neha Grover, Kanishka Sharma, and Manoj K. Sharma^a

School of Physics and Materials Science, Thapar University, Patiala-147004, India

Received: 29 September 2017 / Revised: 9 November 2017

Published online: 15 December 2017 – © Società Italiana di Fisica / Springer-Verlag 2017

Communicated by F. Gulminelli

Abstract. The decay mechanism of $^{47}\text{V}^*$ formed in direct kinematics ($^{20}\text{Ne} + ^{27}\text{Al}$) is investigated within the collective clusterization approach of dynamical cluster decay model (DCM). All calculations are done for quadrupole (β_{2i} -deformed) choice of fragments by taking optimum orientations over a wide range of center of mass energies ($E_{c.m.} \sim 83\text{--}125\text{ MeV}$). According to the experimental evidence, there is a strong competition between fusion fission (FF) and deep inelastic collision (DIC) in the decay of $^{47}\text{V}^*$, which are recognized as compound nucleus process and non-compound nucleus process, respectively. The decay cross sections of $^{47}\text{V}^*$ for both FF and DIC decay modes are addressed using DCM, and are found to be in agreement with the experimental data. It is important to mention that emitting fragments in both these decay channels maintain their homogeneity in terms of charge number, that lies in the region $3 \leq Z \leq 9$. Hence, all possible isotopes contributing towards $3 \leq Z \leq 9$ are taken into consideration here. Calculations of both FF and DIC are segregated on the basis of angular momentum windows, where $0 \leq \ell \leq \ell_{cr}$ has been taken for FF and $\ell_{cr} < \ell \leq \ell_{gr}$ for DIC, as the later operates only due to the partial waves near grazing angular momentum. In DIC, preformation probability (P_0) is divided equally amongst the most favoured outgoing fragments. Moreover, the behavior of fragmentation potential, preformation probability, penetrability and emission time etc. is examined, in order to identify the most favorable isotopes contributing towards FF and DIC.

1 Introduction

In the last few decades, collisions involving heavy ion charged particles forming a compound nucleus in the light mass region ($A_{CN} \leq 80$) have been studied extensively [1–6]. The study regarding the decay of compound nucleus having mass in the mentioned region provides a lot of interesting opportunities to analyze competing compound nucleus formalisms such as evaporation residues (ER) ($A_2 \leq 4$), intermediate mass fragments (IMF) ($A_2 \leq 21$), heavy mass fragments (HMF) ($A_2 \leq A_{CN}/2$) and fusion fission (FF) ($A_{CN}/2 \pm 20$) etc. along with other non-compound nucleus paths. Collisions or fusion processes forming the composite systems in the specified region may invite various (nCN) non-compound nucleus exotic processes like quasi elastic (QE), deep inelastic (DI) processes, etc. Our main focus here is to address FF and DIC mechanism. The exercise concerning the indicated nuclear reactions may provide some input to investigate the mononuclear or dinuclear system more precisely [7]. Many reactions from this region like $^{16}\text{O} + ^{27}\text{Al}$, $^{16}\text{O} + ^{28}\text{Si}$, $^{20}\text{Ne} + ^{27}\text{Al}$, $^{20}\text{Ne} + ^{59}\text{Co}$ [8], $^{20}\text{Ne} + ^{20}\text{Ne}$, $^{20}\text{Ne} + ^{16}\text{O}$ [9],

$^{20}\text{Ne} + ^{12}\text{C}$ [10], $^{16}\text{O} + ^{12}\text{C}$ [11], etc. have been examined in the last few years. Information extracted from the above mentioned reactions unfold distinctive interesting aspects about the system formation and decay. As mentioned above, the most efficiently recognized forms of decay modes through compound nucleus are ER, IMF, HMF and fission. But there are distinctive parameters like energy, mass, angular momentum, etc. which inhibit these decay modes with some other anomalous processes. These parameters influence differently disintegration of compound nucleus. It is found that for lighter nuclei at energy much higher than the Coulomb barrier, the compound nucleus dissipates an enormous component of its own mass, hence in disintegration process, fragments possessing mass comparable to projectile or target come out with the highest probability [9]. Apart from energy, in some cases the structure of the colliding nuclei has been observed to play a crucial role. Reactions $^{20}\text{Ne} + ^{12}\text{C}$ [12], $^{24}\text{Mg} + ^{12}\text{C}$ [13], and $^{28}\text{Si} + ^{12}\text{C}$ [14] have α cluster amalgamating nuclei and inquisition on these reactions demonstrates that excitation functions of the outgoing channel are similar to the entrance channel, which is an explicit indication of the presence of deep inelastic collisions (DIC). Deep inelastic collisions define the phenomenon

^a e-mail: msharma@thapar.edu

Effect of Particle Size on Magnetic and Dielectric Properties of Nanoscale Dy-Doped BiFeO₃

Gitanjali Dhir · Poonam Uniyal · N.K. Verma

Received: 7 December 2013 / Accepted: 5 January 2014
© Springer Science+Business Media New York 2014

Abstract In the present report, influence of Dy-substitution and size on the structural, magnetic and dielectric properties of BiFeO₃ nanoparticles has been investigated. The synthesis of pure and Dy-doped BiFeO₃ nanoparticles has been done successfully using sol–gel method. Size of Dy-doped BiFeO₃ nanoparticles was tailored by varying the calcination temperature. Structural analysis reveal that substitution of Dy³⁺ leads to a change in structure from rhombohedral ($x = 0$) to orthorhombic ($x = 0.15$). The average crystallite size varies from 6 to 15 nm. Magnetic study reveals the enhancement in magnetization with the doping of Dy³⁺. Further, this value decreases as the particle size increases. Dielectric property improves with the Dy³⁺ substitution. All the nanoparticles display Debye-type relaxation. The low dielectric loss values observed are attributed to the nano-sized grains. Remarkably, enhanced saturation magnetization value (13.8 emu/g) and dielectric constant value (95.8) were observed for Dy-doped BiFeO₃ nanoparticles having the smallest particle size. Thereby, the study indicates strong correlation between size and multiferroism.

Keywords Size-dependent · Nanoparticles · Magnetic materials · Dielectric · Ferromagnetism

1 Introduction

Multiferroics categorize the materials that exhibit simultaneous presence of any of the two ferroic orders, namely, ferroelectric, ferromagnetic, ferroelastic or ferrotoroidic, in

the same phase [1–3]. Multiferroics with magnetoelectric effect (ME) possess coupling between (anti)ferroelectric and (anti)ferromagnetic orders over some range of temperature [4]. The term ‘multiferroic’ coined by Hans Schmid, represents a rare class of materials owing to the contrary prerequisites of ferroelectricity and ferromagnetism [3]. Much attention is paid to these materials due to a wide range of applications provided by them such as multiple state memories, spintronics, spin valves, sensors, transducers, quantum electromagnets and many more. Also, the fascinating physics involved makes them attractive apart from the immense technological applications [1–4]. Amongst the various single-phase ME materials, BiFeO₃ is a strong candidate having immense potential in technological applications owing to its high Curie ($T_c \sim 1103$ K) and Néel ($T_N \sim 643$ K) temperature [4]. Although the exhibition of ferroelectric and G-type antiferromagnetic order above room temperature is promising from the application point of view, however, it has few inherent problems associated with it. Bulk BiFeO₃ possesses weak magnetism due to orientation of magnetic moments perpendicular to the rhombohedral axis, magnetic moment canting and spiral spin structure having wavelength of 62 nm [5]. The superimposed spin spiral structure over the G-type antiferromagnetic order prevents the net magnetization as well as linear magnetoelectric coupling [6]. Also, the non-stoichiometry issues and defects lead to low resistivity which in turn makes the complete polarization impossible [7]. It possesses low magnetoelectric coupling coefficients and wider difference between the ferroic transition temperatures. These altogether contribute towards the disappointingly low values of polarization and magnetization when compared to the standard ferromagnetic and ferroelectric materials.

Several studies have been devoted to the enhancement of multiferroic properties in BiFeO₃ [4–12]. It has been

G. Dhir (✉) · P. Uniyal · N.K. Verma
Nano Research Lab, School of Physics and Materials Science,
Thapar University, Patiala 147 004, India
e-mail: gitanjali.thaprian@gmail.com



Cite this: *New J. Chem.*, 2017, 41, 8320

Augmenting the catalytic performance of spinel nanoferrites (CoFe₂O₄ and NiFe₂O₄) via incorporation of Al into the lattice†

Ankita Goyal,^a S. Bansal,^b B. Chudasama,^c K. B. Tikoo,^d V. Kumar^d and Sonal Singhal^{*a}

Spinel nanoferrites have emerged as outstanding catalysts for a variety of organic transformations and reactions. Spinel nanoferrites also possess the complementary benefit of facile and complete external magnet-aided recovery. Further improvement in the catalytic performance of spinel nanoferrites is currently a vibrant area of research. In this context, in the present investigation, Al has been incorporated into the lattice of spinel nanoferrites. Owing to its octahedral site preference, Al could actively participate in the reaction mechanism as octahedral sites are exposed upon the surface and catalytic activity is predominantly related to the metal ions present in these sites. Al content has varied from $x = 0.2$ to $x = 1.0$ when incorporated into the lattice of CoFe₂O₄ and NiFe₂O₄ as CoAl_xFe_{2-x}O₄ and NiAl_xFe_{2-x}O₄, respectively. Catalytic activity has been evaluated for the reduction of nitrophenols in the presence of NaBH₄ as the reducing agent. The catalytic activity has been found to increase with increasing Al content up to $x = 0.6$, before decreasing with further increase in Al content. The effect of increasing Al content on the catalytic performance is thought to be related to synergistic interactions among the metal ions present in the surface-exposed octahedral sites.

Received 3rd May 2017,
Accepted 3rd July 2017

DOI: 10.1039/c7nj01486d

rsc.li/njc

1. Introduction

Magnetically recoverable nanocatalysts have revolutionized the world of catalysis by facilitating facile recovery using an external magnet.^{1–4} Facile recovery and recyclability of the catalyst are key characteristics of any catalyst and have allowed spinel nanoferrites to assume a strong position in the area of catalysis.⁵ Additional attractions of spinel nanoferrites that have attracted many nanochemists working in the field of catalysis are their fascinating properties, including heterogeneity, facile synthetic procedure, stability, insolubility in most solvents, stability at wider pH ranges, inherent magnetic character and their intriguing structure.^{6–9} A variety of methodologies are available in the literature for the synthesis of these spinel nanoferrites, *viz.* co-precipitation,¹⁰ micro-emulsion,¹¹ hydrothermal,^{12–14} sol-gel,^{15,16} sol-gel auto-combustion¹⁷ *etc.*, with different modifications.

In the case of spinel nanoferrites, catalytic activity predominantly relates to their structure. The structure of spinel nanoferrites is such that the octahedral sites are exposed upon the surface while the tetrahedral sites are present in the bulk.¹⁸ As catalysis is a surface phenomenon, the metal ions present in the octahedral sites are largely responsible for the catalysis offered by spinel nanoferrites. Further, the metal ions in the octahedral sites are placed at comparatively large distances, providing sufficient room for the reactant molecules to interact freely. Therefore, the catalytic activity of spinel nanoferrites is greatly affected by the nature and mutual synergistic interactions of the metal ions present in the catalytically active octahedral sites.¹⁹ The catalytic properties of spinel nanoferrites can easily be tailored by varying the cation distribution; *i.e.* via substitution of existing ions with the guest metal ions.²⁰ The substituent or the dopant guest metal ion can belong to any of the blocks of the periodic table; *i.e.* it can be a transition metal element, a post-transition metal element, or a rare-earth metal element. The doping of transition metal ions^{21–26} and the rare-earth metal ions^{27–31} has been widely studied by researchers in terms of its effect on the catalytic performance of spinel nanoferrites. Both a reduction and an improvement in catalytic performance has been observed by researchers studying doping of this kind in different catalytic applications. However, the effect of doping of p-block elements on the catalytic performance of spinel

^a Department of Chemistry, Panjab University, Chandigarh, 160014, India.

E-mail: sonal1174@gmail.com, sonal@pu.ac.in; Fax: +91-172-2545074;

Tel: +91-172-2534421(o), +91-09872118810(m)

^b Department of Science and Technology, New Delhi, India

^c School of Physics & Materials Science, Thapar University, Patiala, 147004, India

^d HRTEM Lab Facility, NIPER, SAS Nagar-160062, Punjab, India

† Electronic supplementary information (ESI) available. See DOI: 10.1039/c7nj01486d

Complete and incomplete fusion dynamics of ${}^6,{}^7\text{Li} + {}^{159}\text{Tb}$ reactions near the Coulomb barrier

Manjeet Singh Gautam^{1,2}, Neha Grover¹, and Manoj K. Sharma^{1,a}

¹ School of Physics and Materials Science, Thapar University, Patiala-147004, India

² Department of Physics, Indus Degree College, Kinana, Jind-126102, Haryana, India

Received: 21 October 2016 / Revised: 21 December 2016

Published online: 24 January 2017 – © Società Italiana di Fisica / Springer-Verlag 2017

Communicated by A. Ramos

Abstract. The complete fusion (CF) and incomplete fusion (ICF) cross-sections are estimated for ${}^6,{}^7\text{Li} + {}^{159}\text{Tb}$ reactions using the energy-dependent Woods-Saxon potential model (EDWSP model) and dynamical cluster-decay model (DCM). The CF data of the ${}^6\text{Li} + {}^{159}\text{Tb}$ (${}^7\text{Li} + {}^{159}\text{Tb}$) reaction at above barrier energies is suppressed with reference to expectations of the EDWSP model by 25% (20%) which is smaller than the reported data by $\sim 9\%$ (6%). This suppression is correlated with the projectile breakup effect. The projectiles ${}^6,{}^7\text{Li}$ are loosely bound systems, which may break up into charged fragments prior to reaching the fusion barrier and subsequently one of the fragment is captured by the target leading to the suppression of fusion data at above barrier energies. The sum of CF and ICF, which is termed as total fusion cross-section (TF), removes the discrepancies between theoretical predictions and the above barrier complete fusion data and hence is adequately explained via the EDWSP model over a wide range of energy spread across the Coulomb barrier. In addition to fusion, the decay mechanism of ${}^6\text{Li} + {}^{159}\text{Tb}$ reaction is studied within the framework of the dynamical cluster-decay model (DCM). The breakup of the projectile (${}^6\text{Li}$) in the entrance channel indicates the presence of ICF, which is investigated further using the collective clusterization approach of DCM. The present theoretical analysis suggests that a larger barrier modification is needed to address the fusion data of chosen reactions in the below barrier energy region.

1 Introduction

During the last few decades, the fusion dynamics of weakly bound unstable nuclei with different target isotopes have been extensively worked out for a better understanding of the nuclear behavior. The low breakup threshold of these systems in turn affects the magnitude of fusion excitation functions in the domain of the Coulomb barrier. The fusion reactions with weakly bound nuclei are primarily investigated to understand the possible role of the breakup channel on fusion dynamics [1–7]. Reactions with weakly bound projectiles may undergo both complete as well as incomplete fusion: the complete fusion, where the whole projectile is captured by the target, and incomplete fusion, wherein a part of projectile is fused with the target. In the case of weakly bound nuclei, it is well recognized that the complete fusion cross-section data at above barrier energies is suppressed with respect to the predictions made by the coupled channel approach. The missing fusion cross-sections appear in the form of incomplete fusion cross-sections. The loosely bound system breaks up into

two or more fragments in the field of the target isotope and consequently results in the suppression of fusion data at above barrier energies [8–13]. The various theoretical predictions result in the conflicting statement with regard to the enhancement or suppression of fusion cross-section, due to breakup channel at both above and below barrier energies [14–22]. The authors of refs. [18–22] suggested the enhancement of sub-barrier fusion excitation function data while the authors of refs. [3–12, 14–17] claimed the above barrier suppression of the fusion cross-section data. The breakup channel induces a strong coupling between the elastic channel and the continuum states and hence results in inhibition of above barrier fusion excitation function data. The weakly bound nuclei such as ${}^6,{}^7\text{Li}$ and ${}^9\text{Be}$ have large breakup probabilities and are most suitable candidates to investigate the role of the projectile breakup channel on the fusion mechanism.

Very recently, Rath *et al.* [23–25] pointed out that the above barrier fusion data is suppressed due to the breakup of the projectile in the entrance channel by 32% for ${}^6\text{Li} + {}^{144}\text{Sm}$, 24% for ${}^7\text{Li} + {}^{144}\text{Sm}$, 28% for ${}^6\text{Li} + {}^{152}\text{Sm}$ and 25% for ${}^7\text{Li} + {}^{152}\text{Sm}$ reaction. Dasgupta *et al.* [5–7] have highlighted the suppression of above barrier fu-

^a e-mail: msharma@thapar.edu



CrossMark
click for updates

Cite this: *Environ. Sci.: Processes Impacts*, 2014, 16, 2191

Antibacterial activities of silver nanoparticles and antibiotic-adsorbed silver nanoparticles against biorecycling microbes

Chandni Khurana,^a Anjana K. Vala,^b Nidhi Andhariya,^a O. P. Pandey^a and Bhupendra Chudasama^{*a}

Silver nanoparticles have a huge share in nanotechnology based products used in clinical and hygiene products. Silver nanoparticles leaching from these medical and domestic products will eventually enter terrestrial ecosystems and will interact with the microbes present in the land and water. These interactions could be a threat to biorecycling microbes present in the Earth's crust. The antimicrobial action towards biorecycling microbes by leached silver nanoparticles from medical waste could be many times greater compared to that of silver nanoparticles leached from other domestic products, since medical products may contain traditional antibiotics along with silver nanoparticles. In the present article, we have evaluated the antimicrobial activities of as-synthesized silver nanoparticles, antibiotics – tetracycline and kanamycin, and antibiotic-adsorbed silver nanoparticles. The antimicrobial action of silver nanoparticles with adsorbed antibiotics is 33–100% more profound against the biorecycling microbes *B. subtilis* and *Pseudomonas* compared to the antibacterial action of silver nanoparticles of the same concentration. This study indicates that there is an immediate and urgent need for well-defined protocols for environmental exposure to silver nanoparticles, as the use of silver nanoparticles in nanotechnology based products is poorly restricted.

Received 30th April 2014
Accepted 21st May 2014

DOI: 10.1039/c4em00248b

rsc.li/process-impacts

Environmental impact

Due to the antibacterial properties of silver nanoparticles (AgNPs), their production and applications have increased. AgNPs can be used in various areas including clinical and hygiene products. During the production, use, and disposal of these products, nanoparticles can be released into the environment. Their exposure to the environment may have a harmful impact on biorecycling microbes. To study their environmental risks, a comprehensive understanding of the source, distribution and toxicity of AgNPs is needed. This article studies the effect of AgNPs and antibiotic-adsorbed AgNPs on environmentally friendly bacterial strains.

Introduction

In a recent project report on “Emerging Nanotechnologies” by Woodrow Wilson International Center for Scholars, it is reported that 1600+ nanomaterial-incorporated consumer products are available on the market for commercial use.¹ The market share of nanotechnology based products has grown at an impressive rate of 379% in the last ten years. In the United States alone, the nanomaterial business will be a trillion dollar industry by 2015.² Antimicrobial silver nanoparticles (AgNPs) are one of the most widely used engineered nanomaterials in nanotechnology based products.³ Thanks to their biocidal activity, AgNPs are routinely incorporated into medical supplements, catheters, wound dressings and implants to

inhibit pathogen growth. AgNPs are added to cosmetics as an antiseptic and used in medical textiles to eliminate microbes in the clinical environment.^{3–6} They are also used for water purification, biosensors, bone prostheses, drug and gene delivery, bioimaging devices, *etc.*^{7–10} The majority of AgNPs released from consumer products are expected to enter terrestrial ecosystems through the land application of biosolids.^{11,12} While environmental concentrations are currently unavailable for AgNPs, and potential environmental exposures are poorly constrained, the increasing use of AgNPs has raised concerns over their likely release into ecosystems. Given the critical role of microbial communities in organic matter and nutrient cycling in ecosystems, environmental exposure of AgNPs has the potential to alter ecosystem productivity.¹³ A large number of studies have been conducted on the clinical applications of AgNPs,^{14–18} while their environmental impacts are largely unclear.^{12,19–25} In addition, the antimicrobial properties of complexes of AgNPs with

^aSchool of Physics & Materials Science, Thapar University, Patiala, 147 004, India. E-mail: bnchudasama@gmail.com; Fax: +91-175-2393020; Tel: +91-175-2393116

^bDepartment of Physics, M.K. Bhavnagar University, Bhavnagar, 364 022, India

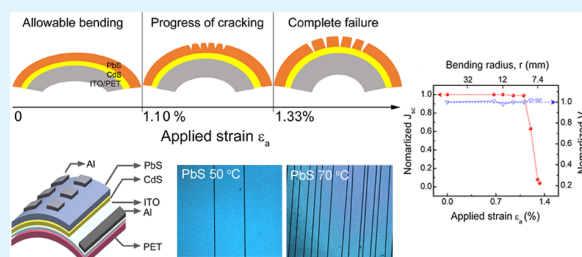
Tensile Stress-Dependent Fracture Behavior and Its Influences on Photovoltaic Characteristics in Flexible PbS/CdS Thin-Film Solar Cells

Seung Min Lee,^{†,§} Deuk Ho Yeon,^{†,§} Bhaskar Chandra Mohanty,[‡] and Yong Soo Cho^{*,†}[†]Department of Materials Science and Engineering, Yonsei University, Seoul 120-749, Korea[‡]School of Physics & Materials Science, Thapar University, Patiala, 147004, India

Supporting Information

ABSTRACT: Tensile stress-dependent fracture behavior of flexible PbS/CdS heterojunction thin-film solar cells on indium tin oxide-coated polyethylene terephthalate (PET) substrates is investigated in terms of the variations of fracture parameters with applied strains and their influences on photovoltaic properties. The PbS absorber layer that exhibits only mechanical cracks within the applied strain range from ~ 0.67 to 1.33% is prepared by chemical bath deposition at different temperatures of 50, 70, and 90 °C. The PbS thin films prepared at 50 °C demonstrate better mechanical resistance against the applied bending strain with the highest crack initiating bending strain of $\sim 1.14\%$ and the lowest saturated crack density of $0.036 \mu\text{m}^{-1}$. Photovoltaic properties of the cells depend on the deposition temperature and the level of applied tensile stress. The values of short-circuit current density and fill factor are dramatically reduced above a certain level of applied strain, while open-circuit voltage is nearly maintained. The dependency of photovoltaic properties on the progress of fractures is understood as related to the reduced fracture energy and toughness, which is limitedly controllable by microstructural features of the absorber layer.

KEYWORDS: lead sulfide, chemical bath deposition, flexible solar cell, fracture behavior



INTRODUCTION

Photovoltaic cells on flexible polymer substrates have been investigated over the past decade because of their great potential for extended applications including as a mobile energy source. Particularly, the choice of absorber layer for the flexible substrate is very limited since the absorber layer needs to be processed below the softening point of the polymeric substrates. Several organic absorber materials, such as poly(3-hexylthiophene) (P3HT) and poly[2-methoxy-5-(2-ethylhexyloxy)-1,4-phenylenevinylene] (MEH-PPV), may be suitable for the flexible applications, but the practical utilization is very limited due to their compatibility issue with polymer substrates and their poor intrinsic long-term stability.^{1,2} On the other hand, typical inorganic absorbers for thin-film solar cells, including Cu(In,Ga)Se₂ and CdTe, have been actively studied for the flexible applications.^{3–5} The selection of substrates for the inorganic absorber is critical since it determines maximum processing temperature for the synthesis and densification of the absorber materials. Only highly thermal resistive substrates including metal foils have been considered as an ideal choice for the inorganic absorbers demanding at least 500 °C for densification to cover the broader range of applications potentially favoring lower softening temperature-polymer substrates including polyethylene terephthalate (PET), poly(ether sulfone) (PES) and polyethylene naphthalate (PEN); however, nonconventional absorber-driven cell structures that are processable below 100 °C are preferred.

Lead sulfide (PbS) has drawn considerable interest as one of the rare p-type absorbers for thin-film solar cells due to its high absorption coefficient of $\sim 1 \times 10^5 \text{ cm}^{-1}$ in the visible light and adjustable band gap toward a higher value ($>1.3 \text{ eV}$) suitable for better band alignment in typical cell structures.^{6–8} There has been no report concerning the deposition of PbS thin films on any flexible polymer substrate even though polycrystalline PbS can be easily formed at temperature below 100 °C by the known chemical bath deposition (CBD) process. There are several reports on the PbS/CdS heterojunction thin-film photovoltaic cells fabricated by CBD on a rigid glass substrate.^{9–11}

In the meantime, there have been extensive studies on mechanical or fracture behavior of thin films deposited onto polymer substrates for a variety of flexible electronic devices.^{12–14} Cracks or macrodefects developed on the surface of thin films as a result of externally applied stress are regarded as the reason for substantial degradation of the devices' functional performance.¹⁵ In the field of flexible thin-film solar cells, surprisingly, there have been no systematic studies about the fracture behavior under tensile stress even though there is a rare report proposing that the photovoltaic performance of Cu(In,Ga)Se₂ cells can be critically affected by flexibility stress and mechanical cycling.⁵

Received: October 21, 2014

Accepted: February 9, 2015

Published: February 9, 2015

Estimation of Particle Concentration in a Nanocomposite Using Magnetization Data

Chandni Rani¹, S. D. Tiwari¹, and Devendra Kumar²

¹School of Physics and Materials Science, Thapar University, Patiala 147004, India

²University Grants Commission-Department of Atomic Energy Consortium for Scientific Research, Indore 452001, India

We report magnetic field dependence of magnetization on nickel oxide nanoparticles, ferrihydrite nanoparticles, and a nanocomposite of both nanoparticle systems. The process of magnetization in these samples is studied. Possibility for estimating concentration of an individual nanoparticle system in a nanocomposite consisting of two or more magnetic phases is discussed in detail.

Index Terms—Magnetization, nanocomposite, nanoparticles, superparamagnetism.

I. INTRODUCTION

NANOMATERIALS have been attracting the attention of researchers from different disciplines of science and engineering for fundamental understanding and useful technological applications. Among different nanomaterials, behavior of magnetic nanoparticles is of great interest. One of the properties that makes magnetic nanoparticles unique is superparamagnetism [1]–[4]. This phenomenon is only shown by small particles of magnetic materials. In last few decades nanoparticles of antiferromagnetic materials have been found to be more interesting in comparison with those of ferromagnetic and ferrimagnetic materials [5], [6]. Among several antiferromagnetic nanoparticle systems, NiO [5]–[16], ferrihydrite [17]–[26], and ferritin [27]–[29], are relatively more interesting.

In addition to pure phase magnetic nanoparticles, works on nanocomposites of magnetic materials have been gaining a lot of attention by researchers in recent years [30]–[33]. Nanocomposites consist of two or more pure phases of nanoparticles. However, there do not exist any convenient and reliable method to estimate concentration of individual nanoparticle system in a nanocomposite. This motivated us to study the magnetization process in a magnetic nanocomposite. This paper is found to be very useful in the estimation of concentration of individual system in a nanocomposite consisting of two or more magnetic phases.

II. EXPERIMENTAL DETAILS

Nanoparticles of nickel oxide are prepared by the thermal decomposition of freshly synthesized nickel hydroxide powder. Ferrihydrite nanoparticles are synthesized by the precipitation of aqueous ferric nitrate solution with sodium hydroxide solution. More details of synthesis of these samples are discussed in [10] and [26]. A nanocomposite is prepared by mixing known masses of nickel oxide and ferrihydrite

Manuscript received April 16, 2015; accepted July 11, 2015. Date of publication July 29, 2015; date of current version November 16, 2015. Corresponding author: S. D. Tiwari (e-mail: sdtiwari@thapar.edu).

Color versions of one or more of the figures in this paper are available online at <http://ieeexplore.ieee.org>.

Digital Object Identifier 10.1109/TMAG.2015.2461677

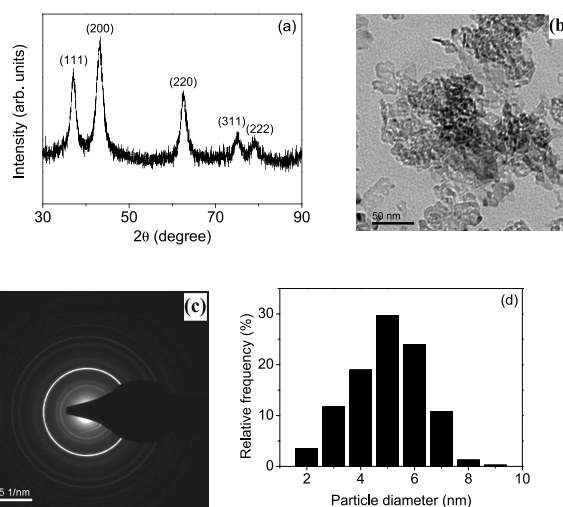


Fig. 1. (a) Room temperature X-ray diffraction pattern. (b) Transmission electron micrograph. (c) Selected area electron diffraction pattern. (d) Histogram of the distribution of particle size in nickel oxide nanoparticles.

nanoparticles homogeneously. This composite consists of 48 weight percent of nickel oxide and 52 weight percent of ferrihydrite nanoparticles. Magnetization measurements are done with a commercial vibrating sample magnetometer (Quantum Design, PPMS).

III. RESULTS AND DISCUSSION

A. Structural Characterization

Structural characterizations of synthesized samples are done by X-ray diffractometer and transmission electron microscope. Room temperature X-ray diffraction data are collected using a PANalytical diffractometer and Cu K_{α} radiation. Transmission electron micrograph and selected area electron diffraction pattern are taken using a FEI Tecnai transmission electron microscope. Figs. 1(a) and 2(a) show the X-ray diffraction patterns of synthesized samples. From these figures, we find that the synthesized samples are single-phase nickel oxide and two lines ferrihydrite nanoparticles [10], [26]. These figures also show that the diffraction peaks are broad. The average crystallite size is calculated by X-ray diffraction line



Cite this: DOI: 10.1039/c5tc03364k

Frequency independent low-*k* lithium borate nanocrystalline glass ceramic and glasses for microelectronic applications

S. K. Arya,^a S. S. Danewalia^b and K. Singh^{*b}

Glasses with composition $B_2O_3-Li_2O-ZnO-TiO_2-V_2O_5$ were prepared with a melt and quench technique with variable concentration of TiO_2 and V_2O_5 . Structural aspects of the as-prepared sample were explored with the help of electron paramagnetic resonance spectroscopy (EPR). Conductivity and dielectric properties of the glasses and nanocrystalline glass ceramic were investigated using impedance spectroscopy. Vanadium was present in these glasses in the V^{4+} state, however, in initial composition, it was in the V^{5+} state. The maximum quantity of TiO_2 contained glasses formed a nanocrystalline rutile phase, which dominated the electronic conduction at lower temperatures with decreased activation energy, *i.e.* 0.21 eV. Moreover, the presence of a nanocrystalline TiO_2 phase reduced the dielectric constant ~ 3 at room temperature and 1 MHz with excellent stability over a wide temperature and frequency range. The present nanocrystalline glass ceramic and glasses can be used in fast communication devices.

Received 16th October 2015,
Accepted 7th March 2016

DOI: 10.1039/c5tc03364k

www.rsc.org/MaterialsC

1 Introduction

Low-*k* materials are being used as substrates in microelectronic devices. It works to enhance the speed of the signals with low noise levels. Basically, the signal speed in conducting media is inversely proportional to the square root of the dielectric constant.¹ The substrate should also have good mechanical, thermal and chemical stability. Silica based glasses meet most of the abovementioned properties. However, during processing and device operation, crystalline cristobalite phase is formed in silica and silicate glasses.² A large volume change is exhibited during a thermal cycle, which leads to thermal stresses between the substrate and signal carrying materials. The fused silica has dielectric constant ~ 4 and changes upon the incorporation of other additives.³ Similarly, polymer based materials exhibit even lower *k* than silica glasses, *i.e.* ~ 2.5 .⁴ However, their thermal and mechanical properties are very poor. It appears that a single phase material could not meet all the abovementioned properties. The properties can be tailored easily in the glasses due to easy accommodation of different constituents. Moreover, according to mixing rules, introduction of the lower polarizable lighter element oxides, such as B_2O_3 , Li_2O and Na_2O , should decrease the dielectric constant. Another possible way to

decrease the dielectric constant is to create pores, but their mechanical properties decrease drastically. Based on these factors, light element oxides based lithium borate glasses were selected for the present study. A small fraction (≤ 10 mol%) of ZnO , TiO_2 and V_2O_5 were added to increase the thermal expansion coefficient as well as to improve the chemical stability. The small fraction of transition elements works as a nucleating agent to form nanocrystalline phases in the glasses, which enhances their chemical durability and thermal stability.⁵ Vaish *et al.* also reported that the nanocrystallites in the glass matrix would be beneficial in non-linear optical applications.⁶ Moreover, the presence of transition metals in different oxidation states may modify the transport/dielectric properties of the glasses. In brief, the transport characteristics of the glasses depend upon the structure, defect states, crystallinity, and internal friction. By optimizing these parameters, the dielectric properties of the glasses can be modified easily. For high-performance microelectronic systems, low-*k* (< 10) glasses are essential components and can be used as substrates and dielectric layer in semiconductor packaging⁷ and in thick film resistors. Therefore, for fast communication applications, it is important to understand the structure and mechanism of dielectric polarization, which arises from the constituent species of the glasses.⁸

The motivation of the present study was to develop low-*k* lithium borate glass with three different transition metal oxides to meet thermal, chemical and mechanical properties for substrates. The chosen glass composition was unique with respect to three different modifiers with different oxidation states such as Li^+ , Zn^{2+} ,

^a Department of Applied Sciences, ABES Institute of Technology, Ghaziabad-201009, UP, India

^b School of Physics & Materials Science, Thapar University, Patiala-147004, India.
E-mail: kusingh@thapar.edu; Fax: +91 1752393005; Tel: +91 1752393891



High-Efficiency Double Absorber PbS/CdS Heterojunction Solar Cells by Enhanced Charge Collection Using a ZnO Nanorod Array

Deuk Ho Yeon,^{†,‡,||} Bhaskar Chandra Mohanty,^{§,||} Che Yoon Lee,^{†,||} Seung Min Lee,[†] and Yong Soo Cho^{*,†,||}

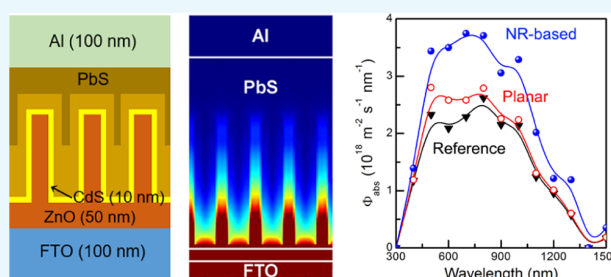
[†]Department of Materials Science and Engineering, Yonsei University, Seoul 03722, Korea

[‡]R&D Center, LG Display Co., Ltd., Paju-si 10845, Gyeonggi-do, Korea

[§]School of Physics and Materials Science, Thapar University, Patiala 147004, India

Supporting Information

ABSTRACT: The device architecture of solar cells remains critical in achieving high photoconversion efficiency while affordable and scalable routes are being explored. Here, we demonstrate a scalable, low cost, and less toxic synthesis route for the fabrication of PbS/CdS thin-film solar cells with efficiencies as high as ~5.59%, which is the highest efficiency obtained so far for the PbS-based solar cells not involving quantum dots. The devices use a stack of two band-aligned junctions that facilitates absorption of a wider range of the solar spectrum and an architectural modification of the electron-accepting electrode assembly consisting of a very thin CdS layer (~10 nm) supported by vertically aligned ZnO nanorods on a ~50 nm thick ZnO underlayer. Compared to a planar electrode of a 50 nm thick CdS film, the modified electrode assembly enhanced the efficiency by ~39% primarily due to a significantly higher photon absorption in the PbS layer, as revealed by a detailed three-dimensional finite difference time-domain optoelectronic modeling of the device.



Compared to a planar electrode of a 50 nm thick CdS film, the modified electrode assembly enhanced the efficiency by ~39% primarily due to a significantly higher photon absorption in the PbS layer, as revealed by a detailed three-dimensional finite difference time-domain optoelectronic modeling of the device.

INTRODUCTION

Solution-processed PbS-based thin-film solar cells have drawn tremendous research interest in recent years for their potential in large area, high throughput, and affordable solar energy conversion.^{1–5} Intensified research has culminated in a remarkable progress in the photoconversion efficiency (PCE) from <1% to better than 8% in a time span of less than a decade.^{1–6} The high performing solar cells utilize a two dimensionally constricted assembly of individually surface passivated PbS quantum dots, which assist in harnessing a wide range of the solar spectrum due to their band gap tunability. Notwithstanding the favorable optoelectronic properties, the surface chemistry resulting from the passivation of the quantum dots and their packing have been shown to critically affect the performance of the devices.^{7,8} The concerted efforts over the years have witnessed diverse techniques employed to achieve the desired passivation with substantially reduced density of trap states on surface and the close packing of the quantum dots, which is critical for efficient exciton dissociation and charge transfer. Despite the promise and rapid progress of the PbS quantum dot-based solar cells, the complex and elaborate processes of surface passivation and poor stability have raised serious issues on the fabrication of scalable low-cost devices.^{9,10}

While seeking an affordable approach to synthesize the PbS absorber layer that would offer the facile tunability of band gap

similar to that of the quantum dots without involving multistep chemical processing and/or without ligand engineering, recently, we have shown that the chemical bath deposition (CBD) method could be a viable option.^{11,12} For the CBD PbS thin films, the optoelectronic properties, including band gap, are determined by the process parameters, such as temperature, composition, etc., that can be easily tailored. A promising PCE, as high as 4.03%, was obtained for photovoltaic devices employing a stack of a pair of CBD PbS layers of varying band gaps.¹² The architectural modification involving stacking of the band gap-tailored PbS films without any intervening layer facilitated better absorption of a wider range of solar spectrum resulting in better PCE, compared to a single PbS layer. Although the obtained photovoltaic performance is the highest for any PbS thin film-based device not involving colloidal quantum dots,^{13,14} we seek to address the need for further improvement in the PCE of the devices.

One of the limiting factors of the performance of the PbS quantum dot-based solar cells has been the inherent compromise between the light absorption and carrier extraction.⁴ Although a complete absorption of above band gap photons requires a film thickness of 1 μm , the very short

Received: July 15, 2017

Accepted: August 11, 2017

Published: August 23, 2017

SCIENTIFIC REPORTS

OPEN

Effect of band-aligned double absorber layers on photovoltaic characteristics of chemical bath deposited PbS/CdS thin film solar cells

Received: 04 February 2015
Accepted: 27 August 2015
Published: 23 September 2015

Deuk Ho Yeon^{1,*}, Bhaskar Chandra Mohanty^{2,*}, Seung Min Lee¹ & Yong Soo Cho¹

Here we report the highest energy conversion efficiency and good stability of PbS thin film-based depleted heterojunction solar cells, not involving PbS quantum dots. The PbS thin films were grown by the low cost chemical bath deposition (CBD) process at relatively low temperatures. Compared to the quantum dot solar cells which require critical and multistep complex procedures for surface passivation, the present approach, leveraging the facile modulation of the optoelectronic properties of the PbS films by the CBD process, offers a simpler route for optimization of PbS-based solar cells. Through an architectural modification, wherein two band-aligned junctions are stacked without any intervening layers, an enhancement of conversion efficiency by as much as 30% from 3.10 to 4.03% facilitated by absorption of a wider range of solar spectrum has been obtained. As an added advantage of the low band gap PbS stacked over a wide gap PbS, the devices show stability over a period of 10 days.

In recent years, solution-processed inorganic thin film photovoltaics have exhibited tremendous potential in the quest for sustainable energy sources^{1–4}. Among the various materials that have been aggressively pursued for the purpose, PbS has emerged as one of the top candidates over the last decade^{3,4}. Although photoresponse of PbS has been long revealed, the recent development is based on its quantum dots that provide with ability to exploit the near infrared (NIR) region due to band gap tunability as a consequence of quantum size effects⁵. Significant and rapid progress has been made on solar cells based on the solution-processed quantum dots from less than 1% efficiency in 2005 to more than 8% in 2014^{6–8}.

Till date, architectures of (i) Schottky junction between a quantum dot film and metal electrode⁹, (ii) depleted heterojunction where a quantum dot film is sandwiched between a metal and an n-type conductor like TiO₂², ZnO¹⁰ or CdS⁴ and (iii) quantum dot-sensitized solar cells¹¹ have been employed for photovoltaic applications. In a true sense, however, the quantum dot thin film is a misnomer; it is rather a two dimensionally constricted assembly of individually surface-passivated quantum dots. Incidentally, surface chemistry of the quantum dots is one of the factors those critically affect the energy conversion efficiency^{12,13}. It has been accepted that the solution-processed quantum dots exhibit poor air stability that can pose serious apprehensions on fabrication of scalable low cost devices^{9,14}. In turn, this has prompted researchers to explore other possibilities that can yield high performance at a reasonably low cost. For example, recently it has been suggested to use pulsed laser ablation-based synthesis of the PbS quantum dots¹⁵. Some other research group has used elemental sulfur, albeit multiple processing steps, instead of the conventional bis (trimethylsilyl) sulfide owing to its pyrophoric nature and high cost¹⁶.

¹Department of Materials Science and Engineering, Yonsei University, Seoul 120-749, Korea. ²School of Physics & Materials Science, Thapar University, Patiala, 147004, India. *These authors contributed equally to this work. Correspondence and requests for materials should be addressed to Y.S.C. (email: ycho@yonsei.ac.kr)

FORMAT - 1

DST – Fund for Improvement in S&T Infrastructure (FIST 2000)

Department of Mechanical Engineering, Thapar University (SR/FST/ETI-329/2012)

Brief Outline College (not more than 5 lines)

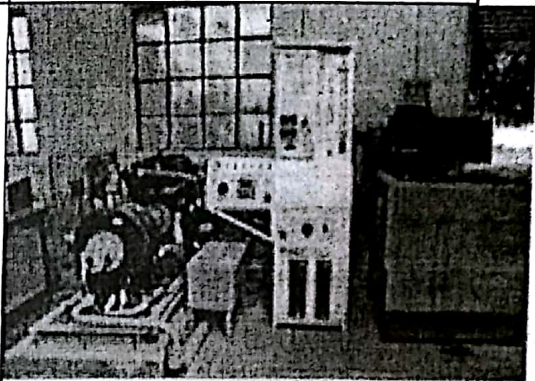
The department offers courses on undergraduate and postgraduate levels. The department boasts of experienced faculty in all the major areas of Mechanical engineering and is actively engaged in teaching and research activities. All the laboratories are well maintained and are upgraded from time to time. Also, a separate research lab with internet and computational facilities is maintained for the PG level students. Several training programmes / workshops and conference have been organized in the department in the recent past.

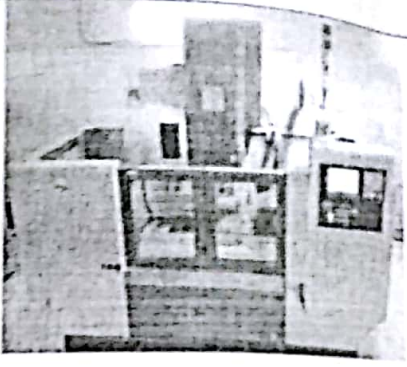

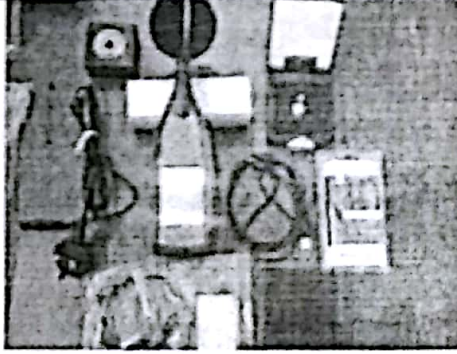
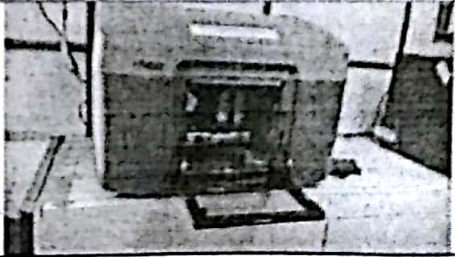
Teaching & Research Activities (not more than 5 lines)

Department offers courses for BE (Mech. Engg.) and ME (CAD/Cam & Robotics) and ME (Prod. & Indl.). The research areas in which the M.E and Ph.D works are being pursued are conventional and non-conventional machining, tribology, composite materials, heat transfer, CAPP, CAM, TQM, ergonomics, Presently 32 Ph.D and 74 M.E thesis works are being pursued in the foresaid areas. Some are experimental while others are analytical in nature.

Facilities Created

[Brief about Facilities costing more than Rs 5 lakh in not more than 3 lines. Attach Photograph (6"x 4" size) of the Facilities created]

Name (with Model & Make)	Cost in INR	
1. APEX Make Computerized 4-Cylinder, 4-Stroke Water cooled Engine MARUTI UDYOG LTD MODEL-226 with Avl Diesel Smoke Meter Pollution Checker	19,99,900	

<p>2. CNC Vertical milling M/C Center Model : Chandra + with fanuc Oi Mate m/c serial No.7184</p>	<p>20,55,925</p>	
<p>3. Artec Spider with calibration kit 1) Artec studio software licence 2) Intel core (Laptop) i7 Make Hp with 16GB Ram 1TB/HDD Nvidia Gefore 2GB Nvidia DDR3 Graphics Card with Window 8.1</p>	<p>13,70,000</p>	
<p>4. (4 channel noise and vibration analyser) 2250/Gr with Bz 7223 frequency Analysis Bz-7226 Sound Recorder option and Bz-7230 FET Analysis Software with some Accessories</p>	<p>8,96,144</p>	
<p>5. MOJO 3D printer pack Include: Equipments and One MOJO 3D printer (Fused deposition modelling machine)</p>	<p>8,12,436.</p>	

Funding: Rs. 43 Lakhs

For further details contact:

Professor S.K.Mohapatra
Head

Mechanical Engineering Department
Thapar University, Patiala

Tel. No. 0175- 393086 (O), 0175- 393086 (R)
Fax no. 0175- 2393005
Email ID. hmed@thapar.edu

Pro-forma for Report for utilization of FIST support

1. Name of College: **Thapar University, Patiala, Punjab-147004**
2. Address for communication: **Prof. (Dr.) S.K. Mohapatra
Sr. professor & head
Mechanical Engineering Department
Thapar University
Patiala-147004
hmed@thapar.edu**
3. Date and ref. No. of DST Sanction letter: **SR/FST/ETI-329/2012, Order Date: 29 August 2013.**

4. Details of the Grants

<i>Budget Heads</i>	<i>Amount Sanctioned with Date</i>	<i>Amount Received with Date</i>
<i>a. Equipment</i>	Rs 77.0 Lakhs (29/08/2013)	33.5 lakh (DST) + 61,873(interest 2013-14) + 31,527(interest in 2014-15)
<i>b. Infrastructure</i>	---	---
<i>c. Networking</i>	---	---
<i>d. Maintenance</i>	Rs. 9.00 Lakhs (29/08/2013)	---
<i>e. Total</i>	Rs 86.00 lakh (50:50 mode)	Rs. 34,43,400

5. Equipment ordered/purchased/installed:

<i>Name (with Model & Make)</i>	<i>Order Date</i>	<i>Installation date</i>	<i>Cost in INR</i>
1. APEX Make Computerized 4-Cylinder, 4-Stroke Water cooled Engine MARUTI UDYOG LTD MODEL- 226 with Avl Diesel Smoke Meter Pollution Checker	25-03-2014	18-09-2014	19,99,900
2. CNC Vertical milling M/C Center Model : Chandra + with fanuc Oi Mate m/c serial No.7184	17-01-2014	22-04-2014	20,55,925
3. Artec Spider with calibration kit 1) Artec studio software licence 2) Intel core (Laptop) i7 Make Hp with 16GB Ram 1TB/HDD Nvidia GEfore 2GB Nvidia	19-08-2014	14-10-2014	13,70,000

DDR3 Graphics Card with Window 8.1			
4. (4 channel noise and vibration analyser) 2250/Ge with Bz 7223 frequency Analysis Bz-7226 Sound Recorder option and Bz-7230 FFT Analysis Software with some Accessories	25-03-2014	09-07-2014	8,96,144
5. MOJO 3D printer pack Include: Equipments and One MOJO 3D printer (Fused deposition modelling machine)	28-12-2013	10/3/2014	8,12,436.

6. Details of Infrastructure developed: N.A.

7. Details of Networking: whole of the campus is equipped with WIFI internet facility

8. Utilization of the facilities created under FIST support:

a. For teaching: list the Classroom use of equipment and new experiments introduced, if any,

Sr. Number	Equipment	Utilization of equipment in the classroom
1.	Computerized 4 stroke 4 cylinder diesel engine	Equipment shall be used in the course UME501(Applied thermodynamics), UME502(Automobile Engineering) in U.G and PTH103(Internal Combustion Engines) in P.G.Programme.
2.	CNC vertical milling machine	Equipment shall be used in the course UME505(Manufacturing Technology), UME 702(Computer aided manufacturing) in under graduate and PPI201(advanced Manufacturing Processes) in P.G Programme
3.	3D scanner with data processing	Equipment shall be used in the course UME 401(Computer aided design), UME 801(Mechanical system design) in under graduate and PCD 106 (Geometric Modeling and Analysis) in P.G. programme

4.	4 Channel Noise & Vibration Analyzer	Equipment shall be used in the course UME 402(Dynamics of machine), and UME 706 (Mechanical Vibration).
5.	Fused Deposition Modeling machine	Equipment shall be used in the course PCD 325 (Rapid Prototyping)

b. For research: Identify the research programs, including names of groups or individual faculty members, who are using the major equipment (> 5 lakhs) acquired with the FIST support

Name of Equipment	Name of faculty	
Computerized 4 stroke 4 cylinder diesel engine	Dr. S.K. Mohapatra Mr. Sumeet Sharma	M.Tech Thesis supervised-02 Ongoing Ph.D Thesis-01
CNC vertical milling machine	Dr. Ajay Batish Dr. Vinod Kumar Singla Dr. Vivek Jain	M.Tech Thesis supervised-06 Ongoing Ph.D Thesis- 01
3D scanner with data processing	Mr. A.S. Jawsanda Dr. Ravinder Devedi	M.Tech Thesis supervised-03 Ongoing Ph.D Thesis-01
4 Channel Noise & Vibration Analyzer	Mr. Daljeet Singh Dr. Ashish Singla	M.Tech Thesis supervised-06 Ongoing Ph.D Thesis-01
Fused Deposition Modeling machine	Mr. A.S. Jawsanda	M.Tech Thesis supervised-01

9. Details of full length research publications (in peer-reviewed journals) during the period under report

Annexure 1.

10. Sponsored research projects in operation during the period under report (please provide name/s of PI/Co-PIs, title of the project, funding agency and total quantum of external support)

Sl. No.	Title of the Project	Funding agency (Scheme)	Duration	Sanction amount (Lacs)	PI/Co-PI
1.	Analysis of metallurgical behavior of weld and	Defence Research and Development	January 2012 –	14.65	Ajay Batish/ Anirban

	heat affected zone during Submerged Arc Welding (SAW) of high strength low alloy (HSLA) steel for different flux compositions, weld parameters with pre and post thermal treatment	Organization (DRDO), New Delhi, India	December 2013 (completed)		Bhattacharya
2.	Experimental investigation for surface improvement of die steels during electric discharge machining with tungsten and titanium powder mixed dielectric	University Grants Commission (UGC), New Delhi, India	August 2012 – July 2014 (completed)	0.90	Anirban Bhattacharya Ajay Batish
3.	Experimental investigation of EDM machined surface of Al-SiC and Al-SiC-B ₄ C metal matrix composites	University Grants Commission (UGC), New Delhi, India	August 2012 – July 2014 (completed)	10.82	Ajay Batish/ Anirban Bhattacharya
4.	Multi-response Optimization of Process Parameters for the Improved Part Accuracy in Fused Deposition Modeling Process	All India Council for Technical Education (AICTE), New Delhi	April 2013 – March 2016 (ongoing)	9.75	Ajay Batish/ Anirban Bhattacharya
5.	Design and control of intelligent autonomous vehicle for Indian sea ports	University Grants Commission (UGC), New Delhi, India	March 2013– March 2015 (Completed)	2.42839	Tarun Kumar Bera
6.	Developing validated scale-up procedure for dense phase pneumatic transport of fine powders using two layer dune flow model	Council of Scientific and Industrial Research, New Delhi, India.	November, 2012– November 2015 (Completed)	7.89167	Soumya Sudha Mallick
7.	Modeling solid friction and transport boundary for fluidized dense-phase pneumatic conveying system	Scientific and Industrial Research Board, New Delhi, India.	February 2012– February 2015 (Completed)	21.95	Soumya Sudha Mallick

8.	Floating wick type vertical multiple effect diffusion solar still with waste heat recovery	Department of Science and Technology, New Delhi, India.	May 2014 – May 2016 (Ongoing)	11.224	Madhup Kumar Mittal
9.	Special assistant programme (SAP-DRS phase 2) for department of mechanical engineering, Thapar University	University Grants Commission (UGC), New Delhi, India	December 2009– November 2014	44.50	HMED, TU
10.	Fund for improvement in S&T infrastructure (FIST)	DST-FIST Project, Department of Science and Technology, New Delhi, India.	September 2013– September 2017 (Ongoing)	86.00	S.K. Mohapatra (HMED)

11. Utilization of Equipment from outside the College

The Computerized 4 stroke 4 cylinder diesel engine and Channel Noise & Vibration Analyzer is utilised by the students of School of Energy and Environment and Chemical Engineering Department.

The facility is being used by PG and research students of neighbouring engineering institutes

12 SELF-ASSESSMENT OF THE IMPACT OF FIST SUPPORT: Please specify if any of the following activity emerged/ improved as a consequence of the FIST support:

- a. New class-room experiments at B.Sc./ M.Sc. or other levels

New experiment for UG and PG courses are being designed

- b. Success of students at national level tests (various PG/Ph.D. entrance tests and tests for JRF etc)

- c. Any new research project that emerged on the basis of the FIST support

1.	Multi-response Optimization of Process Parameters for the Improved Part Accuracy in Fused Deposition Modeling Process	All India Council for Technical Education (AICTE), New Delhi	April 2013 – March 2016 (onging)	9.75	Ajay Batish/ Anirban Bhattacharya
----	---	--	---	------	---

- d. Did the newly created facility lead to betterment of quality of research publications
Yes, the list of research publication is mentioned in Annexure -1

- e. Any training program/ workshop organized by the department during the period of

report, specially those involving the newly created facility)

Date	Theme of the Workshop/Seminar	Organized by	Duration
4th July 2014	Perspective on research	Mechanical Engineering Department, Thapar University, Patiala	1 days
16-17 Aug., 2013	Exposition to research areas in vibration and noise	Mechanical Engineering Department, Thapar University, Patiala.	2 days
19th August 2013	Simulation of engineering system	Mechanical Engineering Department, Thapar University, Patiala.	1 day

13. Is any problem faced in utilization of the grant/facilities?

Lack of in time response from the suppliers delayed the procurement of equipment.

A report highlighting the research activities of the College during the period under review may also be provided.

List of ongoing Ph. D. Thesis

S. No.	Title of the Thesis	Name of the Supervisor(s)
1.	STUDY OF PERFORMANCE AND EMISSIONS OF C.I. ENGINE WITH PONGAMIA BASED BIO-DIESEL	Dr. S.K. Mohapatra
2.	TOOL PATH PLANNING FOR IMPROVED MACHINING OF SCULPTURED SURFACES FOR A WEB. BASED MANUFACTURING SYSTEM	Dr. Sanjeev Bedi Dr. Ajay Batish
3.	DEVELOPMENT OF LIVE MODEL BASED CONTROLLER WITH AN INTEGRATED 3D SCANNER	Dr. Sanjeev Bedi Dr. Ajay Batish
4.	NOISE INVESTIGATION AND MODELLING OF URBAN TRAFFIC UNDER DYNAMIC CONDITIONS	Dr. S.P Nigam Dr. Maneek Kumar

List of M.E. Thesis/Dissertation

S. No.	Title of the M.E. Thesis/Dissertation.	Name of the Supervisor(s)
1	A comparative experimental study between the biodiesel of jatropha and palm oils based on their performance and emissions in a four stroke diesel engine	Dr K. Kundu Mr Sumeet Sharma Dr S. K. Mohapatra
2	STUDY OF PERFORMANCE AND EMISSIONS OF C.I. ENGINE WITH PONGAMIA BASED BIO-DIESEL	Dr. S.K. Mohapatra
3	Traffic Noise Modelling and Investigation for Signalized Intersection	Dr. S.P.Nigam, Daljeet Singh
4	Study on Radial Drilling Machine Noise	S.P. Nigam & Ajay

S. No.	Title of the M.E. Thesis/Dissertation	Name of the Supervisor(s)
		Batish
5	Measurement and Evaluation of Cam Chain Noise and Vibration of Motorcycle Engine	Dr Ajay Batish & Dr S P Nigam
6	Traffic noise modeling considering various traffic compositions at roundabouts	Dr. S.P. Nigam, Mr Daljeet Singh
7	Analysis and validation of traffic noise under dynamic condition near roundabouts using MADM approach	Dr .S.P. Nigam, Dr .V.P. Agrawal, Mr Daljeet Singh
8	NOISE INVESTIGATION AND MODELLING OF URBAN TRAFFIC UNDER DYNAMIC CONDITIONS	Dr. S. P. Nigam, Dr. Maneek Kumar
9	Investigation of noise generated during turning operation on a CNC Lathe	Dr.S.P. Nigam, Mr.Anirban Bhattacharya
10	A Methodology for Simulation and Verification of Tool Path Data for 3-Axis and 5-Axis CNC Machining	Mr. R K Duvedi
11	Automatic NC Toolpath Generation for 3D Sculptured Features Extracted from 2D Image	Mr. R K Duvedi, and Mr. Ravinder Kumar
12	Controlled Scallop Height Tool Path Generation for 3-Axis Vertical CNC Machining of STL Surfaces	Mr. R K Duvedi
13	Structural Design of 3-Axis CNC Machine Tool for Wood Carving	Mr. Sandeep Sharma and Mr. R K Duvedi
14	Automatic tool path generation from b-rep model of sculptured surfaces using cad software API	Mr. Ajayinder Singh Jawanda
15	Investigation on Mechanical Properties, Geometric Accuracy and Surface Roughness Improvement for Fused Deposition Modeling	Dr. Anirban Bhattacharya
16	Methodology for Design and Selection of Components of 3-Axis Granite Carving Machine Tool	Mr. Sandeep Sharma and Mr. R K Duvedi
17	Graphical machining simulator showing overcut-undercut in 3 axis lathe mill sculpturing	Mr. Ajayinder Singh Jawanda

Annexure-I Publication

S. No.	Title of the paper	Name of the Journal with volume, page nos., year	Name of the authors
1.	Command shaped closed-loop control of flexible robotic manipulators	Journal of Vibration Engineering and Technologies, (JVETv4n2-3)	Ashish Singla, Ashish Tewari and Bhaskar Dasgupta
2.	On Surface Finish and Dimensional Accuracy of FDM Parts after Cold Vapor Treatment	Materials and Manufacturing Processes, Taylor and Francis, Accepted: 17 June 2015, DOI: 10.1080/10426914.2015.1070425	Ashu Garg, Anirban Bhattacharya, Ajay Batish
3.	Numeric Implementation of Drop and Tilt Method of 5-Axis Tool Positioning for Machining of STL surfaces	International Journal of Advanced Manufacturing Technology, Springer-Verlag London, Vol. 78, pp.1677-1690, 2015 DOI: 10.1007/s00170-014-	Ravinder Kumar Duvedi, Sanjeev Bedi, Ajay Batish and Stephan Mann

Annexure-1 Publication			
S. No.	Title of the paper	Name of the Journal with volume, page nos., year	Name of the authors
		6636-3	
4.	The Edge-Torus Tangency Problem in Multipoint Machining of Triangulated Surface Models	International Journal of Advanced Manufacturing Technology, Springer-Verlag London, Published online 18 th July, 2015, DOI 10.1007/s00170-015-7532-1	Ravinder Kumar Duvedi, Sanjeev Bedi, Ajay Batish and Stephan Mann
5.	"Modal analysis of Human Body Vibration Model for Indian Subjects under sitting posture"	Ergonomics (Taylor and Francis) published online 17 October, 2014 DOI: 10.1080/00140139.2014.961567	Ishbir Singh, S.P. Nigam & V.H. Saran
6.	A production of biodiesel from waste cotton seed oil and testing on small capacity diesel engine	International Journal of Advance Research in Science and Engineering, IJARSE, 4, (02), Feb (2015), 172-178.	Singh, Sandeep, Sharma, S., and Mohapatra, S. K.
7.	Performance parameters of dual fuel diesel engine using eucalyptus-producer gas as secondary fuel	International Journal of Engineering Technology Science and Research, IJETSR, 2, March 2015, pp 15-22.	Kumar, P., Garg, L., Kumar R., and Mohapatra, S. K
8.	A multipoint method for 5-axis machining of triangulated surface models	Computer-Aided Design, Elsevier, Vol. 52, page 17-26, 2014	R K Duvedi, Sanjeev Bedi, Ajay Batish, Stephen Mann
9.	Hard Turning: Parametric Optimization using Genetic Algorithm for Rough/Finish Machining and Study of Surface Morphology	Journal of Mechanical Science and Technology Vol. 28, No. 5, May 2014, pp. 1629-1640.	Ajay Batish, Anirban Bhattacharya, Manwinder Kaur, Manjot Singh Cheema
10.	Experimental investigation of material transfer mechanism in WEDM of pure titanium (Grade-2)	Advances in Materials Science and Engineering, Vol.2013, Article ID: 847876, PP.1-20, DOI: 10.1155/2013/847876, Hindawi Publishers	Anish kumar Vinod kumar Jatinder kumar
11.	Vehicular traffic noise modeling using artificial neuron network approach	Transportation Research Part-C, v. 40 pp 111-122	Paras Kumar, S.P. Nigam & Narotam Kumar

Annexure-I Publication

S. No.	Title of the paper	Name of the Journal with volume, page nos., year	Name of the authors
12.	Characterisation of biodiesel derived from waste cotton seed oil and waste mustard oil	International Journal of Engineering Science and Technology (IJEST), ISSN: 0975-5467, Vol 5, No 7, July 2013, pp 1443-1448.	Singh S., Sharma S., Mohapatra, S. K., Kundu, K.
13.	Exhaust gas emission revelation during the study of performance of Pongamia oil as biodiesel	International Journal of Engineering Research & Technology (IJERT), ISSN: 2278-0181, Vol 2, Issue 8, August-2013, pp 991-997.	Prasad V.S., Mohapatra, S. K., Pooja LM.
14.	Biomass-based gasifiers for internal combustion (IC) engines – A review	Sadhana, Springer, Vol. 38, Part 3, June 2013, pp 461-476	Malik, A. and Mohapatra, S. K.
15.	Investigation of machining parameters and surface integrity in wire electric discharge machining of pure titanium	Proceedings of the Institution of Mechanical Engineers, Part B, Journal of Engineering Manufacture, 227 (7), pp. 972-992, 2013	Anish kumar Vinod kumar Jatinder kumar
16.	Multi response optimization of process parameters based on Response surface methodology for pure titanium using WEDM process	International Journal of Advanced Manufacturing Technology, DOI 10.1007/s00170-013-4861-9, 2013	Anish kumar Vinod kumar Jatinder kumar
17.	Performance and emission study of Indian brown hemp oil, methyl ester in a 4-stroke single cylinder water cooled diesel engine	International Journal of Engineering Research and Technology, ISSN: 0974-3154, 6, 5, pp 15-19, March 2013.	Ragit S. S., Mohapatra, S. K., Kundu, K., and Patil, GJV
18.	Methanolysis and ethanolysis of raw hemp oil; biodiesel production and fuel characterization	International Journal of Engineering Research and Technology, ISSN: 2278-0181, 2, 3, pp 1-10, March 2013.	Ragit S. S., Mohapatra, S. K., Kundu, K., and Karmakar, R.,
19.	Dynamic analysis of condenser assembly	Journal of The Institution of Engineers (India): Series C	M.Singh, D.Singh,

Annexture-1 Publication

S. No.	Title of the paper	Name of the Journal with volume, page nos., year	Name of the authors
	of automobile air conditioning system using CAE tools	Volume 94, Number 02, 135-145, 2013.	J.S.Saini
20.	Optimization and modelling of process parameters involved in ultrasonic machining of glass using design of experiments and regression approach	American Journal of Materials Engineering and Technology, 2013, vol. 1, no. 1, pp. 13-18, Science and Education Publishing DOI:10.12691/materials-1-1-3	Vinod kumar

FIST Program
STATEMENT OF EXPENDITURE (2 copies)
(for the Year of 1st April, 2014 to 31st March, 2015)

- Sanction Order No. & Date: SR/FST/ETI-329/2012, Order Date: 29 August 2013, vide FIST Sl. No. 104, dated 30.08.2013
- Total Sanctioned Project Cost (in Rs): Rs. 86.0 Lakhs (50:50 mode, DST share – Rs. 43.0 Lakh, Thapar University share 43.0 Lakhs)
Capital Assets: Rs. 77.0 Lakhs
General components: Rs. 9.0 Lakhs
- Date of Commencement of the Project: 11th September, 2013
- Grant Received in each year (in Rs):

1 st Year	2 nd Year	3 rd Year	4 th Year	5 th Year	Interest, if any	Total
33.50 Lakhs (DST)+ 33.50 Lakh (Thapar University) (+ Interest income of 2013-14 year = Rs 61,873)	-	-	-	-	Rs. 31,527	Rs. 67,93,400 (previous expenditure: Rs. 21,30,211) Net available: Rs. 46,63,189

5. Statement of Expenditure

Sr. No.	Sanctioned Budget Heads	Allocation of Funds (in Rs)	Expenditure incurred (Financial year-wise) (in Rs)					Total (Rupees)	Balance as on 1 st April, 2015 (in Rs)	Remarks , if any
			1 st Year	2 nd Year (01/04/14 to 31/03/15)	3 rd Year	4 th Year	5 th Year			
(A) Capital Assets										
1	Equipment (E)		Amount available Rs. 46,63,189, Total expenditure = Rs. 42,66,044					3,97,145		
	(i) Computerized 4 stroke 4 cylinder diesel engine	20.0 Lakhs	-	19,99,900	-	-	-	19,99,900		
	(ii) CNC vertical milling machine	18.0 Lakhs	-	-	-	-	-		Purchased in 2013-14	
	(iii) 3D scanner with data processing	15.0 Lakhs	-	13,70,000	-	-	-	13,70,000		
	(iv) 4 Channel Noise & Vibration Analyzer	10.0 Lakhs	-	08,96,144	-	-	-	08,96,144		
	(v) Fused Deposition Modeling machine	14.0 Lakhs	-	-	-	-	-		Purchase in process	
(B) General Components										
2	Net Working & Computational Facilities (NW)		-	-	-	-	-			
3	Infrastructure Facilities (IF)		-	-	-	-	-			
4	Maintenance (M)	9.00 Lakhs	-	-	-	-	-			
5	Total	86.0 Lakhs*	-	42,66,044	-	-	-	42,66,044	Yet to receive fund in (B) 3,97,145	

* - Received Rs 33.5 Lakhs (DST) + Rs 61,873 (Interest in 2013-14) + Rs 31527 (interest in 2014-15) against Sanctioned Rs 43.0 Lakhs. Amount to be received from DST = Rs. 8,56,600

Name & Signature of Head of Department/ Project Coordinator

Date:

Note:

- Expenditure under the sanctioned Heads, at any point of time should not exceed funds allocated under that Head, without prior approval of DST.
- Utilization Certificate for each financial year ending 31st March has to be enclosed along with request for carry forward permission to next year.

Name & Signature of Competent Financial Authority
Date:

Finance Officer
Thapar University

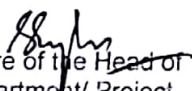
P.

UTILIZATION CERTIFICATE (2 copies)
(for the Year/Period of 1st April, 2014 to 31st March, 2015)

1. Name of the Department & Institute/ University: Mechanical Engineering, Thapar University Patiala
2. Name of the Head of Department/ Project Coordinator: Prof. (Dr.) S. K. Mohapatra
3. Sanction Order No. & Date: SR/FST/ETI-329/2012, Oder Date: 29 August 2013, vide FIST Sl. No. 104, dated 30.08.2013
4. Head of Account as given in original Sanction Order: Capital Assets: Rs. 77.0 L + General Component 9.0 L (on 50:50 share mode)
5. Amount brought forward from the previous financial year: [Order No., Date, & Amount in Rs] Rs. 46,31,662
6. Amount received during the financial year: [Order No., Date, & Amount in Rs] Nil
7. Interest earned, if any: Rs. 31,527
8. Total amount available for expenditure (excluding commitments): Rs. 46,63,189
[Sl. no. 5 + 6 + 7]
9. Actual Expenditure (excluding commitments) incurred during Financial year (up to 31st March 2015): Rs. 42,66,044
10. Balance amount available at the end of the financial year: Rs. 3,97,145
11. Unspent balance refunded if any (give details of Cheques/ Drafts etc): Rs. NIL
12. Amount to be carried forward to the financial year (if applicable): Rs. 3,97,145

Certificate

Certified that out of --- NIL (sanctioned) + Rs 31,527 (interest income) --- amount of grant-in-aid sanctioned during the year **2014-15** in favour of **Registrar, Thapar University, Patiala-147004 (Punjab)** under the Ministry/ Department Order No. **FIST Sl. No. 104** and Rs. **46,31,662** on account of unspent balance of previous year, a sum of **Rs 42,66,044** has been utilized for the purpose of **Capital Assets and General components** for which it was sanctioned and the balance amount of **Rs. 3,97,145** remaining unutilized at the end of the year has been surrendered to Government (vide Challan no.-----X----- dated -----X-----) / will be adjusted towards the grant-in aids payable during the next year **2015-16**.



Signature of the Head of the Department/ Project Coordinator

Date: 30/7/15


Signature of Accounts Officer
Finance Officer
Thapar University
Patiala-147 004

Date:


Signature of the Head of Institute/ University

Date:  Registrar
Thapar University
Patiala-147 004

(To be filled in at DST)

Certified that I have satisfied myself that the conditions on which the grants-in-aids was sanctioned has been fulfilled/ are being fulfilled and I have exercised the following checks to see that the money was actually utilized for the purpose for which it was sanctioned:-

Kinds of Checks exercised:

- 1.
- 2.
- 3.

Signature/ Designation/ Date